The Influence of Hydrodynamic Environment on the Nucleation Mechanism of a Chiral Crystallization

Craig James Callahan

Thesis submitted for the degree of Doctor of Philosophy

Centre for Oscillatory Baffled Reactor Applications (COBRA)

School of Engineering and Physical Sciences

Heriot-Watt University

July 2014

Abstract

This thesis presents the results and discussions of an investigation into nucleation mechanisms in a cooling crystallization of sodium chlorate in both a stirred tank crystallizer (STC) and an oscillatory baffled crystallizer (OBC) under various crystallizer configurations and operational conditions.

The key question to be addressed was why nucleation took place in an OBC without seeds, while seeds were essential in an STC for the same chemistry and at the same process conditions. Various hypotheses have been initiated, tested and verified in both primary and secondary nucleation experiments, and new scientific insights and better understanding have been achieved on the parameters that have influenced the nucleation mechanisms and some explanations as to why seeds were not necessary in the OBC are put forward.

For the seeded nucleation, the fluid dynamic environment and mixing mechanics were responsible for dictating the nature of the nucleation mechanism. The unique scraping action of the baffles against the crystallizer wall in the OBC enabled a different enantiomorphism of the product crystals compared to the seed crystal. Removing such a motion in the OBC provided product crystals similar to that seen in the STC. The degree and the means of mixing near the single seed crystal also affected the crystal handedness. For the primary nucleation experiments, it was found that the handedness of the product crystals in the STC was strongly orientated towards a single enantiomorph, while both enantiomorphs were formed in the OBC. The results were suggestive of a lower free energy barrier in the OBC, in turn resulting in primary nucleation being favoured in the OBC as opposed to rapid secondary nucleation being dominant in the STC.

Acknowledgements

I would like to take the opportunity to thank a number of people who have helped me immensely in my research. It is with their help that this project was possible.

Firstly, thanks to my supervisor, Professor Xiong-Wei Ni, for his continuous guidance, support, encouragement and providing the opportunity to work on this project. I would also like to thank the members of the continuous crystallization discussion group: Chris Price, Gerry Steele, Amy Robertson, Thomas Rammelo, Kevin Girard and Alex Caillet for the valuable expertise and guidance on the subject matter.

Thanks to the technicians, Ronnie Millar and Curtis Abbot for assistance in getting the apparatus up and running. Thanks also to Craig Bell for his assistance in acquiring elusive pieces of apparatus. I would also like to thank Marian Millar and Eileen McEvoy for the useful discussion on analysis of the crystalline material. I would like to extend thanks to Cameron Smith of the department stores for his assistance in acquiring suitable equipment and the ordering of materials. Thanks to Andrew Haston for his assistance in repairing and configuring the electrical apparatus and for the construction of the turbidity probe and control box. Thank you to Naomi Briggs and Dimitrios Lamprou of the University of Strathclyde for kindly supplying AFM imaging of the baffle surfaces. For valuable assistance with the acquisition and analysis of the Nanosight data, I thank Anna Jawor-Baczynska. For assistance in the primary nucleation experimental work, I thank Andrew Baillie.

My thanks to Professor Graeme White and Doctor Cameron Brown for the useful discussions and advice, as well patience and time for organising lab space and helping to set up apparatus. I also want to thank Doctor Alison Nordon and Doctor Jaclyn Dunn for the invaluable advice regarding statistical analysis of the results.

For helping me to keep a work/life balance and a much needed creative outlet, I thank Ben, Dave, Emma and Ross.

Finally, I must thank my family and my wife, Katie for the constant support, love and encouragement throughout all of this work.

ACADEMIC REGISTRY
Research Thesis Submission

Name*:*	Craig James Callahan		
School/PGI:	Engineering and Physical Sciences		
Version: *(i.e. First, Resubmission, Final)*	Final	Degree Sought (Award **and** Subject area)	Doctor of Philosophy, Chemical Engineering

Declaration

In accordance with the appropriate regulations I hereby submit my thesis and I declare that:

1) the thesis embodies the results of my own work and has been composed by myself
2) where appropriate, I have made acknowledgement of the work of others and have made reference to work carried out in collaboration with other persons
3) the thesis is the correct version of the thesis for submission and is the same version as any electronic versions submitted*.
4) my thesis for the award referred to, deposited in the Heriot-Watt University Library, should be made available for loan or photocopying and be available via the Institutional Repository, subject to such conditions as the Librarian may require
5) I understand that as a student of the University I am required to abide by the Regulations of the University and to conform to its discipline.

* *Please note that it is the responsibility of the candidate to ensure that the correct version of the thesis is submitted.*

Signature of Candidate*:*		Date:	

Submission

Submitted By *(name in capitals):*	CRAIG JAMES CALLAHAN
Signature of Individual Submitting:	
Date Submitted:	

For Completion in the Student Service Centre (SSC)

Received in the SSC by *(name in capitals):*			
Method of Submission *(Handed in to SSC; posted through internal/external mail):*			
*E-thesis Submitted (**mandatory for final theses)***			
Signature:		Date:	

Table of Contents

List of Tables

List of Figures

Nomenclature

Symbol	Definition	Units
a	Standard activity, solution phase	(--)
a^*	Equilibrium activity	(--)
A_{PISTON}	Cross sectional area of piston	(m^2)
A_{PIPE}	Cross sectional area of pipe	(m^2)
A_1	Column cross sectional area	(m^2)
A_2	Baffle orifice area	(m^2)
c	Solution concentration	(kg m^{-3})
c^*	Equilibrium concentration	(kg m^{-3})
C_D	Discharge coefficient (0.7)	(--)
D	Pipe diameter	(m)
D'	Effective width of obstacle	(m)
D_b	Baffle diameter	(m)
D_c	Column diameter	(m)
D_o	Orifice diameter	(m)
D_s	Diameter of stirrer	(m)
f	Pulsating frequency	(Hz)
G_S	Surface excess free energy	(J)
G_V	Volume excess free energy	(J)
ΔG	Free energy difference	(J)
ΔG_{crit}	Critical free energy (homogeneous nucleation)	(J)
$\Delta G'_{crit}$	Critical free energy (heterogeneous nucleation)	(J)
H	Half channel width	(m)
H_{MAX}	Maximum channel width	(m)
ΔH_f	Enthalpy of fusion	(J mol^{-1})
J	Nucleation rate	($kgm^{-3}min^{-1}$)
k	Boltzmann constant (1.38 x 10^{-23})	(J K^{-1})
K	Nucleation rate constant	(--)
l	Mixing length	(m)

L	Baffle spacing	(m)
m	Order of nucleation	(--)
N_T	Total number of crystals	(--)
N'	Number of seed-dissimilar crystals	(--)
N''	Number of seed-similar crystals	(--)
N_b	Number of baffles per unit length	(--)
N_s	Speed of stirrer	(RPS)
P	Power	(W)
P_O	Power number	(--)
P/V	Power density	(W m^{-3})
r	Radius of nucleus	(m)
r_{crit}	Critical radius	(m)
R	Gas constant (8.3143)	(J mol^{-1} K^{-1})
Re	Reynolds number	(--)
Re_p	Pulsating Reynolds number	(--)
Re_o	Oscillatory Reynolds number	(--)
S	Supersaturation	(--)
St	Strouhal number	(--)
T	Absolute temperature	(K)
ΔT	Supercooling	(°C)
ΔT_{max}	Metastable zone width	(°C)
T_b	Baffle thickness	(m)
V	Volume	(m^3)
u	Mean flow velocity	(m s^{-1})
u_p	Pulsating velocity	(m s^{-1})
u_{PEAK}	Peak velocity	(m s^{-1})
V_L	Volume of liquid in STC	(m^3)
x_o	Centre to peak amplitude	(m)
α	Baffle free area ratio	(--)
α_s	Surface roughening factor	(--)

β	Cooling rate	(°C min^{-1})
γ	Interfacial surface tension	(J m^{-2})
γ_{cl}	Interfacial surface tension between crystal/liquid	(J m^{-2})
γ_{cs}	Interfacial surface tension between crystal/solid	(J m^{-2})
γ_{sl}	Interfacial surface tension between solid/liquid	(J m^{-2})
θ	Contact angle	(°)
μ	Chemical potential	(J mol^{-1})
ν	Fluid kinematic viscosity	(m^2 s^{-1})
ν_m	Molecular volume	(m^3 mol^{-1})
ξ	Anisotropy factor	(--)
ρ	Fluid density	(kg m^{-3})
σ	Relative supersaturation	(--)
ϕ	Contact angle function	(--)
ω	Angular frequency	(rad s^{-1})

+	Dextrorotatory
−	Levorotatory
LH	Left handed
RH	Right handed
OBC I	Oscillatory baffled crystallizer (oscillating baffles)
OBC II	Oscillatory baffled crystallizer (oscillating baffles + gap)
OBC III	Oscillatory baffled crystallizer (oscillating fluid)
COBC	Continuous Oscillatory Baffled Crystallizer
STC I	Stirred tank crystallizer
STC II	Stirred tank crystallizer with scraping stirrer
STC III	Stirred tank crystallizer with baffles

List of publications

1. Callahan, C. J. and X. Ni, *Probing into nucleation mechanisms of cooling crystallization of sodium chlorate in a stirred tank crystallizer and an oscillatory baffled crystallizer*, Crystal Growth & Design, 2012, **12,** (5), pp 2525-2532 – Chapter 5

2. Callahan, C. J. and X. Ni, *An investigation into the effect of mixing on the secondary nucleation of sodium chlorate in a stirred tank and an oscillatory baffled crystallizer*, CrystEngComm, 2014, **16**, pp 690-697 – Chapter 6

3. Callahan, C. J. and X. Ni, *On the investigation of the effect of apparatus configurations on the nucleation mechanisms in a cooling crystallization of sodium chlorate*, CJChemE, **Accepted**, January 2014 – Chapter 7

4. Callahan, C. J. and X. Ni, *An investigation into the effect of agitator materials of construction on the nucleation mechanism in an oscillatory baffled crystallizer*, **Manuscript ready for submission** – Chapter 8

5. Callahan, C. J. and X. Ni, *Probing the primary nucleation mechanisms of cooling crystallization of sodium chlorate in a stirred tank crystallizer and an oscillatory baffled crystallizer*, **Manuscript ready for submission** – Chapter 9

6. Ni, X and C. J. Callahan, *Device for inducing nucleation*, WIPO patent number **WO2013/088145 A1**, June 2013

List of conference presentations

Poster presented at European Conference of Crystal Growth 4 (ECCG4), Strathclyde University, June 2012

Oral presentation at The British Association of Crystal Growth (BACG) conference, Manchester University, June 2013

Oral presentation at The Northern Postgraduate Chemical Engineering Conference (NPCEC), Newcastle University, August 2013

Oral presentation at The Centre for Continuous Manufacturing and Crystallization (CMAC) 2nd Annual open day, Glasgow Science Centre 2013

Chapter 1 – Introduction

This chapter discusses the purpose and inspiration of the research as well as gives a general overview of the layout of the thesis.

1.1 – Basis of Research

Crystallization is an important separation technique in the chemical and pharmaceutical industries. Although many theories are available in the literature[1-5], the fundamental science behind crystal nucleation and growth is not fully understood and in an industrial setting, operator experience rather than sound scientific understanding often plays a major role in the success or failure of a crystallization process. The scale up of crystallization processes also poses further challenges for chemical engineers and process chemists in that although batch processes are well understood, the scale up is often marred with batch to batch variations with additional problems not encountered in the laboratory scale. This is largely due to different fluid mechanical conditions present at different scales of operation[6]. It is widely accepted that discrepancies in mixing and flow patterns have profound influence on 0parameters such as metastable zone width (MSZW)[7], nucleation and growth mechanisms[8, 9]. This consequently affects the final crystal specifications such as size distribution and morphology[10]. A drive to minimize these differences in fluid dynamics at different scales of operation has led to the use of continuous crystallization by means of plug flow crystallizers such as the continuous oscillatory baffled crystallizer (COBC)[11-13].

Due to the uniform mixing, plug flow characteristics[14], enhanced mass[15] and heat transfer rates[16], together with the ease and readiness of controlling temperature profiles along the length of the crystallizer, this provides a constant fluid mechanical condition for the nucleation and subsequent growth of crystals. This has led to uniform crystal sizes[17] with significantly enhanced filtration rates[18]. The transition of a lab scale COBC of typically 10 – 15 mm diameter to a pilot/full scale COBC of 40 – 80 mm diameter is a linear process[19], which means that there is little variation in fluid mechanical conditions as well as the metastable zone widths and this facilitates a direct and smooth scale up operation. In addition, analytical tools and monitoring techniques can be used at all scales without modification, enabling direct knowledge and know-how of transfer from lab to industrial volumes.

In recent studies of continuous crystallization of active pharmaceutical ingredients (APIs), some interesting results were consistently observed. For example, higher nucleation temperatures and narrower MSZW were observed in an OBC than in an STC[20]; rapid growth of crystals in an OBC without the entrainment of impurities was possible[21]; also seeding was not necessary in an OBC while it was essential in an STC for the same operation[22]. This current PhD work aims to address the latter finding which has been exhibited in the following two available case studies:

Case study 1 – Crystallisation of an API product after fermentation

In the benchmarking operation, the solid crude chemicals were dissolved in acetone (40% w/w) at 45 °C, and then crash cooled to 20 °C. Solid seeds (~1% w/w) were added at 20 °C. The crystallizing solution was then cooled to 2.5 °C at a rate of 0.3 °C /min. There was an aging period of 4 hours after crystallisation. In the OBC, it was cooled from 45 to 25 °C at a rate of 3 °C/min, and then at 0.6 °C/min from 25 to 2.5 °C. Nucleation took place without seeds and the same or better purity and yield was obtained in comparison to the benchmark data, but with no aging time.

Case study 2 – Crystallisation of a fine chemical compound

In the benchmark STC operation, 1% seeds (w/w) in water were added to the solution at 40 °C. The solution was then cooled to 20 °C over a number of hours. A two-step cooling profile was used in the OBC, where nucleation was achieved without seeding at cooling rates of up to 1.2 °C/min. All tests gave good purity and high yield.

The hypotheses are that a different nucleation mechanism could be observed in an OBC compared to a STC. Such differences could be due to different styles of mixing, or mixing mechanisms, while all other operational conditions remain constant, such as supersaturation, temperature, mixing intensity and etc. Different nucleation mechanisms may have resulted in different crystallization specifications. Understanding and controlling these differences of nucleation in an OBC will be essential in order to scale up a batch operation to an industrially relevant process with ease and confidence. It is however nearly impossible to observe nucleation directly due to the facts that the event of nucleation is too fast to be recorded and the concentration of nuclei is too low to be detected by any modern measuring tools. The focus of this PhD work is therefore directed at finding a crystal compound whose solid state properties could retrospectively be related to the nucleation mechanism. This

relationship can then be probed in order to further understanding into how and why the OBC yielded different properties to an STC operation.

In the work described in this thesis, it has been shown how the use of an enantiomorphic compound has allowed the determination of the nucleation mechanism in both the OBC and STC. All of the data generated confirms the hypotheses that it is the fluid mechanical environment which plays an important role in the nucleation mechanism. Through further hypothesising and testing, it has been shown that it is in fact the scraping action of the baffles on the inner surface of the wall in the OBC that is the main culprit for the differences in the nucleation mechanisms when compared to the STC where no scraping takes place between the agitator and the vessel wall.

1.2 – Structure of thesis

This thesis is split into ten chapters. Following this introduction, a review of the current theories on crystallization and a more detailed description of the mechanism of mixing seen in an OBC are reported in Chapter two. A number of model compounds that would be suitable for the investigation is also outlined. This section also reviews the background literature and discuss the possible benchmark data for comparison.

Chapter three describes the experimental and analytical setup and the experimental plans that will be implemented to probe the effect of mixing mechanism on nucleation.

Chapters four to eight presents and discusses the results of the experimental work for seeded and non-seeded cooling crystallization of sodium chlorate in the OBC and STC, and draws conclusions for each condition investigated.

Chapter nine summarises the key differences and observations on the effects of crystallizer configurations and operating conditions on nucleation mechanisms observed in the OBC and STC. Chapter ten recommends future studies based on the outcome of this research. Finally, after the main body of the thesis, the appendices are given followed by a list of literature references.

Chapter 2 – Literature Review

This chapter considers the relevant background literature and general theories for crystallization and reviews crystallization hardware, specifically the OBC, as well as potential model compounds.

2.1 – Crystallization

This section of the literature review discusses the relevant background of crystallization beginning with nucleation and progressing onto crystal growth. The topic of chiral crystals is also examined.

2.1.1 – Introduction

Crystallization is a separation process that has important uses in many different industries ranging from food such as chocolate[23] and ice cream[24]where crystallization directly impacts product quality to the pharmaceutical industry where crystal size of a drug compound affects downstream operations such as filtration and drying[25], and ultimately the bioavailability of the compound to the patients [26-28].

Crystallization is the process of forming a solid crystalline state from either a solution or a melt of a substance and can generally be considered in two stages. Firstly nucleation must occur and is a critical stage in any crystallization process where a number of molecules undergo some manner of self-assembly process to form embryos, which must reach a certain minimum size to be stable. Secondly, these nuclei undergo growth to become crystals with well-defined crystal faces. Both steps can be considered much like any other chemical process wherein there is an energy barrier that must be overcome to allow the process taking place. The driving force for nucleation and growth is defined by supersaturation, which is a relationship between the temperature and concentration of a solution and is closely related to the solubility of a compound.

2.1.2 - Supersaturation

If a solution containing a given solute is in equilibrium with a solid phase, the chemical potentials of the solute in solution ($\mu_{solution}$) and the solute in the solid phase (μ_{solid}) must be equal, as shown below.

$$\Delta\mu = \mu_{solution} - \mu_{solid} = 0 \qquad (2.1.01)$$

Where $\Delta\mu$ is the difference in chemical potential (J mol^{-1}).

In this state of equilibrium the solution is termed as saturated and a graph of concentration versus temperature is the solubility profile, depicted in more detail in Figure 2.1.1.

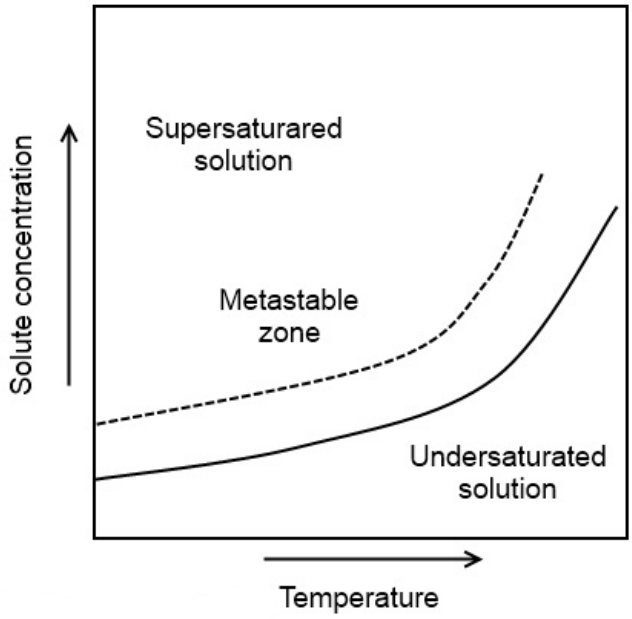

Figure 2.1.1 - Typical solubility curve (solid line) and metastable limit (dashed line). The area between the two represents the metastable zone. Image adapted from [29]

If the $\Delta\mu$ value is positive ($\mu_{solution} > \mu_{solid}$), more of the solute exists in the solution state and the solution is then supersaturated. Conversely when the value of $\Delta\mu$ is negative ($\mu_{solution} < \mu_{solid}$), more of the solute exists in the solid state and the solution must be undersaturated. The chemical potential can be expressed in terms of the standard potential, μ_o, and the standard activity, a, as shown below.

$$\mu = \mu_o + RTlna \tag{2.1.02}$$

Where R is the gas constant (8.3143 J mol^{-1} K^{-1}) and T the absolute temperature (K). Note that a can take the form of "a" to denote the activity of the solution phase or "a^*" the activity of the solid phase or the equilibrium activity. Substituting the above into equation (2.1.01), the following can be derived.

$$\frac{\Delta\mu}{RT} = \ln\left(\frac{a}{a^*}\right) \tag{2.1.03}$$

The ratio of the standard activities, a/a^* can be replaced by supersaturation, *S*, giving the equation (2.1.04).

$$\frac{\Delta\mu}{RT} = ln\left(\frac{a}{a^*}\right) = lnS \tag{2.1.04}$$

Assuming that the solution being studied is an ideal solution, the activity will not vary with concentration; the supersaturation can then be expressed in terms of concentration. An excess of concentration above the equilibrium will drive the formation and growth of crystals, i.e. the solution phase has a higher concentration of solute than the solid phase.

$$lnS = ln\frac{c}{c^*} \tag{2.1.05}$$

Where S is the fundamental supersaturation, c^* the equilibrium concentration (kg m^{-3}) (solute in solution in equilibrium with the solid phase) and c the solution concentration (kg m^{-3}) (solute in solution phase). If c/c^* is approximately 1, then equation (2.1.06) can be used.

$$ln\frac{c}{c^*} \approx \frac{c-c^*}{c^*} = \sigma \text{ or } S = \sigma + 1 \tag{2.1.06}$$

Where σ is the relative supersaturation.

A typical solubility curve will consist of three distinct regions as shown in Figure 2.1.1: the stable, metastable and labile regions.

The stable region lies beneath the solubility curve and refers to an undersaturated solution where no nucleation could occur. This is typical of a high temperature. If a stable solution is cooled, evaporated, or undergoes an addition of an antisolvent, the solution will then become supersaturated and enter the metastable zone. Crystallization is unlikely to be spontaneous, instead seeding would be necessary to induce nucleation.

Further increasing the supersaturation by cooling, evaporating or anti-solvent addition will push the solution past the boundary of the metastable zone and into the labile region. It is in this region that the solution is the most unstable and most likely to spontaneously nucleate.

A number of nucleation mechanisms can occur under the correct conditions of supersaturation. Figure 2.1.2 displays the possible mechanisms of nucleation.

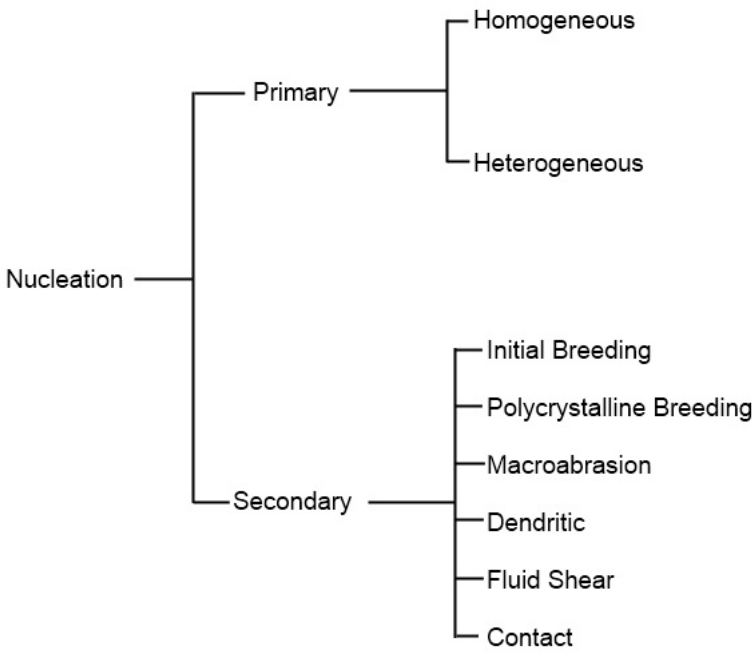

Figure 2.1.2- Mechanisms of nucleation [3]

2.1.3 – Primary nucleation

When a new solid phase is spontaneously formed from the supersaturated solution, this is an example of primary, homogeneous nucleation.

The "transition state" to nucleation as described by the classical nucleation theory is a cluster of molecules held together by intermolecular forces. These clusters of molecules are defined by Volmer [30] as being constructed by means of an addition process:

$$A + A = A_2$$

$$A_2 + A = A_3$$

$$A_{c-n} + A_n = A_c$$

Such an addition process proceeds until a critical cluster size has been reached and a nucleus established, as demonstrated in Figure 2.1.3.

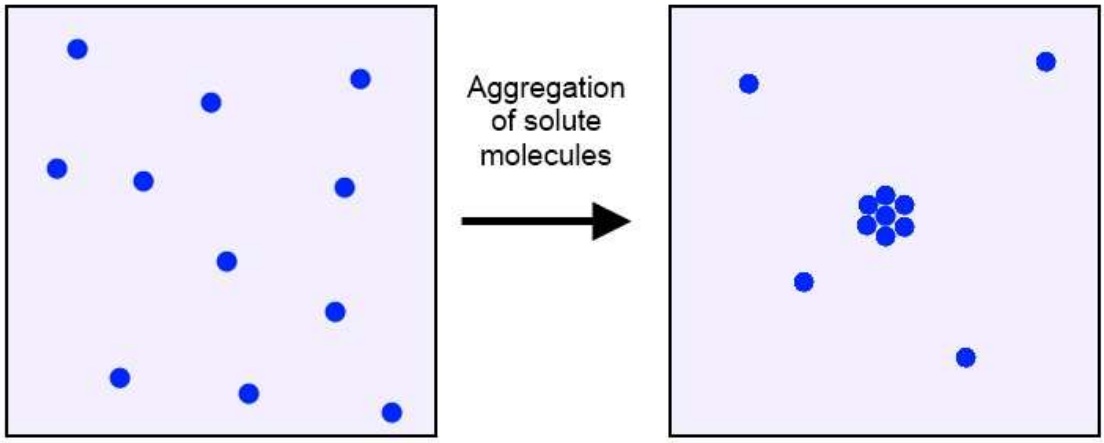

Figure 2.1.3 - Formation of clusters in solution. Solute molecules are represented by the blue circles. Adapted from [29]

In a saturated solution, these clusters, or embryos are constantly forming and dissolving in a state of equilibrium. Once the solution is supersaturated, the formation of tangible solid surfaces becomes possible. The coalescence of the solute molecules to form a three dimensional nucleus carries an energy barrier as this is essentially the formation of a new solid surface from the solution. The likelihood of this forming a stable nucleus (as opposed to re-dissolving) will be determined by the energy of the nucleus' formation and subsequent growth.

The overall free energy difference, ΔG (J), between a solid particle of the solute and the solute being in solution is the sum of the surface excess free energy, G_S (J) and the volume excess free energy, G_V (J):

$$\Delta G = G_V + G_s \tag{2.1.07}$$

Where G_V *and* G_S are defined by:

$$G_V = \frac{-4\pi r^3 \Delta\mu}{3v_m} \quad G_S = 4\pi r^2 \gamma \tag{2.1.08}$$

Where r is the radius of the nuclei (m), v_m the molecular volume (m^3 mol^{-1}) and γ the interfacial surface tension (J m^{-2}).

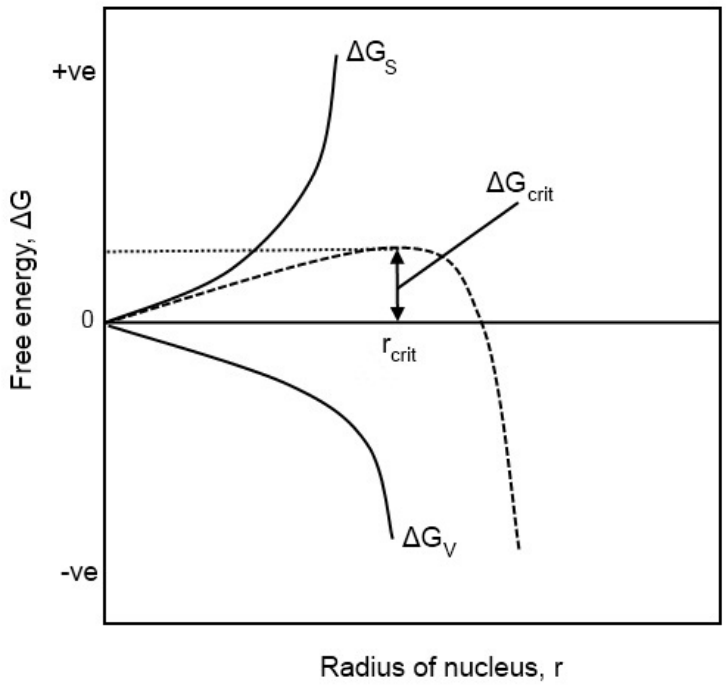

Figure 2.1.4 – Critical free energy (ΔG_{crit}) and critical radius (r_{crit}) of nucleation. Figure derived from [29]

In order to determine the value of ΔG_{crit}, the radius, r, can be replaced with the critical radius, r_{crit}, which is the minimum size of radius needed for a nucleus to become stable and then grow, as denoted in Figure 2.1.4.

$$r = r_{crit} = \frac{2\gamma v_m}{\Delta\mu} \tag{2.1.09}$$

Substituting the above into the equation (2.08) results in equation 2.1.10.

$$\Delta G_{crit} = \frac{16\pi\gamma^3 {v_m}^2}{3\Delta\mu^2} \tag{2.1.10}$$

In dealing with nuclei, the formulae must relate to solid particles instead of moles of gas. Because of this, the gas constant, R in equation (2.1.04) can be replaced by the Boltzmann constant, k (1.38×10^{-23} J K^{-1}). By substituting Δμ from equation (2.1.04) and S from equation (2.1.06) into equation (2.1.10) we have:

$$\Delta G_{crit} = \frac{16\pi\gamma^3 {v_m}^2}{3[kTln(\sigma+1)]^2} = \frac{16\pi\gamma^3 {v_m}^2}{3k^2T^2(lnS)^2} \tag{2.1.11}$$

From equation (2.1.11), it can be seen that at higher levels of supersaturation, the critical free energy for nucleation will be reduced in comparison to that at lower levels of supersaturation. This is illustrated in Figure 2.1.5.

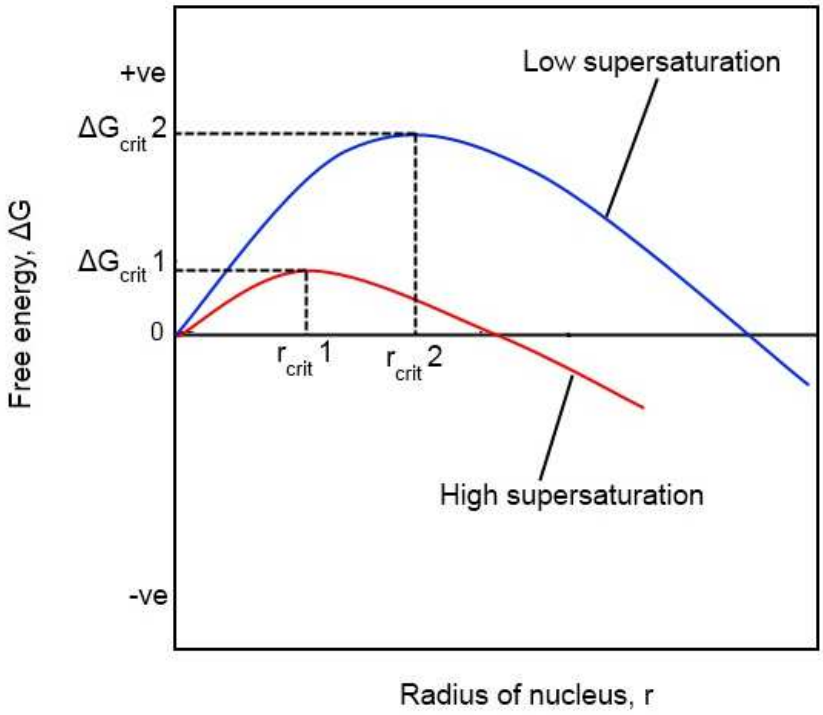

Figure 2.1.5 - Free energy difference with respect to supersaturation. Note the reduction in both r_{crit} and ΔG_{crit} when supersaturation is increased (red curve) [29]

Supersaturation will also have an effect on the rate of nucleation as demonstrated in Figure 2.1.6, where the nucleation rate is plotted against supersaturation.

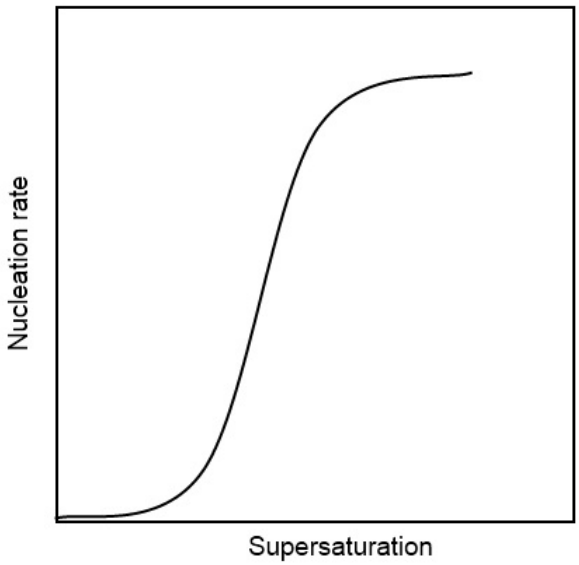

Figure 2.1.6 - Nucleation rate with respect to supersaturation. The critical supersaturation is where the nucleation rate increases exponentially [29]

The rate of nucleation, J (kg m^{-3} min^{-1}), is described by the equation:

$$J = Ke^{\left(\frac{-\Delta G}{kT}\right)} \tag{2.1.12}$$

Where K is the nucleation rate constant which varies depending on the order of nucleation rate.

By combining equations (2.1.10) and (2.1.12) it can be seen that higher values of surface tension (γ) give large ΔG, leading to smaller values of J. Similarly, higher values of chemical potential ($\Delta\mu$) lead to lower values of ΔG, hence higher J values.

It is likely that homogeneous nucleation is rarely ever seen in industrial crystallization. Instead, some form of heterogeneous nucleation is taking place wherein some sort of impurity, possibly remnants of a previous batch or dust from the environment is triggering the nucleation event.

In "dirty" systems, nucleation temperatures and rates tend to be higher than that in "clean" systems. For example, pure water will freeze at around -30 °C, but tap water will readily freeze at -9 °C[31]. This phenomenon occurs because solid impurities in the fluid provide an opportunity for solute molecules to adsorb onto the surface of the impurity. Essentially, the impurity acts as a nucleus and allows crystal growth due to a reduction in ΔG_{crit}. This type of nucleation is known as heterogeneous nucleation. The more the impurity resembles the surface of the desired nucleus, the lower the value of ΔG_{crit} and the more effective the impurity acts as a seeding material. In the case of the impurity, or nucleant, yielding an exact crystallographic match for the desired nucleus, the seed will then orientate the solute molecules such that the nucleant behaves as part of the crystal structure. This phenomenon is known as epitaxy, as illustrated in Figure 2.1.7.

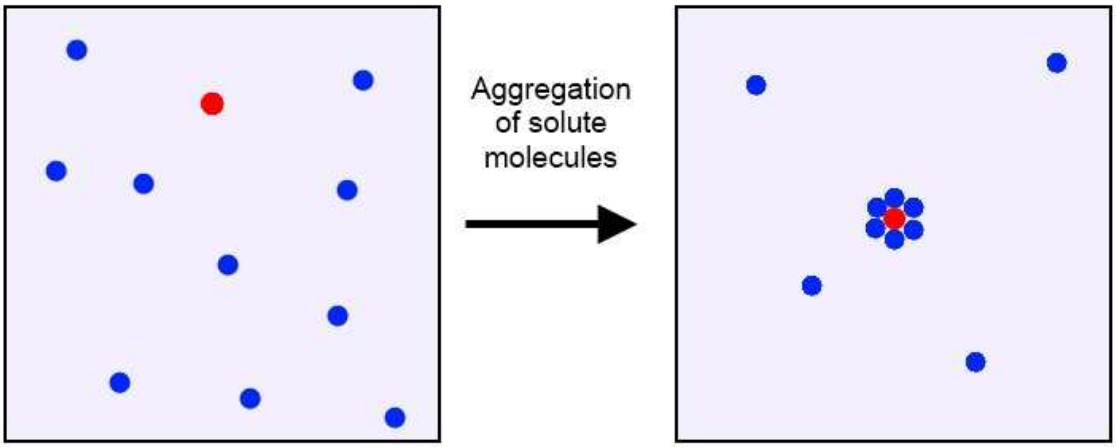

Figure 2.1.7 - Heterogeneous nucleation due to the presence of a nucleant indicated by the red circle [29]

This reduced free energy for a heterogeneous nucleation can be defined as $\Delta G'_{crit}$ and is differentiated from ΔG_{crit} of a homogenous nucleation by the following equation:

$$\Delta G'_{crit} = \phi \Delta G_{crit} \tag{2.1.13}$$

The term ϕ is a function of the contact angle (θ) between the solid impurity and the new crystalline deposit. This term also takes into account the surface tension, γ. The surface tensions between the crystalline, liquid and impurity species will determine the contact angle of wetting involving the solution and the solid impurity. Mullin[5]presented a nice figure demonstrating this, shown below in Figure 2.1.8:

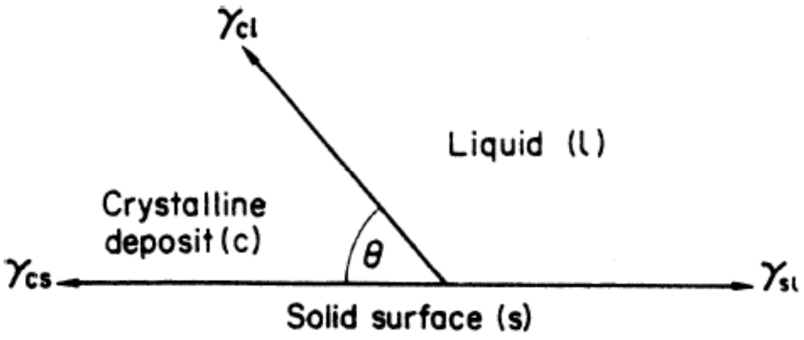

Figure 2.1.8 - Interfacial tension and contact angles in heterogeneous nucleation[5]

The angle and tensions can be resolved and defined by:

$$cos\theta = \frac{\gamma_{sl} - \gamma_{cs}}{\gamma_{cl}} \tag{2.1.14}$$

Where the subscript *sl* stands for the surface tension between the solid and liquid, *cs* between the growing crystal and the solid surface and *cl* between the growing crystal and the liquid.

Volmer [30] suggested that ϕ can be defined as:

$$\phi = \frac{(2+cos\theta)(1-cos\theta)^2}{4} \tag{2.1.15}$$

In such a situation, the contact angle relates to the epitaxy of the solid impurity.

If the solid impurity shows no correlation to the crystal structure of the solute, no epitaxy will be displayed and the contact angle, θ, of the system will be 180° as seen with a completely non-wetting liquid-solid interface. In such a situation, ϕ will be equal to 1 and $\Delta G'_{crit}$ will be equal to ΔG_{crit} and no heterogeneous nucleation will take place.

If there is some degree of epitaxy between the solid impurity and the crystalline structure of the solute, the contact angle can then take any value between 0 and 180°. This will give ϕ a value of less than one and therefore $\Delta G'_{crit}$ will be less than ΔG_{crit}. Heterogeneous nucleation will take place due to the reduced critical free energy requirement.

2.1.4 – Primary nucleation kinetics

Just as understanding of chemical reaction kinetics are important for the scale up and operation of any other chemical processes, crystal nucleation kinetics are of great importance in order to achieve true control of nucleation and growth. Determination of nucleation kinetics relies on understanding and control of the metastable zone width [32].

Nývlt (1968) proposed a method for evaluating the nucleation kinetics based on the metastable zone width [33]. Modifying equation (2.1.12) allows the expression of nucleation rate as:

$$J = K\Delta c_{max}{}^{m} \tag{2.1.16}$$

Where Δc_{max} is the maximum possible supersaturation (kg m^{-3}) and m is the order of nucleation.

The maximum possible supersaturation is a function of the maximum supercooling in the system due to the fact that solution concentration is dependent on the solution temperature. From equation (2.1.16) it can be seen that the nucleation rate depends on the rate of generation of supersaturation (the faster supersaturation is generated, the faster the nucleation rate will be), which in turn depends on the cooling rate, the metastable zone width can be related to the cooling rate according to equation (2.1.17).

$$log\beta = (m-1)log\frac{dc^*}{dT} + logK + mlog\Delta T_{max} \qquad (2.1.17)$$

Where β is the cooling rate (°C min^{-1}), T the temperature (K), ΔT_{max} the metastable zone width (°C) and dc^*/dT represents the dependency of concentration to temperature.

From this, a plot of log(β) against log(ΔT_{max}) would give a straight line of gradient, m, and the nucleation constant, K, evaluated from the intercept.

One drawback to the Nývlt method lies in the degree of accuracy of the determination of the metastable zone width. Many different techniques exist which allow the observation of the nucleation point (more precisely, post-nucleation) but the perceived MSZW may differ for each method used [34]. Tools such as turbidity [35, 36], ATR-FTIR spectroscopy [37, 38], FBRM [39, 40], bulk video imaging [41, 42] and analysis by eye [43] have been employed previously, but each method requires the nuclei to grow to a certain minimum size in order to be detected. It should be noted that these above methods provide a retrospective glimpse of post-nucleation events in a crystallizer. The smaller the minimum size of nuclei, the more accurate the determination of MSZW would be.

In order to account for the accuracy of the analytical tool, Kubota (2008) [44] considered the minimum number of detectable nuclei for a given volume, i.e. the number density in the kinetic extraction as given in equation (2.1.18).

$$\log(\Delta T_{max}) = \frac{1}{m+1}\log\left[\left(\frac{N_m}{KV}\right)(m+1)\right] + \frac{1}{m+1}\log\beta \qquad (2.1.18)$$

Where N_m/V is the number density, the minimum number of nuclei required for detection. As with the Nývlt method, the slope of a plot of MSZW vs. cooling rate yields the gradient, m, but the nucleation constant can only be evaluated provided that the number density is given for each nuclei detector. For a turbidity probe, Mitchell *et al.* suggested a value of N_m/V as 10^{11} # m^{-3} [36].

2.1.5 - Secondary nucleation

Should the solid impurity be an exact crystallographic match for the crystalline structure, the contact angle will be 0° and $\Delta G'_{crit}$ will equal zero. Such a situation would arise when a pure seed crystal of the solute is introduced to the solution. Nucleation will result because of the introduction of a crystalline material and is termed secondary nucleation.

This type of nucleation has been studied in detail by a number of researchers, see for example: Strickland-Constable[45]; Denk and Botsaris [46, 47]; Qian and Botsaris[48-50]; Garside and Davey [25, 51] and Nývlt[52]. There are a few mechanisms through which secondary nucleation can take place. The first mechanism is contact nucleation, a process where a single crystal is split into numerous crystals by mechanical means.

Powers(1963)[53] and Sung *et al.* (1973)[54] suggested that fluid shear, an aspect of mixing, was responsible for secondary nucleation and fluid flow could cause micro-crystalline dust from a crystal to be swept into solution and into areas of high supersaturation. Alternatively, growth on the crystalline surface could be sheared off and taken into the solution in a similar fashion, leading to secondary nucleation.

Once crystals have been established within the crystallizer from some sort of primary nucleation, or secondary nucleation described above, it becomes likely that there will be collisions between crystals and crystallizer walls/impeller surfaces or crystals with other crystals. Such interactions are known as collision breeding interactions yielding further crystals.

The other method of initiating nucleation through crystal presence is by deliberately introducing crystals into the solution. This is known as seeding. Seeding a crystallizer involves introducing crystalline solute to the solution in order to initiate nucleation, by either single crystal, or a certain mass of crystals. The use of seeds is an important procedure in industrial crystallizers where control over the nucleation process is essential to prevent problems such as rapid nucleation that could lead to deviation from desired crystal parameters. Seeding can also help control phenomena such as scaling or blockage in an industrial crystallizer.

In order for seeding to be effective, the seeds should be introduced to the solution within certain conditions of supersaturation, ideally within the metastable zone width, as shown in Figure 2.1.9 below.

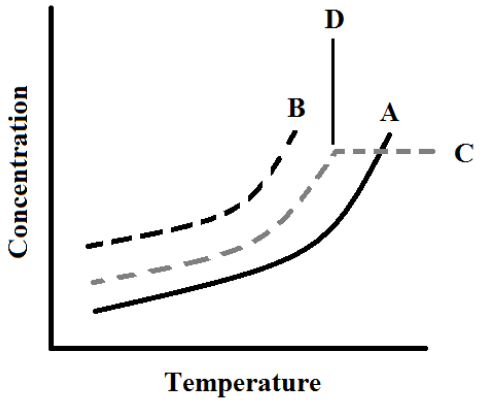

Figure 2.1.9 - Supersaturation pathway of a seeded crystallization

From Figure 2.1.9, an undersaturated solution at point C is cooled beyond the solubility curve A and into the metastable zone. An ideal seeding point would lie in the metastable zone before the line B where the supersaturation would allow spontaneous nucleation to occur. As an example, the point D would be a suitable point for seed crystals, although this would vary on a compound to compound basis, as well as the experimental conditions such as cooling rate and mixing.

If seeds are added at the point C where the solution is undersaturated, seeds would be dissolving. Conversely, if seeds are added to the left of the curve B where the solution is too supersaturated, primary nucleation is likely to occur, offsetting the effect of seeding. By using seeds, the nucleation can be controlled, in turn allowing control over final product specifications such as crystal size distribution and morphology. Further to the use of seeding, ultrasonic cavitation and laser light were also used to trigger nucleation events[55, 56].

2.1.6 – Alternative nucleation theories

As well as the classical nucleation theory, a number of recent studies have suggested alternative models. Qian and Botsaris (1997) suggested the embryos coagulation secondary nucleation (ECSN) model which addressed the attractive forces acting between the solute molecules and the molecular clusters, a parameter overlooked by the classical nucleation theory. The behaviour of the molecules in this model was

described in a similar manner to a colloidal suspension. Essentially, this model postulated that near the surface of a seed crystal, for example, the attractive forces of the seed surface could orient the molecules of the solute into an ordered cluster prior to the nucleation event[48].

This model was used to describe not only the KCl crystallization work by Qian and Botsaris, but also some previous research involving enantiomorphic crystallization. Davey *et al.* (1990) reported the case of triazolylketone crystallization wherein the product crystals had incorporated the opposite enantiomer into the surface and the bulk of the crystal[57]. Qian and Botsaris described this as the attractive forces involved do not discriminate between optically active enantiomers, which explains the incorporation of the chiral impurity into the crystal structure.

Qian and Botsaris also used the ECSN model to explain the work of SCMC crystallization by Yokota and Toyokura (1992) where product crystals displayed mixed enantiomorphism when seeded with a single enantiomer seed[58]. The ECSN model interpreted that the unexpected enantiomers could have occurred due to ordering around the seed crystal prior to nucleation.

More recently, Vekilov (2005) pointed out that in the classical nucleation theory, the structure and the density of the solid and liquid phases were not addressed. By investigating the crystallization of lysozyme, Vekilov suggested that a solution first adopted a dense liquid state before the molecules within this dense droplet became ordered to form a new crystal solid[59] as depicted in Figure 2.1.10.

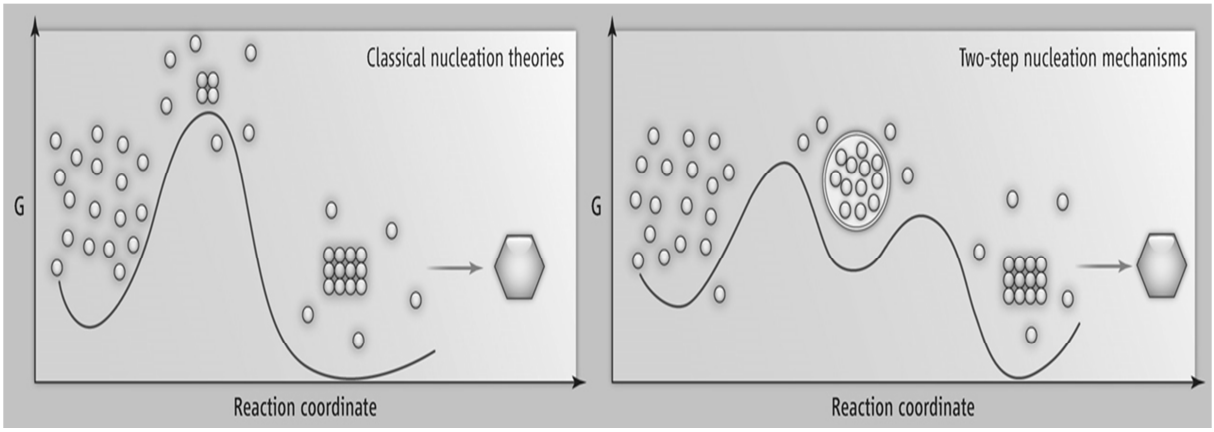

Figure 2.1.10 – The classical nucleation model (left) compared to the two-step nucleation model [60]

This density fluctuation followed by a structure fluctuation was termed the two-step nucleation mechanism, as presented in the right hand side of Figure 2.1.10. In a recent paper, Vekilov (2010) described how this model was applicable to not only protein crystallization, but also small organic molecule and nanoparticle crystallization with significant improvement over the predictions made by the classical nucleation theory[61]. This two-step nucleation theory was praised by Chen *et al.* (2011) as one of the biggest advances in our understanding of the mechanisms of nucleation[62], who also presented a thorough list of literature references demonstrating that the two-step nucleation mechanism was a major improvement over the classical nucleation theory.

The following is a brief list of the works cited. Georgalis *et al.* (1997) showed, by dynamic and static light scattering, that lysozyme solutions displayed "mass-fractals undergoing diffusion limited-like aggregation" prior to nucleation[63, 64]; Igarashi *et al.*(1999) demonstrated by means of differential scanning calorimetry (DSC) that prior to crystal nucleation and growth lysozyme solutions adopted a structured aggregate which was promoted through hydrophobic bonding between the protein molecules[65]; Chattopadhyay *et al.* (2005) used small-angle X-ray scattering (SAXS) to demonstrate that glycine nucleated via a liquid like cluster in a supersaturated aqueous solution[66]; Garetz *et al.* (2002) utilized nonphotochemical light-induced nucleation (NPLIN) to control polymorphism in glycine crystallization[67]. Chen *et al.* (2011) argued that the alignment of molecules by the pulsed LASER alone would not be sufficient to cause nucleation without some sort of clustering by means of dense droplet formation[62].

Recent evidence of the two-step nucleation model has comprehensively been collected and presented in a review by Gebauer and Cölfen (2011) [68] who highlighted a previous work involving amorphous calcium carbonate precipitation, where transmission electron microscopy (TEM) imaging revealed clear evidence of pre-nucleation nanostructures within the solution [69]. High resolution cryo-TEM experiments were also employed to investigate crystallization of calcium carbonate revealing evidence of pre-nucleation clusters in the 9 mM solution[70].

More recently, by using a combination of techniques such as Cryo-TEM, dynamic light scattering (DLS) and Brownian microscopy/nanoparticles tracking analysis (NTA) in the investigation of the crystallization of glycine and alanine, the presence of mesostructured clusters was able to be detected by Jawor-Baczynska *et al.* (2013). Furthermore, they proposed an alternative phase diagram for the crystallization

of the studied amino acids from solution, which split the metastable zone width of the classical nucleation model into two distinct regions: the mesostructured liquid phase region, and afterwards, the metastable region similar to that described in Figure 2.1.1 presented earlier.

2.1.7 - Crystal Growth

Once a nucleus has been established, whether through heterogeneous or homogeneous nucleation, it will continue to grow so long as the rate of growth units joining the crystal surface exceeds the rate of crystal growth units leaving the surface due to dissolution. In the case of a supersaturated solution, this will be the case, where $\Delta\mu$ will be high and ΔG will be low, which results in a high rate of nucleation or growth. More supersaturation means that there will be more solute molecules available in the solution.

As crystals grow, distinct faces will be formed. The rate of growth also depends on the strength and number of interactions between faces and growth units. The mechanism of growth is based on growth units being free to migrate to more favourable positions. For crystals to grow in such a way, it must be assumed that the growth occurs by the incorporation of growth units in a sequential manner. This creation and propagation of growth layers will determine the shape of the crystal being grown. Surface interactions are dictated by the underlying packing of molecules, or ions, in the crystal structure or lattice.

A study of the crystal growth can allow understanding of the unit cell structure and symmetry. Crystal shape is very rarely the same as the unit cell. Crystals tend to grow in a manner such that the number of intermolecular interactions is maximised. These interactions are reflected in the three fundamental types of crystal faces: kinked faces that have 3 interaction sites; stepped faces that have 2 interaction sites and flat surfaces that have only one interaction site, as shown in Figure 2.1.11.

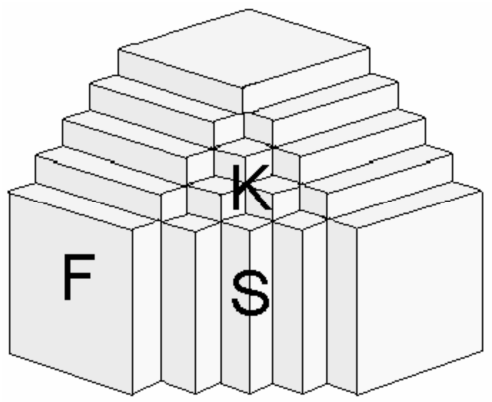

Figure 2.1.11 - Types of growth faces [29]

Growth units absorbed onto one of the rough surfaces (kinked or stepped) would not yield a smooth surface normally visible on a crystal. It tends to be the smooth flat surfaces that bind a crystal's structure. Since flat surfaces only have one interaction site available, the binding there would be relatively weak, e.g. the strongest intermolecular interactions are around 20 kJ/mol[25]. The more interactions available on a crystal face, the faster it will grow. Growth units adsorbing onto flat surfaces tend to desorb readily, whereas on kinked surface, the three binding sites allow growth units to be incorporated into the growing crystal. Because of this binding mechanism, kinked faces tend to grow rapidly whereas flat surfaces grow the slowest. The slow growing surfaces will dominate the crystal shape. It is the study of flat surface growth mechanisms that allows the prediction of a crystal shape. The surfaces do not always remain flat, surface roughening would occur as demonstrated in Figure 2.1.12.

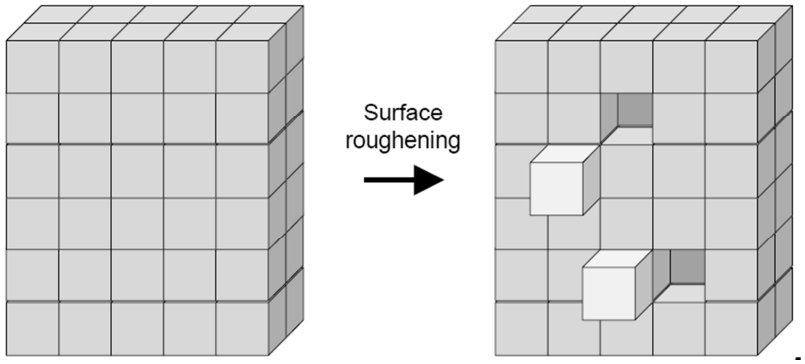

Figure 2.1.12 - Surface roughening [29]

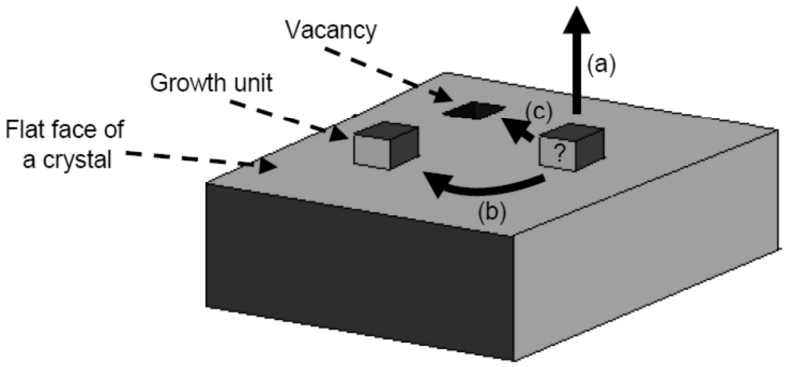

Figure 2.1.13 - Migration of growth units [29]

A growth unit that happens to adsorb onto a crystal surface has three possible actions which are indicated in Figure 2.1.13:

a) It can desorb back into the bulk solution
b) It can diffuse across the crystal surface to find another growth unit.
c) It can diffuse across the crystal surface to a vacancy

When dealing with crystallization from solution, the surface roughening factor (α_s) can be calculated from the equation:

$$\alpha_s = \xi \left[\frac{\Delta H_f}{RT} - lnc^*\right] \tag{2.1.19}$$

Where ξ is an anisotropy factor (a unitless ratio) which relates the bonding energy in the crystal surface layer to the total lattice energy, ΔH_f the heat (or enthalpy) of fusion (kJ mol^{-1}). Typical values of α_s range from 2 to 20 [25].

When α_s < 3, the surface can be considered as rough. This is like having a kinked face where there are lots of interaction sites to incorporate new growth units.

If 3< α_s <5, surface roughening is to a lesser extent and some growth units would not find a suitable attachment site and would therefore desorb back to the bulk solution. Growth units that do become attached would act as an interaction site for further growth units.

When α_s >5, little or no surface roughening is then observed and it is unlikely for growth units to adsorb onto the growing crystal face, see Figure 2.1.14 below:

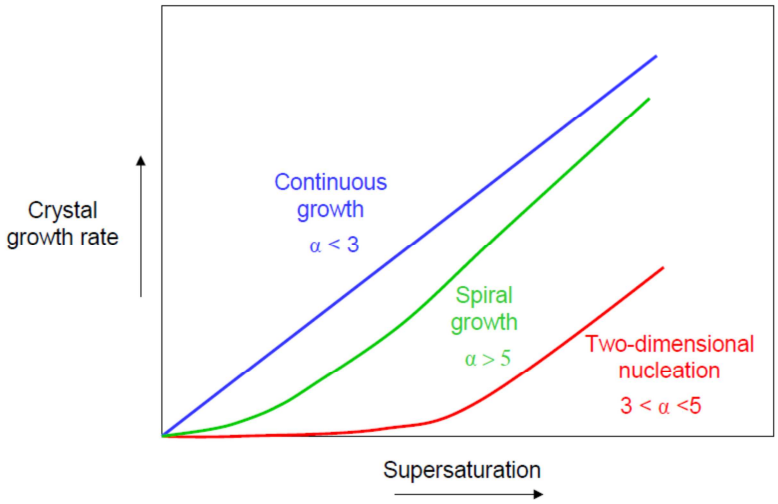

Figure 2.1.14 - Types of growth with respect to alpha [29]

The final shape of a crystal is determined by the rates at which the different faces grow:

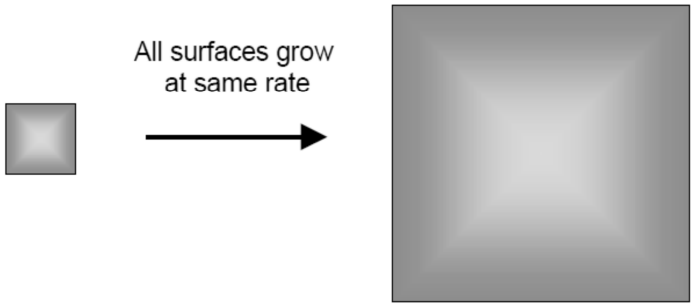

Figure 2.1.15 - Crystal shape with uniform face growth rates [29]

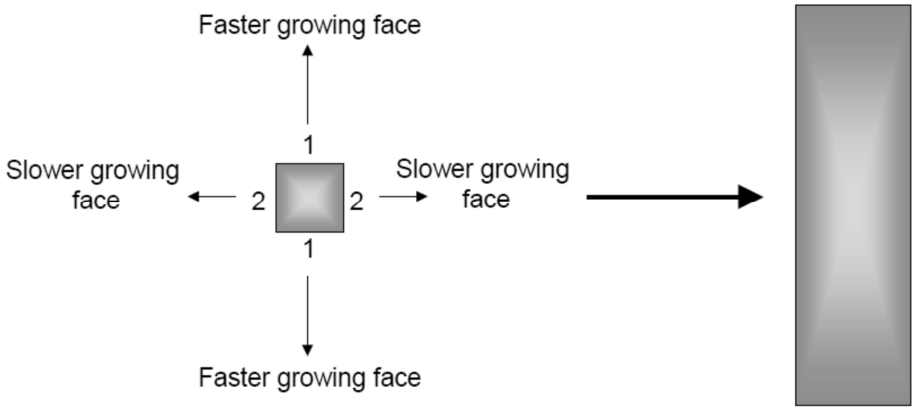

Figure 2.1.16 - Crystal shape with different face growth rates [29]

The crystal would be bound by its slowest growing faces, as Figures 2.1.15 and 2.1.16 show. This would have a direct impact on the processability of the crystals, for example, the filtration as shown schematically in Figure 2.1.17:

Figure 2.1.17 - Cubes allow for free flowing filtrate, plates can slow or even block filtration [29]

Crystal shape may be manipulated by selective adsorption of impurities. Such impurities can poison a growth surface causing a reduction of growth rate, as sketched in Figure 2.1.18. Such additives are useful, for example in diesel fuels. At low temperatures, diesel forms large plate like crystals that could block a pump or fuel lines. Additives can prevent this from happening.

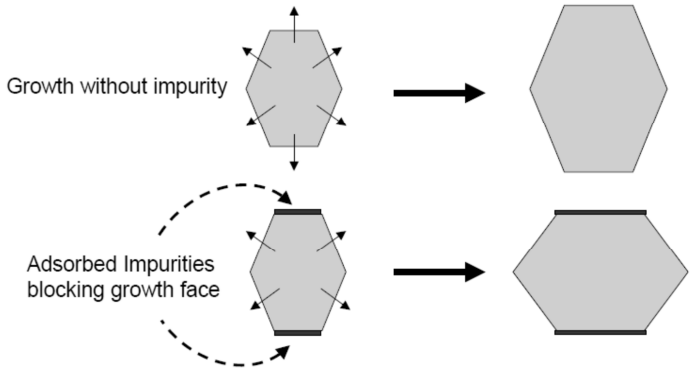

Figure 2.1.18 - Growth in the presence of impurities [29]

There are a number of other variables that could affect crystal growth:

a) Solvent selection would impact growth rates as polar solvents would adsorb onto polar crystal surfaces acting as impurity and inhibiting growth;
b) Supersaturation clearly affects growth as high supersaturation means high growth rates;
c) The volume of supersaturated solution available would affect growth rates; The more supersaturated solution present, the more growth units are available for crystal growth;

d) Crystal density in solution would also influence growth. If there are a lot of crystals in solution they would compete for growth units. This speeds up the consumption of growth units from the solution;

e) Crystal size would also alter growth. The larger a crystal becomes, then the more growth units are required for each growing face or layer (Figure 2.1.19);

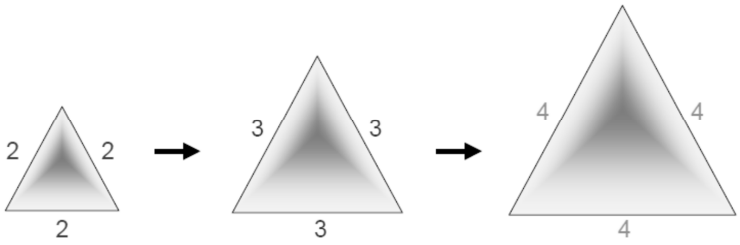

Figure 2.1.19 - Increase in growth unit requirement with size [29]

f) Growth would slow down as mass transfer from the solution is diffusion limited. As the solution becomes depleted, growth would level off as shown in Figure 2.1.20.

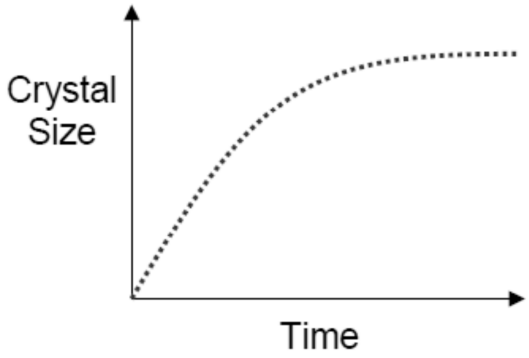

Figure 2.1.20 - Crystal size with time [29]

2.1.8 - Chiral crystals

The concept of chirality is an important principle in physical science. In biological chemistry it governs the behaviour of important amino acids and complex biological structures such as DNA. Chiral molecules are molecules with two different types of handedness. The left and right handedness of molecules can be considered as non-superimposable mirror images of one another. In terms of molecules, chirality occurs due to the presence of a stereogenic atom which has a number of different functional groups attached to it[71]. An example of this would be in lactic acid where a

stereogenic carbon atom has four different functional groups that adopt certain positions in a three dimensional space according to which stereoisomer is being considered, see Figure 2.1.21 below.

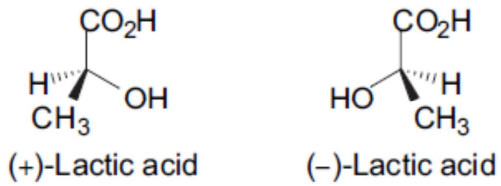

Figure 2.1.21 - Lactic acid

The two molecules are a special type of isomer known as a stereoisomer. The structure and molecular formula is the same in both handedness, but the order of the molecules is different resulting in the mirror image demonstrated above. The two mirror images cannot be superimposed on top of one another and such a molecule is referred to as an enantiomer, or an enantiomorph.

In order to distinguish between the two enantiomers, the optical activity of the substance can be examined. The measurement of the rotation of plane polarised light would allow the determination of which handedness the chirality is. One enantiomer rotates the light clockwise, denoted by the "+" sign, and the other anticlockwise, indicated by the "-" sign. The use of a polarimeter allows the analysis of the rotation of the plane polarised light. Another terminology for chiral compounds uses the prefixes D and L as opposed to + and – prefixes respectively. The prefix D comes from the term "dextrorotatory", the polarised light is rotated in a clockwise direction and the prefix L from the term "levorotatory", the polarised light is rotated in an anti-clockwise direction. Although it is common to use the D and L nomenclature, the IUPAC recommendations in 1996 suggested that optical activity should be described by the + and – nomenclature[72].

The above description is particularly suited for the discussion of individual molecules and solutions of substances such as lactic acid. When describing crystalline solids, the idea of non-superimposable mirror images is still valid. In the case of a compound such as sodium chlorate (Figure 2.1.22) the molecule itself is not chiral:

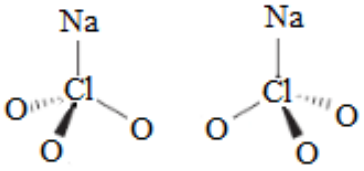

Figure 2.1.22 - Sodium chlorate

Instead, it is the crystal structures obtained that will be chiral as shown in Figure 2.1.23:

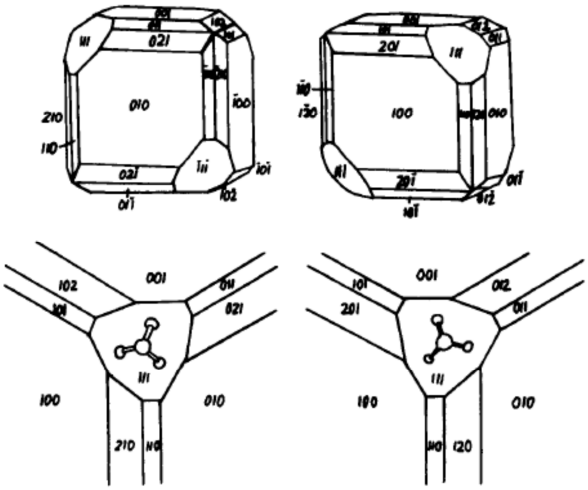

Figure 2.1.23 - Sodium chlorate crystal structures[73]

Normally in an industrial setting, the presence of enantiomorphs presents somewhat a problem in terms of processing. When enantiomers (or racemates) exist in a bulk product, there tends to be a mixture of both + and – enantiomers. This is referred to as a racemic mixture. There are a number of techniques available for obtaining exclusively one enantiomer. It is possible to use selective compounds to react with a certain enantiomer resulting in either chromatographic resolution of an enantiomer or kinetic resolution where reaction rates can be exploited to obtain enantiomeric purity. By using crystallization processes, racemic mixtures can also be resolved, e.g. using a chiral complexing agent during the crystallization, the solubility of an enantiomer can be altered to yield resolution. Another method which is more relevant to this work is the use of a chiral seed. Seeding with the desired enantiomer under certain conditions would yield exclusively the seed enantiomer in the final product.

For this work, the ability to obtain different enantiomers provides the opportunity of using plane polarised light to determine which handedness of crystals are obtained during a crystallization. Sodium chlorate crystals would rotate plane polarised light yielding a colour change. An article in the April 2005 publication of Physics

Today described the work of Viedma where the sodium chlorate crystals were observed through a linearly polarized light source. By rotating a second polariser at the point of observation the following colour changes were observed. The rotation in the clockwise direction of the second polarizer showed the right handed crystals appearing to transmit a blue light (the top row of Figure 2.1.24), whilst the left handed crystals remained a pale white colour. Conversely, rotating the polarizer in an anti-clockwise direction, the left handed crystals would appear in red, with the right handed crystals remaining white as shown in the bottom row of Figure 2.1.24[74]:

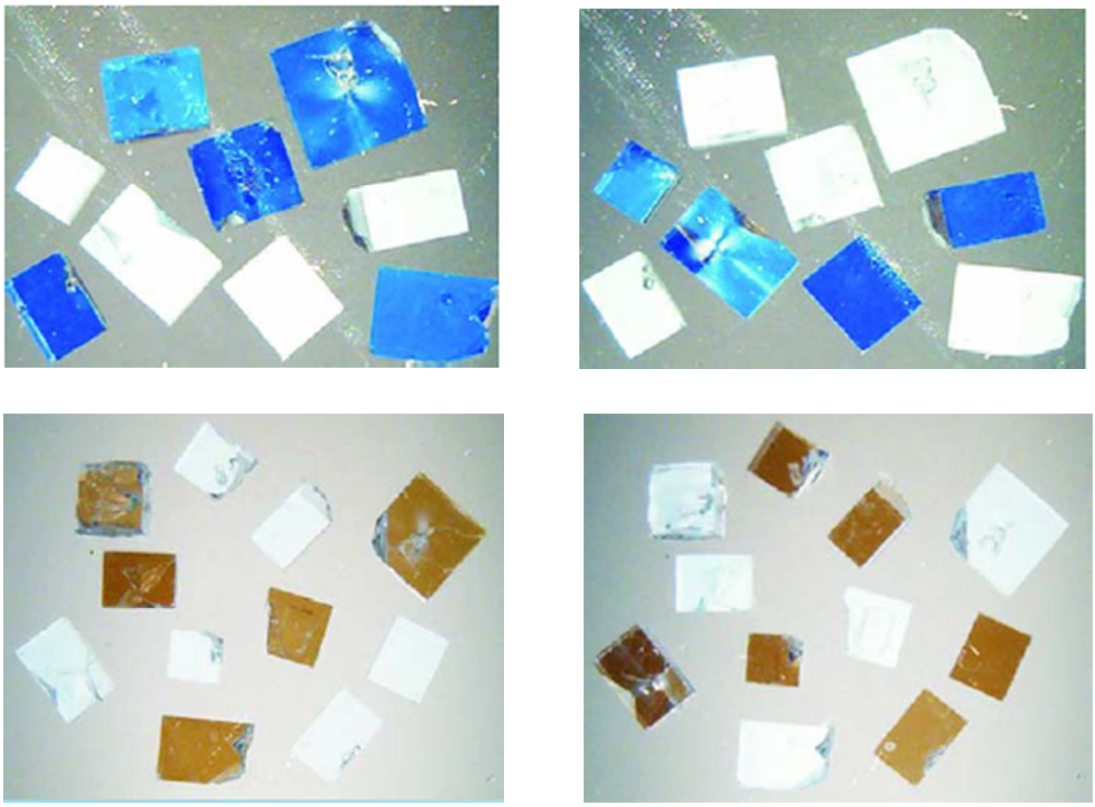

Figure 2.1.24 - Rotating polariser clockwise, top and bottom left; and anticlockwise top and bottom right, indicates the handedness of the crystals [74].

Exploiting this property of optical activity would allow an understanding of the mechanism through which the crystals are nucleating and growing. For example, if a solution of an enantiomorphic compound was seeded with a crystal of known handedness, the handedness of the product crystals could infer the nucleation process through which the crystals have been formed. All crystals could either be generated directly from the seed crystal through contact nucleation, dendritic growth or another secondary nucleation mechanism; or appear through a primary nucleation mechanism.

2.2 – Oscillatory Baffled Crystallizers

In this work, oscillatory baffled crystallizers are used. A brief review of the relevant literature is presented in the following sections.

2.2.1 - Introduction/History

Oscillatory baffled flow (OBF) has been a growing area of research since the mid-1980s, which stemmed from the study of oscillatory flow in the form of the pulsed sieve plate column as described by Van Dijick (1935)[75] and the reciprocating plate column as described by Karr (1959)[76]. This research led to studies of oscillatory flow in furrowed channels for applications in membrane filtration as reported by Bellhouse in the early 1970s[77]. It was in 1980 that Sobey *et al*. reported a numerical characterisation for the vortex style mixing within Bellhouse's system[78, 79]. These findings were consistent with data published around the same time by Knott and Mackley (1980) who reported that when sharp edges were present in a flow field, enhanced mixing was achieved due to vortex formation that was observed[80].

The first conception of what would have become the oscillatory baffled reactor (OBR) was proposed by Mackley (1987) in the form of the oscillatory baffled tube[81]. This simple device consisted of essentially a cylindrical tube with a series of periodically spaced annular baffles onto which the fluid was oscillated. The oscillation of the fluid produced vortices as the means of mixing. The efficiency of this mixing was quantified by Brunold *et al*. (1989) who demonstrated the generation and cessation of large scale eddies [82]. In considering a scenario of continuous flow, Dickens *et al*. (1989) demonstrated the effectiveness of the eddy mixing and reported conditions for near plug flow operation[83]. This pioneering research led to significant work in the 1990s which developed understanding on how the OBR could yield improvements over traditional stirred tank reactor (STR) in terms of heat transfer (some 30 fold improvement in Nusselt number was achieved)[16, 84], mass transfer[15, 85], residence time distribution[86] and in scale up correlations[19, 87]. This subsequently paved the way for the development of the oscillatory baffled reactor (OBR) for studies in more industrially relevant processes such as biodiesel production[13], polymerization[88], mixing and particle suspension[89] and more related to the objectives of this work, crystallization[7, 20, 90, 91].

2.2.2 - Mixing in an OBR

From the early research in OBF, the mixing in an OBR can be explained as the formation of vortices or eddies due to the motion of a fluid through the baffle which acts as a sharp edge. The oscillation of the fluid allows the constant generation and cessation of eddies which creates a complex series of flow patterns within the reactor resulting in highly efficient axial and radial mixing. Figure 2.2.1 below demonstrates the eddy motion within an OBR[92].

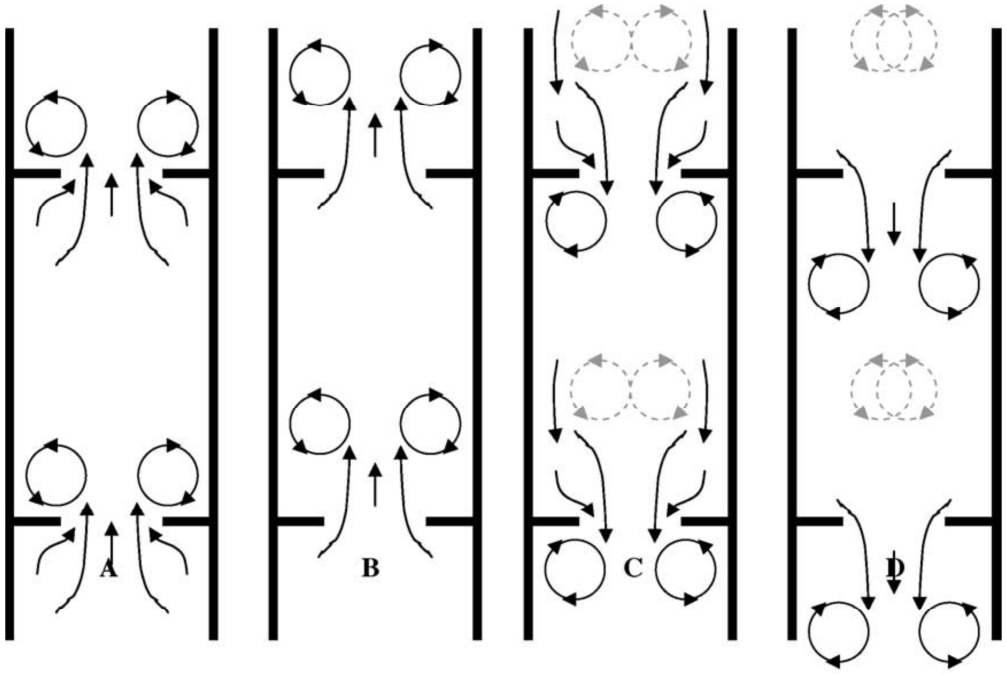

Figure 2.2.1 - Eddy motion in an OBR[92]

As seen in Figure 2.2.1, the oscillation causes mixing vortices within each inter baffle cavity. This effectively allows each cavity to act as a perfectly mixed stirred tank, with the mixing intensity controlled by varying the oscillation frequency and amplitude. Oscillation of the fluid can be achieved through a bellows or piston unit. Alternatively, a rotary or linear motor can be used to oscillate the baffles through the fluid within a vessel. Typical reactor designs for each method of oscillation will be discussed in more details in section 4.1.

At low mixing intensity, the generation of vortices can be said to be axisymmetric. As the intensity of the mixing increases, the vortices then become more chaotic and mixing more thorough. This mixing intensity has been simulated by Mackay (1991)[93], Howes (1991)[94],Wang (1994)[95] and Roberts (1996)[96]. More recent studies into the flow patterns generated within an OBR have been conducted with the aid of digital particle image velocimetry and laser induced fluorescence (Ni *et al*., 1995[97] and Fitch *et al*., 2001/05[92, 98]).

2.2.3 - Characterisation of fluid mechanics

Flow of a fluid in a pipe is characterised by the dimensionless Reynolds number. The Reynolds number is the ratio of inertial force to viscous force within the flowing material as defined by equation (2.2.1).

$$Re = uD/v \tag{2.2.1}$$

Where D is the pipe diameter (m), u the mean superficial flow velocity (ms^{-1}) and v the kinematic viscosity of fluid (m^2s^{-1}). When Re < 2000, flow in the tube is streamlined in nature, or laminar. Once the Reynolds number exceeds 2000, the layered structure of laminar flow will no longer be in effect and the flow is said to be turbulent. The Reynolds number is essentially a description of the state of flow; it gives a numerical value to the degree of turbulence in the fluid and involves all of the factors shown below in Figure 2.2.2.

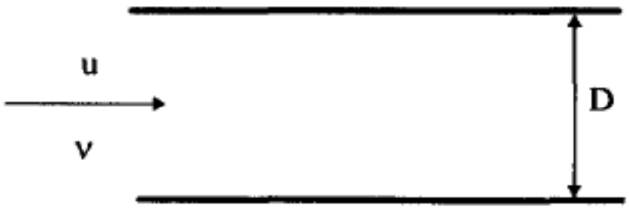

Figure 2.2.2 – Flow in a tube of diameter D [99]

Once an oscillatory motion is applied to the above scenario, the Reynolds number becomes insufficient to describe all of the motions occurring within the tube, shown in Figure 2.2.3.

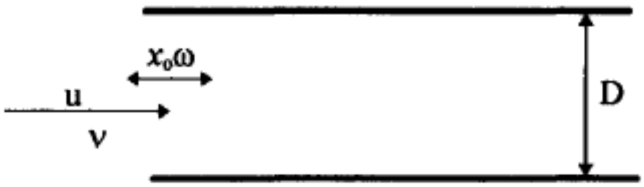

Figure 2.2.3 - Oscillatory motion applied to flow in a tube [99]

The characterisation of a pure oscillatory flow can be attributed to the work of Binnie (1945)[100]. Since then there have been a number of publications wherein the characterisation of oscillatory flow has been made using the pulsating Reynolds number defined by equation 2.2.2.

$$Re_p = u_p D/v \tag{2.2.2}$$

Where u_p is the pulsating velocity (ms^{-1}). This factor was defined by Sarpkaya (1966)[101] as the amplitude of periodic component of cross-sectional mean velocity ($=\pi f x_o A_{piston}/A_{pipe}$) where f is the pulsating frequency (Hz), x_o the pulsation centre to peak amplitude (m) and A_{piston} and A_{pipe} are the cross sectional areas of the subscript term (m^2). In most applications, the pulsating velocity can be taken as the product of the amplitude and angular frequency i.e. $u_p = x_o\omega$. The pulsating Reynolds number therefore describes the oscillatory motion applied to the system, while the net flow Reynolds number describes the measurement of the state of flow within the system. Combining both Re and Re_p, all of the parameters of pulsated flow as shown in Figure 2.2.3 can be covered.

Pulsed oscillatory flow can be complicated further by the addition of inserts such as baffles within the tube being studied. In this case, Re and Re_p do not sufficiently characterise the flow involved. To account for the new parameters shown in Figure 2.2.4; the Strouhal number was introduced[78], defined by equation 2.2.3.

$$St_f = fH/u_{peak} \tag{2.2.3}$$

Where H is the half channel width (m) and u_{peak} the peak velocity at the maximum channel width, H_{max}. The physical meaning of the Strouhal number was later defined as the ratio of the channel length scale to the scale of a fluid particle displacement[102].

Research in the late 1980s into generating unsteadiness in a laminar flow[81, 82] found that oscillatory flow around a baffle configuration as shown in Figure 2.2.4

caused the formation of vortex rings downstream of the baffles. On each reversal of the direction of flow, the vortices are swept into the centre of the tube and the cycle of vortex formation, growth and ejection yields a state of chaotic advected mixing in each inter-baffle cavity (the mixing effect is propagated downstream).

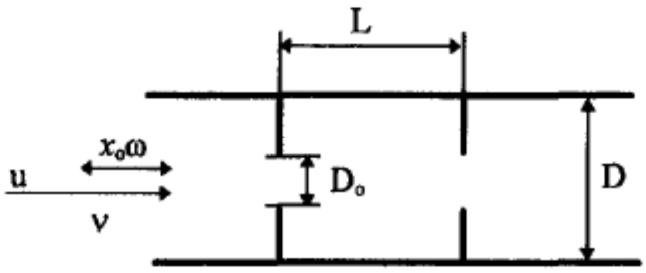

Figure 2.2.4 - Oscillatory baffled flow [99]

Brunold *et al*.[82] proposed the fluid mechanics of oscillatory baffled flow using two dimensionless groups: the oscillatory Reynolds number and the Strouhal number defined by the equations 2.24 and 2.25 below.

$$Re_o = \frac{u_p H_{max}}{v} = \omega x_o D/v \tag{2.2.4}$$

$$St = \frac{\omega H_{max}}{4\pi u_p} = D/4\pi x_o \tag{2.2.5}$$

The Strouhal number was based on the study of vortex shedding in flow around restrictions such as orifices. The von Karman vortex street is an example of how vortices develop behind a cylindrical object in a flowing fluid, shown in Figure 2.2.5.

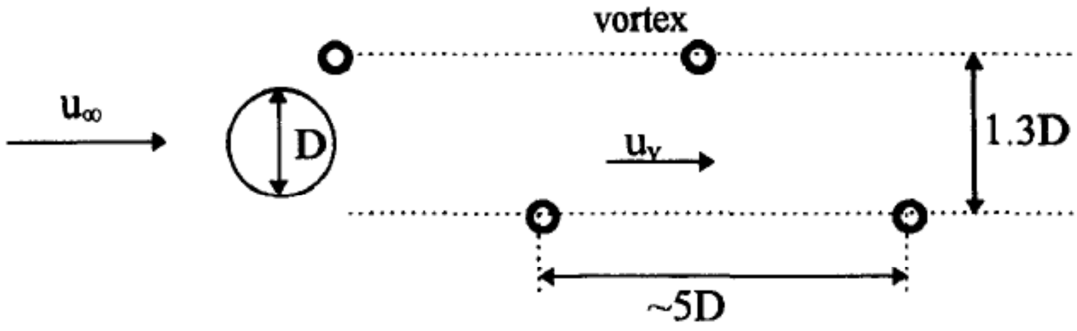

Figure 2.2.5- von Karman Vortex Street [99]

In the above example, the velocity of the vortex street, u_v would be equal to $0.86u_\infty$, the free stream velocity of the liquid[99]. It was suggested by Rouse[103] that

the frequency of vortex shedding could be defined from the Strouhal number as shown in equation 2.2.6.

$$St_v = \frac{f_v D'}{u_\infty} \tag{2.2.6}$$

Where *D'* is the effective width of the obstacle (m) and is the cylinder diameter in the case of a tubular reactor. In transferring the Strouhal number to an OBF application, f_v was replaced by the angular frequency of oscillation. This can only be true for values of ω that are equal to f_v but not close to resonance. Also, the free stream velocity of the liquid can be replaced by the oscillatory velocity in OBF. This makes sense as the oscillatory velocity would be the factor responsible for reciprocal vortices in OBF. One flaw with the Strouhal number above is that D' did not consider the obstacle diameter. This is given as the tube diameter in OBF. Ni and Gough (1997)[99] suggested that the Strouhal number for OBF should consider the orifice diameter instead.

$$St = \frac{\frac{\omega}{\pi} D_o}{x_o \omega} = \frac{D_o}{\pi x_o} \tag{2.2.7}$$

Despite this suggestion, recent publications continue to utilise the original Strouhal number. For this reason, the original number (Equation 2.2.5) will be considered in this work.

In summary, the oscillatory Reynolds number defines the intensity of mixing within a system and the Strouhal number determines the length of eddy propagation, i.e. how effective the system is at generating the mixing vortices. When a through flow is present in the tube, then the original Reynolds number equation is also valid.

2.2.4 - Reactor Geometry

Understanding the geometry of any type of reactor is essential in order to optimize the mixing conditions for a maximum efficiency in terms of heat and mass transfer. The main geometric parameters that govern mixing in an OBR are the baffle type, baffle orifice size, baffle thickness and the baffle spacing. A typical schematic of a set of baffles is shown below in Figure 2.2.6.

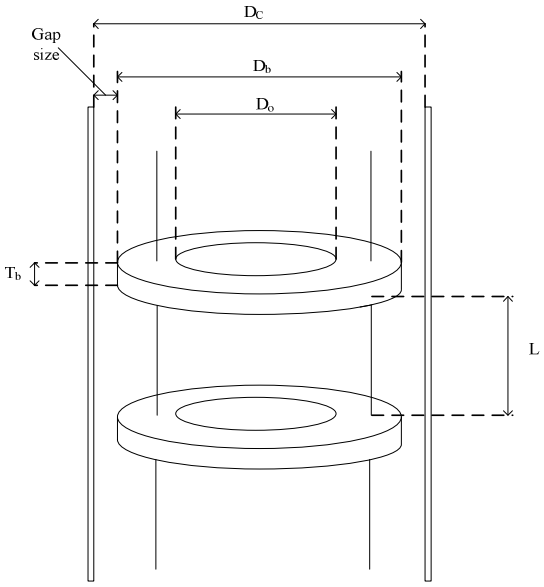

Figure 2.2.6 - Typical baffle schematic

Where T_b is the baffle thickness (m), D_C the column diameter (m), D_b the baffle diameter (m), D_o the orifice diameter (m) and L the baffle spacing (m).

Baffle spacing plays an important role in vortex generation. For instance, if the baffles were spaced very closely together this would result in a scenario where the vortices may never be generated or propagated through the column. When the baffles are spaced infinitely far apart it would result in the eddies being dispersed within the baffled cavity leading to poor mixing or stagnant regions within the OBR.

Zhang *et al*. (1996) suggested that a baffle spacing of 1.5 times the column diameter yielded the optimal mixing conditions for the dispersion of oil-water systems[104]. For mass transfer in an air-water system, Ni and Gao (1996) reported that a spacing of 1.8 times the column diameter was better[85]. Gough *et al*. (1997) studied flow patterns and stated that an optimal mixing was achieved with a baffle spacing of up to two times the column diameter coupled with an oscillation amplitude of one quarter the baffle spacing[105]. Ni *et al*. (1998) performed a thorough investigation into the effects of baffle geometry and concluded that for oscillatory fluid, an optimal mixing was achieved with a baffle spacing of 1.8 column diameters. For the case of oscillating baffles, a spacing of 2 column diameters was the optimal spacing[106]. In these trials, a baffle thickness of 2-3 mm was identified as optimal. This was backed up with research into methylmethacrylate suspensions (Ni *et al*., 1998) where a baffle thickness of 3 mm was identified as yielding the best outcome[107].

The investigation by Ni *et al*. (1998) also probed the effect of the baffle free area ratio. In these trials, a free area ratio of 20-22 % was considered as the optimal value. The baffle free area ratio, α, is defined by:

$$\alpha = \frac{A_2}{A_1} \tag{2.2.8}$$

Where A_2 is the baffle orifice area (m^2) and A_1 the column cross-sectional area (m^2).

Ni and Stevenson (1999) investigated the effect of gap size between the outer diameter of the baffle and the wall of the column on mixing time and reported that the larger the gap size, the longer the system took to reach a state of thorough mixing, the lower the axial dispersion coefficient and the less efficient the OBR becomes[108]. It can be taken for this thesis work that the gap size is negligible, i.e. the baffles used are tight fitted to the vessel.

An investigation by Ni *et al*. (2000) reported the effect of baffle geometry on flow patterns in a much larger vessel than previously reported. For a 0.38 m diameter column, the effect of baffle spacing and orifice diameter on mixing was on the same order of magnitude as seen with a bench scale OBR. This is an interesting conclusion as it reinforces that an OBR can yield a linear scale up[109].

Further to baffle geometry, the baffle type has also been an area of investigation. A number of baffle types have been studied including annular doughnut baffles, disc baffles, a combination of disc and annular baffles[110], as well as helical baffles. Disk baffles were found to yield the poorest mixing but with higher shear forces. Helical baffles yielded better mixing than disk baffles, however, optimal mixing was obtained through the use of annular baffles where the best vortex mixing was seen[15, 93, 94].

2.2.5 - Power consumption

An important factor in the design of any mixing apparatus is an understanding of the power consumption of the device[111]. The power dissipation can be used as a guide for how efficient a mixing method is and as a basis of comparison between two different mixing devices[21].

In order to establish the power consumption in an OBR, two main models can be considered: the quasi-steady flow model and the eddy enhancement model of power density. The former was initially proposed by Jealous and Johnson (1955) who applied

the power density to a pulsed plate column[112]. This idea of a quasi-steady model has since been applied to the OBR as described by Mackley (1991)[113], Mackley and Stonestreet (1994)[84] and Baird and Stonestreet (1995)[114]. The power density (power per unit volume) can be defined by the equation:

$$\frac{P}{V} = \frac{2\rho N}{3\pi C_D^2}\left(\frac{1-\alpha^2}{\alpha^2}\right) x_o^3 \omega^3 \ (Wm^{-3}) \tag{2.2.9}$$

Where ρ is the fluid density (kg m^{-3}), N the number of baffles per unit length of reactor (m^{-1}) and C_D a discharge coefficient for the orifice (normally taken as 0.7[7, 115, 116], although the value will depend on the baffle thickness and α value[117]). α is the baffle free area ratio, defined by the area of the orifice divided by the tube cross-sectional area.

Baird and Stonestreet (1995) suggested that the quasi-steady model was suited for high amplitudes (in the region of 5-30 mm) and low frequencies (order of 0.5 – 2 Hz) oscillation[114, 118].

At higher oscillation frequencies (1 to 6 Hz, Baird and Rama Rao, 1995; 3 to 14 Hz, Baird and Stonestreet, 1995) and lower amplitudes (1 to 5 mm, Baird and Stonestreet, 1995; 1 to 10 mm Baird and Rama Rao, 1995), the quasi-steady model becomes ineffective at describing the power density. Baird and Stonestreet (1995) proposed the eddy enhancement model, which is defined as:

$$\frac{P}{V} = 1.5\frac{\rho\omega^3 x_o^2 l}{L\alpha} \ (Wm^{-3}) \tag{2.2.10}$$

Where l is the mixing length (m), which is in the same order of magnitude as the column diameter. The challenge for this model would be the determination of the mixing length. For this thesis, the oscillation conditions fall into the remit of the quasi-steady model of power density.

Investigations by Ni and Mackley (1993) and Ni *et al*. (2000) suggested that the OBR yielded a much more energy efficient process than seen in a STR[109, 119]. Interestingly, an increase in scale did not call for an increase in power consumption, i.e. the power density remained constant[109].

2.3 - Model Compounds

As mentioned in Chapter 1, a hypothesis for this thesis research is that the mixing observed in an OBC could account for the differences in product properties when compared to a STC. Specifically the requirement of seeding was not necessary in an OBC whereas seeding in an STC was essential. In order to gain some insight into this, the nucleation mechanism must be further exploited since the knowledge of the origin of the nuclei would allow for the realisation of the mechanism through which the nuclei were created. The aim is to differentiate whether or not the nuclei originated directly from a seed crystal or other means and to link each event with the possible mixing mechanisms.

Davey *et al.* (2001) used a retrospective method to probe the molecular self-assembly which occurred during crystal nucleation. By examining the polymorphism of 2,6-Dihydroxybenzoic acid, they discovered a direct link between the crystal polymorphism and the molecular clusters that preceded the nucleation event[120]. This suggests the use of polymorphism as a potential tool for evaluating the nucleation mechanism.

By using a similar approach, Ferrari *et al.*(2003) employed optical microscopy, X-ray diffraction and FTIR analysis to follow the solution mediated transformation of metastable β glycine to the stable α glycine[121]. According to the Ostwald's rule of stages[122], β glycine should be nucleated first, followed by transformation to the α polymorph. Ferrari *et al.* (2003) pointed out that the rate of transformation depended greatly on process conditions such as stirring (they compared a magnetic stirrer to an overhead stirrer), cooling and, of relevance to this work, the nucleation mechanism[121].

In the same paper, Ferrari *et al.* (2003) cited the work of Yokota *et al.* (1999), Garside and Davey (1980), and Doki *et al.* (1999) which described another parameter which influenced the transformation: process scale. Different transformation rates and unexpected polymorphs were seen as scale increased [1, 123, 124]. This would certainly be an interesting phenomenon to investigate in the OBC; however this lies out with the scope of this thesis work.

Towler *et al.* (2004) utilized polymorphism to investigate the influence of pH on the nucleation of glycine. By altering the pH, they found that the introduction of

charged particles “poisoned” the system and inhibited nucleation of α glycine. Instead, the more stable, but less kinetically favourable, γ glycine was observed[125]. Studying the product crystal polymorphism allowed retrospective determination of the possible nucleation mechanism. This again suggests glycine and polymorph analysis as suitable tools to probe nucleation in the OBC where instead of pH, fluid mechanical environment can be altered and the resulting polymorphism recorded.

As well as using polymorphism as a tool to probe the nucleation mechanism, much can also be learned by analysing crystal enantiomorphism. A suitable compound would be the one wherein the solution phase displays no optical activity while the crystalline solid does. The formation of a solid phase can adopt either a left or right handed screw-like configuration. The product crystals can be isolated by filtration and then analysed, the ratio of the left to right handed crystals could then be studied in order to relate to the origin of the nuclei.

There are a number of potential candidates considered as model compounds for this work:

a) 1, 1'-binaphthyl
b) 4, 4'-dimethyl-chalcone
c) Magnesium sulphate
d) Sodium bromate
e) Sodium chlorate

Studies of 1, 1’-binaphthyl crystallization from the melt showed that spontaneous nucleation in non-stirred conditions resulted in a 50-50 split of left to right handed crystals[126, 127]. Kondepudi *et al*. (1999) further evaluated this system and reported that the act of stirring with a Teflon stirrer bar resulted in breaking of chiral symmetry and enantiomeric excess could reach as high as 80 %. The excess handedness was just as likely to be left or right handed as shown by the bimodal probability distribution[128]. However, 1,1’-binaphthyl requires operating temperatures of greater than 158 °C in order to reach a molten state. Analysis of the product crystals must also be performed within 9 hours to prevent interconversion of the enantiomers when the products are dissolved in benzene for analysis[128]. Due to such a complicated analytical procedure, this is not a suitable compound for this study.

A similar scenario applied in solution crystallization of 4, 4' –dimethyl-chalcone, where Penzien and Schmidt (1969) reported that enantiomorphism was observed in the crystal product[129]. Kondepudi *et al*. (2002) again demonstrated that continuous stirring resulted in chiral symmetry breaking[130]. What is interesting about Kondepudi's work is that continued stirring has resulted in enantiomeric excess of a certain handedness of crystal. However, 4, 4'-dimethyl-chalcone presents difficulties in analysis where the product crystals must be reacted with bromine vapour prior to analysis. This is again excluded from this work.

Sodium chlorate is a non-chiral substance, which on crystallization produces crystalline solids that possess either a left or right handed enantiomorphism as shown in Figure 2.1.22[73]. This material is ideal as it crystallizes readily from water, is inexpensive and readily available. Magnesium sulphate and sodium bromate are two similar compounds. Magnesium sulphate would yield mostly left handed crystals if spontaneous nucleation was allowed to occur. The use of seeds, specifically right handed seeds, would alter the ratio of left to right handed crystals[131]. Sodium bromate is readily crystallized from water and when viewed under initially crossed polarisers, the handedness of the material is easily determined[132]. Because of the configuration of the atoms within the $P2_13$ space group, the orientation of the crystal under the polarizer does not affect the direction of which plane polarized light is rotated. This makes analysis straightforward. On balance, sodium chlorate has been chosen for this work because there is a lot benchmark data for comparison, which is one of the essential criteria.

Two such benchmarking studies were reported in 1972 by Denk and Botsaris[46, 47]. In studying the secondary nucleation of sodium chlorate, they reported that a supercooling of 3 °C at 350 RPM stirring yielded a crop of product crystals of 100 % right handedness (unfilled circles) when seeded with a single right handed crystal as indicated below in Figure 2.3.1. The equivalent outcome was seen with a left handed crystal (filled circles). This would indicate that secondary nucleation was dominating, i.e. nucleation was dependent on a seed crystal being introduced to the solution. This also excluded primary nucleation as the cause of product crystals at supercoolings of less than 7 °C. Again from Figure 2.3.1, it can be seen that without seeding and at supercoolings of greater than 7 °C, primary nucleation was observed (filled triangles), a 50:50 mixture of left and right handed product crystals were

observed. This would suggest that if spontaneous, or primary nucleation was occurring, a mixture of both left and right handed crystals would be expected.

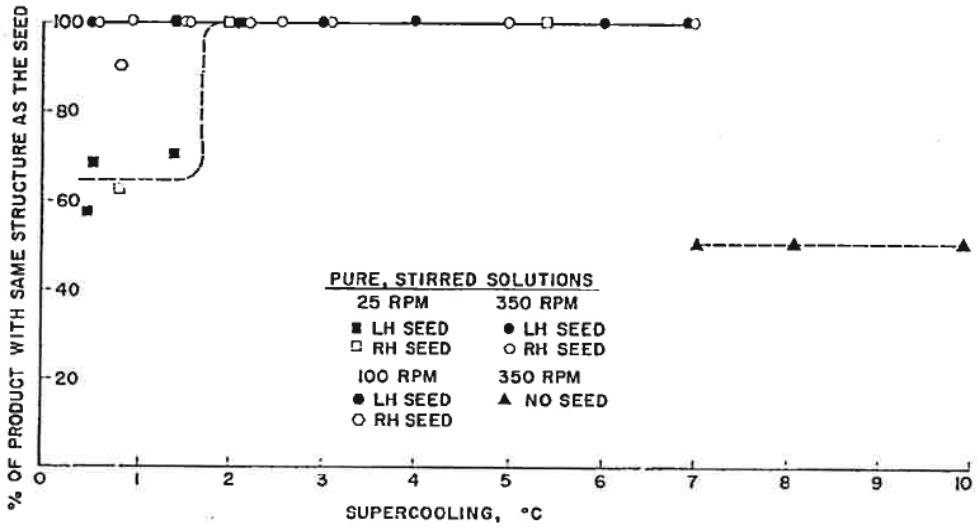

Figure 2.3.1 - Types of product crystals obtained in stirred solutions[46]

Clearly sodium chlorate is such a useful compound in that the ratio of handedness in product crystals is closely linked with nucleation, the fundamental step in crystallization. By performing similar trials in the OBC, it should be possible to gain some insight into the nucleation mechanism when the hydrodynamic environment is changed.

Chapter 3 - Experimental setup and procedures

This chapter describes the setup of experimental apparatus and the procedures of both experimental and analytical methods.

There are three types of batch crystallizer that have been studied: the STC; the OBC I with oscillating baffles; and the OBC II with oscillating fluid. For the STC, both a regular stirrer and the one that scrapes the vessel wall are employed. For the OBC I both tight and loose fitting baffles are investigated. This gives five crystallizer configurations to be examined.

3.1 - The stirred tank crystallizer – Un-scraped (STC I)

Figure 3.1 shows the setup of the STC I. The STC I consisted of a jacketed round bottom glass vessel with a volume of 500 mL. A PTFE anchor type stirrer on a PTFE coated stainless steel shaft was driven by the motor and the stirrer was 70 mm in diameter, 15 mm in width, with a clearance of around 10 mm from the vessel floor. With a volume of 500 mL, the height of the liquid in the vessel is approximately 80 mm. The rotation was adjustable from 50 to around 2000 RPM. For the STC, the surface area to volume ratio was calculated to be approximately equal to 71.25.

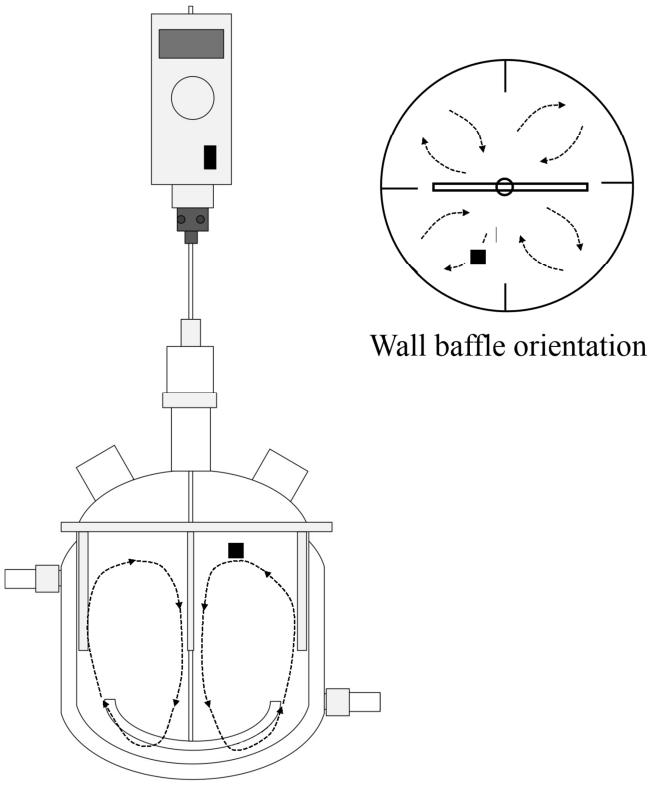

Figure 3.1 - Image of the STC I setup (not to scale). The approximate flow patterns are indicated by the dotted lines and the seed position for the seeded experimental work is indicated by the black square

The power density of a stirred tank crystallizer is defined by[133]:

$$\frac{P}{V} = \frac{P_O \rho {N_S}^3 D_S^5}{V_L} \quad (Wm^3) \tag{3.1}$$

Where *P/V* is the power density (W m^{-3}), ρ the fluid density (1456 kg m^{-3} at 40 °C[134]), N_s the speed of the stirrer (rps), D_S the diameter of the stirrer (0.07m), V_L the volume of liquid in the STC (0.0005m^3) and P_O the dimensionless power number of the agitator which was estimated at 1 based on data from Nagata (1975) [111].

For this STC, the power density can be approximated by the equation:

$$\frac{P}{V} = 13.2 N_S^3 \tag{3.2}$$

For the STCs considered in this work, the shear rate can be determined using the equation[135]:

$$\dot{\gamma} = K_S N_S \tag{3.3}$$

Where $\dot{\gamma}$ is the fluid shear rate (s^{-1}) and K_S is a constant related to the stirrer geometry. In this work, K_S can be assumed to be equal to 3.2 [136].

3.2 - The stirred tank crystallizer – Scraped (STC II)

The scraped STC utilised the same apparatus as that in the un-scraped STC. In order to achieve scraping in the system, the anchor impeller was simply lowered to rub against the floor of the glass vessel as indicated in Figure 3.2 below.

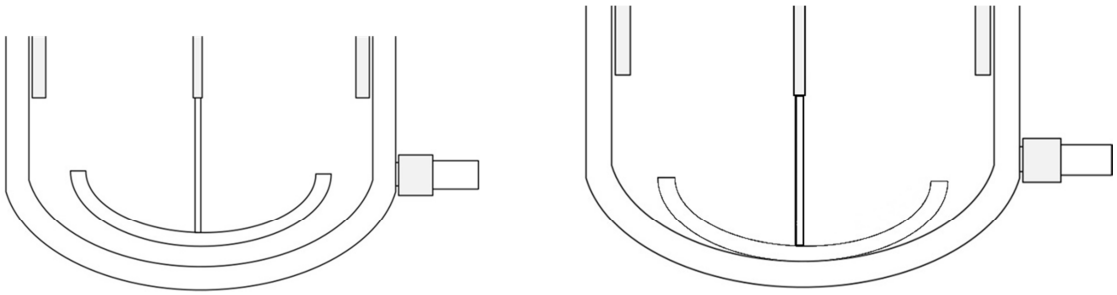

Figure 3.2 – Schematic setup of the STC II (not to scale). The non-scraping impeller (left) is lowered to touch the bottom of the crystallizer (right) in order to achieve scraping. The seed location is the same as in the previous STC

For this STC, the power density can be approximated by the equation:

$$\frac{P}{V} = 9.54N_S^3 \tag{3.6}$$

3.3 - The oscillatory baffled crystallizer – tight fit baffles (OBC I)

Figure 3.3 shows the setup of the OBC I. The OBC I consisted of a jacketed glass column of an internal diameter 50 mm and a height of approximately 500 mm. This allowed a working volume of 500 mL. The vessel was held in position by a stainless steel flange. The baffles were oscillated in the vessel by means of a linear motor (Copley Controls Corp.), which was held by an aluminium/plastic frame above the OBC. Frequencies of 0-10 Hz and amplitudes of 0-50 mm were possible. The baffle string comprised of 4 PTFE baffles with an outer diameter of 48 mm, an orifice diameter of 24 mm and a thickness of 3 mm. The baffles were spaced at 65 mm by stainless steel spacers. For the scraped OBC described here, the surface to volume ratio was found to be approximately 127.38.

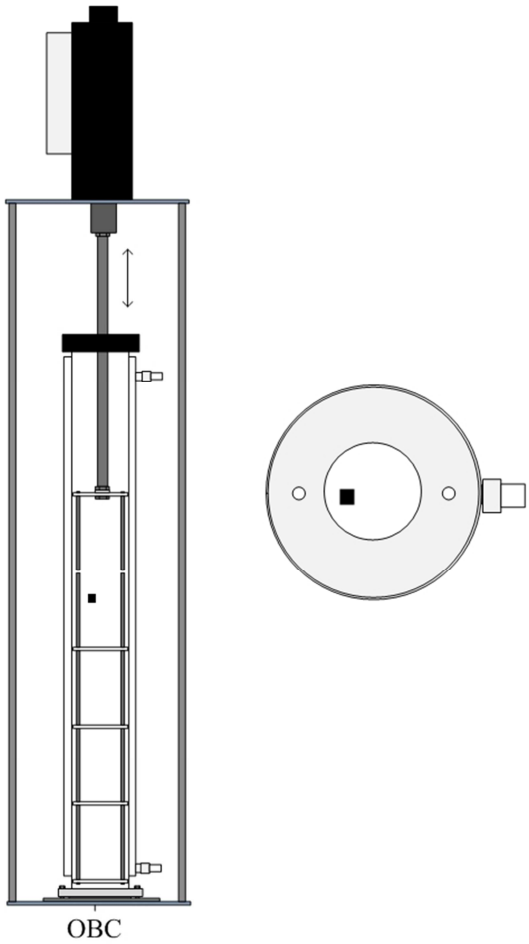

Figure 3.3 - Schematic of the OBC I setup (not to scale). The seed location is indicated by the filled square in the side and top views to the left and right hand side of the Figure respectively. For clarity, the flow pattern has been omitted, however this can be seen clearly in Figure 2.2.1

The power density of the OBC is estimated using the quasi steady flow model proposed by Baird and Stonestreet (1995)[114]:

$$\frac{P}{V} = \frac{2\rho N_b}{3\pi C_D^2}\left(\frac{1-\alpha^2}{\alpha^2}\right) x_o^3 (2\pi f)^3 \qquad (3.7)$$

Where N_b the number of baffles per unit length of OBC (15.38 m^{-1}), C_D the discharge coefficient of the baffles (taken as 0.7), x_o the centre to peak amplitude of oscillation (this is fixed at 0.0016 m throughout the investigation), f the oscillation frequency (Hz) and α the baffle free area ratio (0.23 for this OBC). The free area ratio, α is defined by the area of the orifice divided by the tube cross-sectional area.

For this OBC, the power density can then be approximated by:

$$\frac{P}{V} = 187f^3 \tag{3.8}$$

For an OBC, the shear (strain) rate is given by the change of oscillatory velocity ($x_o f$) at the gap according to:

$$\dot{\gamma} = \frac{x_o f}{D} \tag{3.9}$$

Where $\dot{\gamma}$ is the fluid shear rate (s^{-1}) and D is the baffle diameter (m) [137].

3.4 - The Oscillatory baffled crystallizer – with baffle gap (OBC II)

Figure 3.4 shows the schematic setup of the OBC II. The OBC II utilised the same setup as the OBC I, but the baffle diameter was reduced to remove the scraping action seen with the previous vessel configuration. The baffles were 37 mm diameter and had α = 0.87. Baffles were spaced 65 mm apart (N_b = 15.38 m^{-1}). For the OBC with baffle gap described here, the surface area to volume ratio was found to be 117.88.

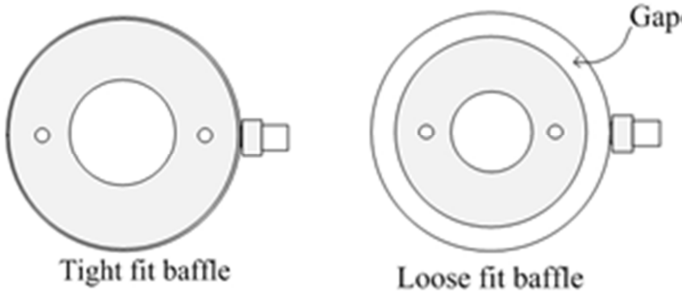

Figure 3.4 – The difference in baffle diameter between the OBCI and OBCII. For each crystallizer configuration, the seed location is identical

For this OBC, the power density can be estimated from:

$$\frac{P}{V} = 2.2f^3 \tag{3.6}$$

3.5 - The Oscillatory baffled crystallizer – Moving fluid (OBC III)

The setup of OBC III is given in Figure 3.5. Again, the OBC III consisted of a jacketed glass column of 40 mm diameter. The PTFE baffles had an outer diameter of 37 mm,

an internal diameter of 17 mm (α= 0.21) and a thickness of 3 mm. The baffles were spaced at 65 mm by stainless steel spacers (N_b = 15.38 m^{-1}) and remained stationary during operation. A rotary motor drove a bellows unit at the base of the column; the speed of the motor controlled the frequency of oscillation, and the amplitude could be adjusted by altering the cam position on the motor. A nitrile rubber sheath was sandwiched between the PTFE bellows and the jacketed column. For the moving fluid OBC, a surface to volume ratio of 136.47 was calculated.

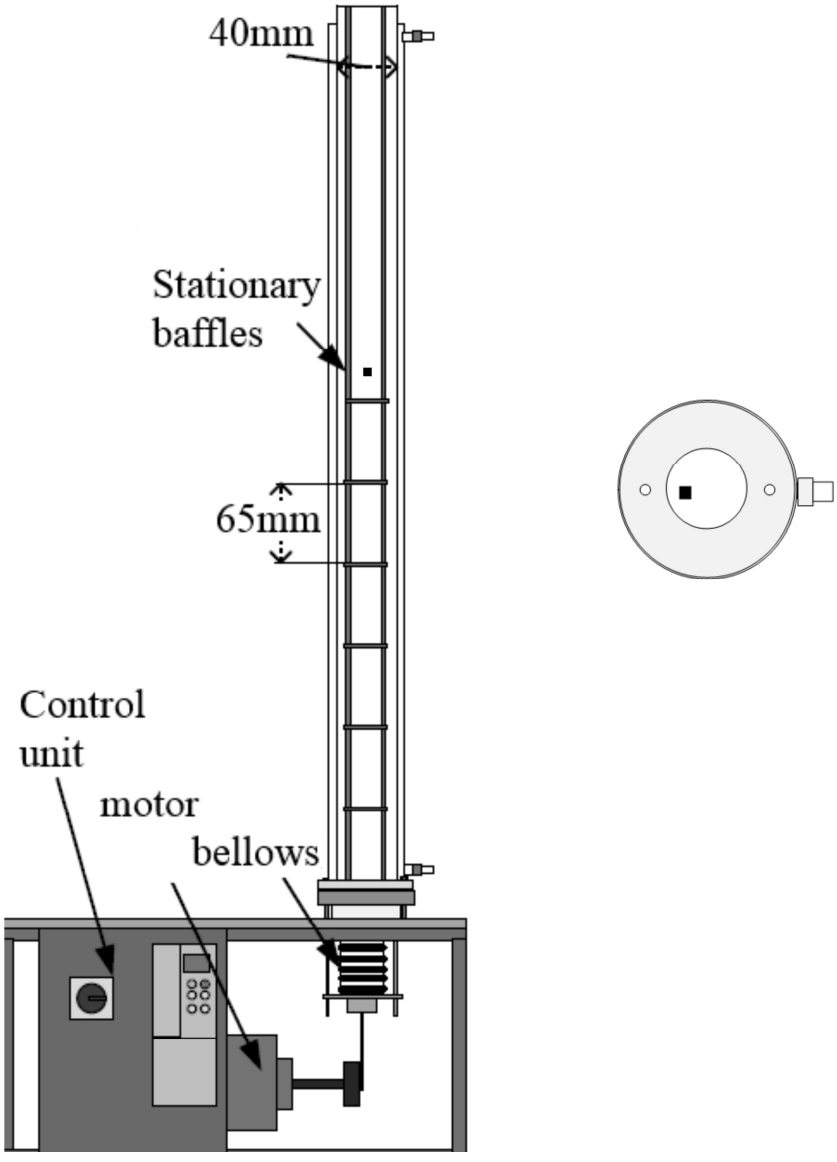

Figure 3.5 - Schematic of the moving fluid OBC setup (not to scale, dimensions given in mm). As with the previous schematics, the seed location is indicated here by the filled black square. Similarly to the moving baffle OBC, the flow pattern can be seen in Figure 2.2.1

By setting the operating amplitude of 0.0075 m, the power density of this OBC can be estimated from:

$$\frac{P}{V} = 175.6f^3$$

3.6 - Measurement tools

Heating and chilling were provided to the crystallizers by the use of a Grant GP200R2 heater/chiller. The jacket fluid was water. Temperature was monitored by using stainless steel T-Type thermocouples and a 4 channel temperature display.

For the primary nucleation work, the temperature and the solution turbidity was measured using a HEL Crystaleyes turbidity system, consisting of a stainless steel PT100 temperature probe and stainless steel turbidity probe fitted with a hastelloy mirror. The probes were connected to a control box, which was interfaced to a PC for the collection of raw data. The turbidity system allows for a real time monitoring and data logging during the course of a cooling crystallization and yields a typical graph of turbidity and temperature vs. time as illustrated in Figure 3.6 below:

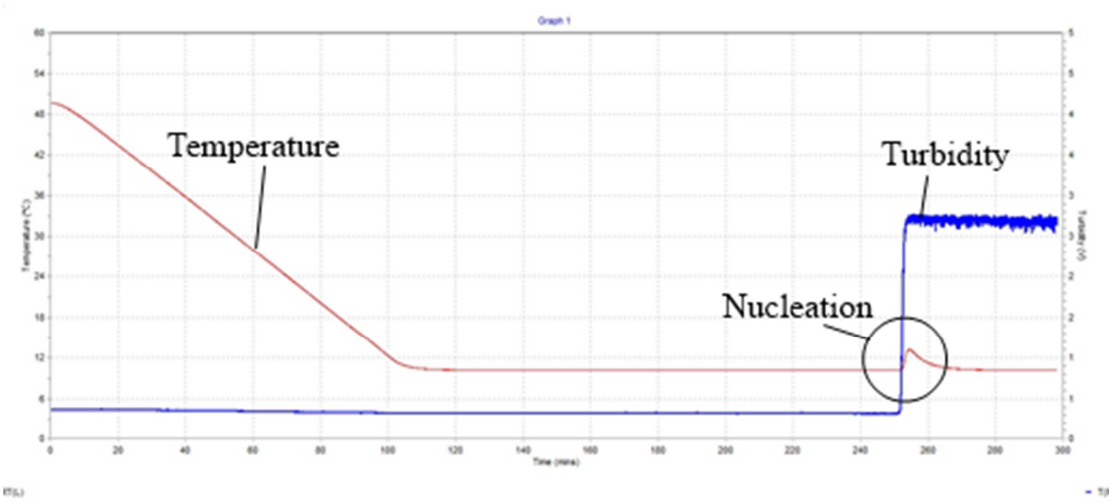

Figure 3.6 – Turbidity (blue line) and temperature (red line) vs. time as displayed on the interface screen on the HEL Crystaleyes turbidity system. The onset of nucleation is evident by an increase in both solution turbidity and temperature

From the example in Figure 3.6 above, the nucleation point is clearly visible on the trend lines, where a clear spike in both temperature and turbidity can be seen. Using this indication of the onset of nucleation would allow the determination of the

metastable zone width and in turn the nucleation kinetics of a given process to be determined.

Further to the turbidity system, the primary nucleation experiments were also monitored by FTIR spectrophotometry. The solute concentration was measured in each device using a Shimadzu IR-Prestige 21 via a probe inserted into the crystallizing solution during the experiment. The detector system was cooled with liquid nitrogen. For sodium chlorate, the spectrum shown in Figure 3.7 was collected, and the peak of particular interest in this case lies between 850 and 1100 cm^{-1}. The height of this peak, in terms of absorbance, was recorded with time and can be considered as being directly proportional to the solute concentration. It is important to note that, due to time constraints, the device was used un-calibrated as a general guide to any change in the solute concentration with time in both the STC and OBC. Prior to each experiment, the air background was subtracted from the sample spectrum via the built in function of the Shimadzu FTIR software.

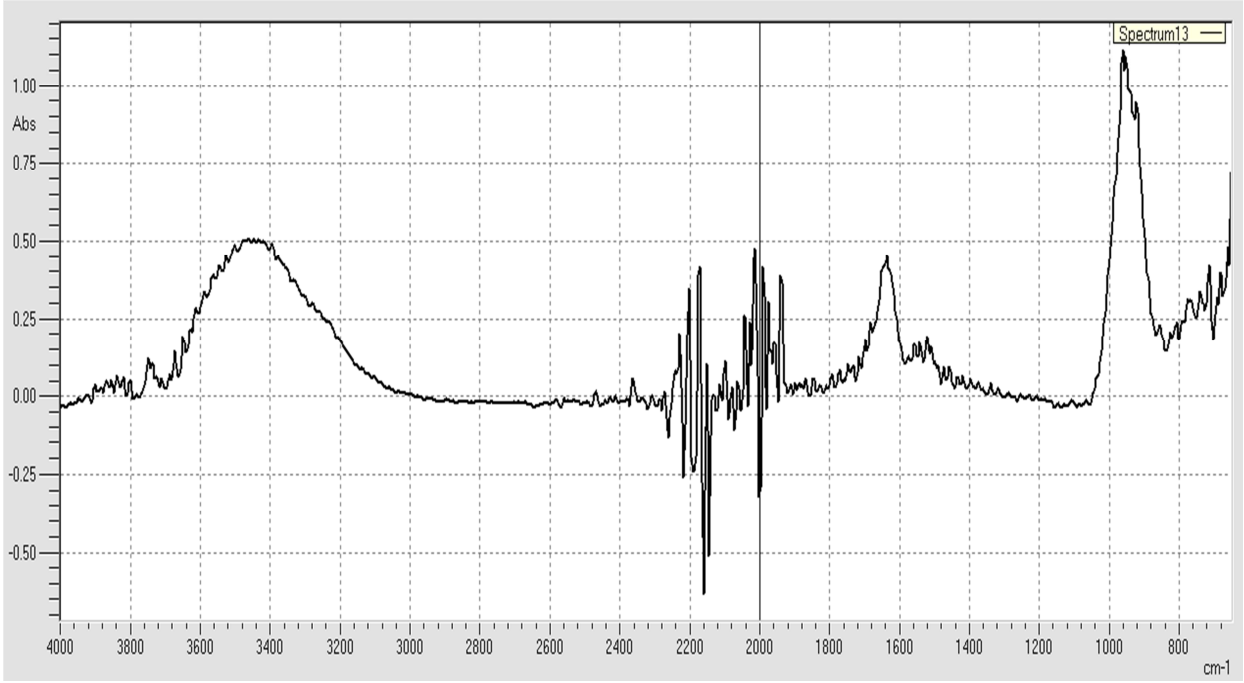

Figure 3.7 – The FTIR trace for sodium chlorate

Polarimetry was used to determine the handedness of the product crystals as shown in Figure 3.8.

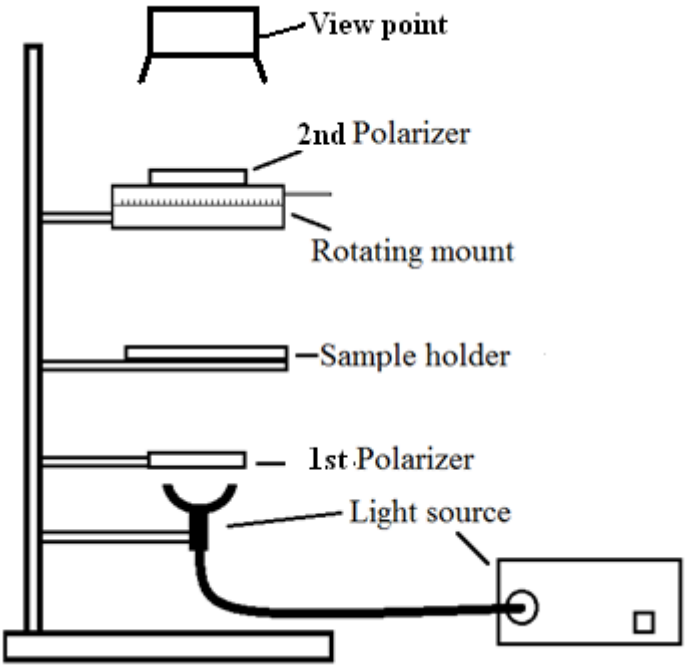

Figure 3.8 - Schematic setup of polarimeter

The light source was powered on and the second polarizer rotated such that the indicator on the mount was indicating a rotation of 0° when minimum light was detectable at the view point. This corresponded to the polarizers being crossed. The crystals to be analysed were placed on the slide and held above the first polarizer. All of the crystals appeared a transparent, pale blue colour. Rotating the second polarizer clockwise revealed the right handed crystals as dark blue/orange coloured whilst the left handed crystals remained pale blue. The left and right handed crystals can then be separated into separate beakers for weighing. This setup was used in all of the experimental work performed.

One problem found with the original setup was that the light source was too small, resulting in a very small bright circle of light and affecting the analysis. In order to remedy this, a LED array was constructed, with nine white LEDs soldered in parallel onto a copper strip board. This proved to be effective.

3.7 - Reagents

The laboratory grade sodium chlorate used for the experiments was sourced from Fisher Scientific UK (99+ % purity). This is termed as the fresh material in the later discussions. For some experiments, recycled sodium chlorate from previous mother liquors was also used. To obtain the recycled material, the mother liquor of the seeded

trials was collected and evaporated to increase the concentration of sodium chlorate in the solution; the concentrated solution was then cooled, filtered and dried to give what is referred to as "the recycled starting material" in the later sections. Recycling mother liquor has become a common technique for not only meeting "green chemistry" requirements, but also achieving the maximum possible yield from a crystallization process[138]. Distilled water was used in all experiments, which had been filtered using a Whatman glass fibre filter (Grade GF/C, nominal pore size 1.2 µm). By using data from Denk's thesis[134] (taken from solubility data published by Seidell[139]), the mass of sodium chlorate required to prepare saturated solutions at our operating conditions are shown in Table 3.1. Note that the solubility data was also verified experimentally and detailed in Chapter 4.

Table 3.1 - Supersaturation values from Denk/Seidell[134, 139]

T_{SAT} (°C)	C (g $NaClO_3$/100 mL sat. sol.)	ρ (kg m^{-3})	Mass $NaClO_3$ (g)	Volume H_2O (mL)
31	73.79	1435	369	349

In some of the later research, a second method of material recycling was employed. Mother liquor from the previous trials was placed in a rotary evaporator and all of the water removed. The resulting dry powder should have a similar purity profile to the original starting material as no mother liquor remained to be filtered from the solids. Appendix D shows the qualitative analysis of the three types of starting material.

3.8 - Seeds

Seeds were prepared by naturally cooling a quiescent sodium chlorate solution in a 250 mL conical flask. Sodium chlorate and water was mixed in the sealed flask which was immersed in a water bath at 30 °C. Once the material had dissolved, the flask was removed and allowed to cool to room temperature. After leaving the solution overnight, the crystals were extracted by filtration using a Buchner funnel and filter paper (Whatman Grade 1). The crystals were immediately washed with 20 mL of cold water to remove any traces of mother liquor and then dried between filter papers. These were the seed crystals used for these trials.

The handedness of the seed crystals were determined by polarimetry prior to experiments. An example is depicted in Figure 3.9; when the polarizers were initially

crossed, all of the dried crystals are transparent with pale blue colour (Figure 3.9a). Rotating the second polarizer clockwise revealed the right handed (dextrorotatory) crystals as dark blue (Figure 3.9b), with further rotation the crystals became orange (Figure 3.9c). The left handed (levorotatory) crystals remained pale blue.

Figure 3.9 - Determination of seed handedness a) initially crossed polarizers b) second polarizer rotated clockwise c) further rotating second polarizer clockwise

3.9 - Experimental procedure

The trials are conducted at a constant set of process conditions, such as supersaturation, concentration, cooling, etc. while only varying the mixing mechanism. This would allow comparison between the two types of crystallizer and gain some insights as to why seeding was not required in the OBC.

For this research work, both seeded and non-seeded crystallization of sodium are investigated. The general experimental procedure involved weighing out the required amounts of reagent within each crystallizer (values in Table 3.1). The solution was cured at either 40 °C (for seeded experiments) or 50 °C (for non-seeded experiments) for one hour under the experimental agitation conditions to ensure that all solid particles had dissolved. After dissolution, the solution was filtered using a Whatman glass fibre filter to remove any foreign particles. The solution was then cooled to the required supersaturation under controlled conditions. For the seeded crystallization experiments, the solution was cooled at a rate of 1 °C/minute until the solution was at the seeding temperature of 30 °C. For the primary nucleation experiments, four cooling rates of 0.4, 0.2, 0.1, and 0.04 °C/minute were investigated. Details of this will be given in Chapter 9.

In experiments where seeding was implemented, a single seed crystal of known handedness was washed with cold distilled water before being suspended in the crystallizing solution by means of a wire for three minutes. The seed crystal was then

removed from the solution and the agitation stopped to allow the product crystals to grow overnight to form larger crystals (this aids in analysis and counting). In the experiments where no agitation was applied, the agitation was stopped prior to seeding. Product crystals were collected and quickly washed with 20 mL of cold HPLC grade water and dried on filter paper. Analysis of the crystals was performed using the polarimeter described in Figure 3.8. The left and right handed crystals were then separated and weighed. Each experiment was repeated a further two times in order to determine the margin of error within the data. The apparatus was thoroughly cleaned between trials using detergent and three rinses of hot water at around 60 °C.

Experimental data, i.e. the similarity to the seed crystal for the seeded trials or the enantiomeric excess for the primary nucleation trials, are recorded using Microsoft Excel. Statistical analysis of the data was performed in MatLab using the Kruskal-Wallis test. Analysis of the data using either Student's T-test or a 2-way analysis of variance (ANOVA) method was considered but rejected due to the requirement of a normal distribution of data, while the results could exhibit either 0 and 100 % similarity to the seed crystal. The Kruskal-Wallis test removes the need for the data to be normally distributed and provides a valid method of statistical analysis. It returns a probability (P value) of the difference between two or more data sets occurring by chance. A low P value would indicate a low probability of the results being due to chance. In this work, a P value of less than 0.05 is considered as being indicative of a statistically significant difference between two sets of data. A value of P greater than 0.05 does not necessarily indicate that two data sets are the same, but it is unlikely that the difference between two sets of data would be significant.

Chapter 4 – Experimental preparation

Prior to a thorough experimental programme being undertaken, a number of important experimental calibration and preparations were conducted, including establishment of operational protocols and verification of the existing solubility data. As seen in Chapter 2, solute solubility is one of the most important parameters to consider when investigating crystallization. Confidence that the crystallizer is being operated with the correct solute concentration is critical, ensuring the correct solute concentration for the seed and minimizing any errors during experiments.

4.1 – Solubility of sodium chlorate

Verification of the solubility of sodium chlorate was performed in the laboratory and compared to existing literature data [39, 134]. Solutions were made up with a fixed mass of water, 300 g, at 10, 20, 30, 40 and 50 °C respectively. Excess amounts of sodium chlorate (based on literature data) were added to each vessel and the systems sealed to prevent any evaporation of water. The solutions were agitated overnight at a fixed temperature. The solutions were filtered through a Whatman Grade 1 filter paper and any remaining sodium chlorate collected and weighed. The sodium chlorate was initially air dried on the filter paper, before being oven dried overnight. The mass of sodium chlorate undissolved in the solution was recorded after loss on drying ceased.

The solubility test was repeated, giving four sets of solubility data as shown in Table 4.1. It can be seen that the obtained solubility data match well with the literature values at all temperatures. The solubility of sodium chlorate is now verified.

Table 4.1 – The concentration of sodium chlorate (gNaClO3/gH2O) at certain temperatures.

Temperature	Callahan1	Callahan2	Denk [134]	Chen [39]
10	0.887	0.846	0.88	0.85
20	0.9645	0.93	0.96	0.94
30	1.0545	1	1.05	1.03
40	1.0885	1.091	1.15	1.12
50	1.18	1.179	1.25	1.21

The data from Table 4.2 was amalgamated and plotted in MatLab. The best fit model was determined to be a linear plot as shown by the dark red line in Figure 4.1. The degree of uncertainty in the data at a 95 % confidence level was also computed within MatLab. The pale pink lines running parallel to the dark red line indicate the uncertainty in the solution concentration at each temperature.

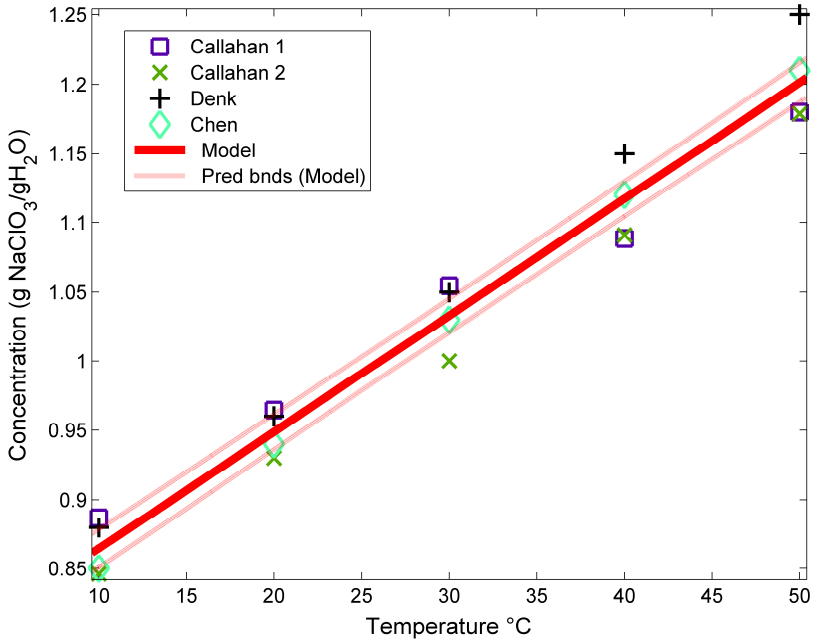

Figure 4.1 – The plot of sodium chlorate concentration vs. temperature from four sets of experimental data. The red line indicates the model used in this investigation and the pink lines indicate the error, or uncertainty of the solute concentration, and subsequent supersaturation.

Linear model Polynomial:

f(x) = p1*x + p2

Coefficients (with 95% confidence bounds):

p1 = 0.008417 (0.008068, 0.008767)

p2 = 0.7805 (0.7689, 0.7921)

Goodness of fit:

R-square: 0.9995; RMSE: 0.003476

Based on the plot of the data in Figure 4.1, the solubility of sodium chlorate in water can be defined by the equation:

$$c = 0.008417\,T + 0.7805 \tag{4.1}$$

For example, a solution saturated at 40 °C would have a concentration of 1.117 g/g. Based on the root mean square error, the concentration would have an uncertainty of ± 0.003476 g/g, or ± 0.31 %. This equation is used throughout this work and based on the confidence level of 95 %, will give an acceptable trust in the values of supersaturation determined later.

4.2 – Experimental problems and solutions

In order to determine the suitability of the experimental procedure for this investigation, two experiments were performed, one in the OBC and one in the STC as outlined in Chapter 3. A single crystal of a known handedness was used as the seed as described earlier. Both crystallizers were operated under similar power density conditions and with identical solutions. The experiment was repeated three times in each vessel to ensure the reproducibility of the results and the robustness of the procedure. For the STC, the experiment seemed to behave as expected, with the product crystals having the same handedness as the seed as shown in Table 4.2 below.

Table 4.2 – The mass of the left and right handed sodium chlorate crystals obtained from the initial STC experiments at a stirrer speed of 57 RPM. The power dissipation is approximately 12 Wm^{-3} and the shear rate is around 3 s^{-1}

Seed type	Trial	Mass right (g)	Mass left (g)	Total mass (g)	Percentage of products with same handedness as seed (%)
Right	1	8.9	0	8.9	100
	2	1.4	0	1.4	100
	3	4.3	0	4.3	100

The mass of the crystals obtained is to be expected based on the supercooling used (1 °C). It is interesting to note that all of the crystals were of the same enantiomorphism as the seed crystal, perhaps giving an indication as to the nucleation mechanism present in the STC. It would seem that all of the product crystals are generated directly from the seed crystal. This could be due to dendrite growth, followed by breakage on the seed crystal.

The same experiment was performed with the OBC and the results were presented in Table 4.3. There are two notable features here: the mass and the percentage similarity to the seed are different from those in the STC (Table 4.2 above).

Table 4.3 – The mass of the left and right handed sodium chlorate crystals obtained from the initial OBC experiments at a frequency of 0.4 Hz and an amplitude of 30 mm. The power dissipation is approximately 12 Wm^{-3} and the shear rate is roughly 0.25 s^{-1}

Seed type	Trial	Mass right (g)	Mass left (g)	Total mass (g)	Percentage of products with same handedness as seed (%)
Right	1	22.5	3.0	25.5	88
	2	28.2	1.4	29.6	95
	3	30.4	1.5	31.9	95

Contrary to the STC data in Table 4.2, the masses of crystals obtained in Table 4.3 are some 10 times greater than the expected mass based on the supersaturation of the solution at the time of seeding. This was identified due to the bottom section of the OBC being unjacketed. This could effectively act as a cold spot, where after leaving the vessel overnight to allow crystal growth, the jacket temperature was held at 30 °C but the cold spot was recorded at 23 °C. This 7 degrees difference corresponds to a supercooling of 8 °C. It is important to note that as soon as the seeding process had finished; agitation was stopped, essentially yielding a stagnant solution. According to data presented by Denk and Botsaris (1972) [46], no spontaneous nucleation was seen at 8 °C supercooling. This phenomenon was not observed until 10 °C supercooling as indicated by the triangles in Figure 4.2 below.

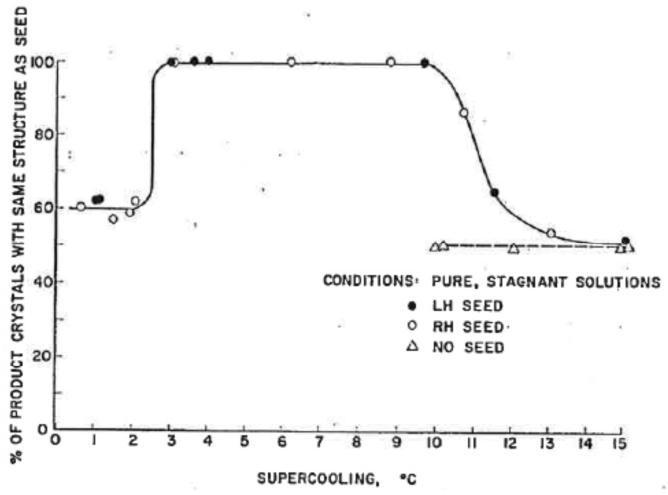

Figure 4.2 – Types of product crystals obtained in pure, stagnant solutions [46]

It became apparent that after agitation has stopped, the nuclei sank to the bottom of the OBC. The increased yield in the OBC was the direct result of the decrease in temperature in the cold spot.

When the bottom of the OBC was immersed in a water bath at 30 °C overnight (Figure 4.3), the crystal mass from the experiments were within the expected range (Table 4.4).

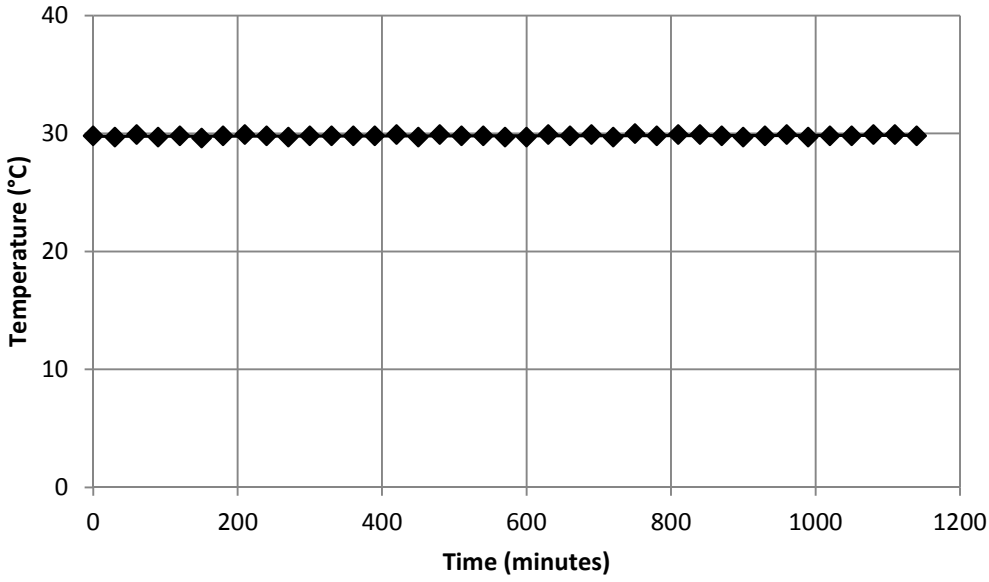

Figure 4.3 – Temperature of cold spot during growth period for a partially immersed OBC

Table 4.4 – The mass of the left and right handed sodium chlorate crystals obtained from the immersed OBC experiments at a frequency of 0.4 Hz and an amplitude of 30 mm

Seed type	Trial	Mass right (g)	Mass left (g)	Total mass (g)	Percentage of products with same handedness as seed (%)
Right	1	8.1	0.6	8.7	93.10
	2	5.4	0.4	5.8	93.10
	3	2.6	0.1	2.7	96.30

The important note here is that the percentage similarity to the seed crystal remains largely unchanged with and without the cold spot present in the system. This confirms that the cold spot only influenced crystal growth, and therefore product yield,

and had no impact on the product crystal handedness or nucleation mechanism. More tests were undertaken in the STC as shown in Tables 4.5 and 4.6.

Table 4.5 – The mass of the left and right handed sodium chlorate crystals obtained from the STC trials at a stirring speed of 160 RPM, corresponding to a power dissipation of approximately 180 Wm^{-3} and a shear rate of about 8.5 s^{-1}

Seed type	Trial	Mass right (g)	Mass left (g)	Total mass (g)	Percentage of products with same handedness as seed (%)
Left	1	0.762	9.427	10.189	92.5
	2	0.627	10.956	11.583	94.8
	3	0.107	10.196	10.303	99.0

Average similarity – 95.53 % S.D. – 2.53

Table 4.6 – The mass of the left and right handed sodium chlorate crystals obtained from the STC trials at a stirring speed of 260 RPM, corresponding to a power dissipation of approximately 776 Wm^{-3} and a shear rate of around 13.8 s^{-1}

Seed type	Trial	Mass right (g)	Mass left (g)	Total mass (g)	Percentage of products with same handedness as seed (%)
Left	1	0.063	4.58	4.643	98.6
	2	0.591	7.848	8.439	93.0
	3	2.247	5.777	8.024	72.0

Average similarity – 92.02 % S.D – 10.81

The initial results suggest that a higher mixing rate reduces the similarity of the product crystals to the seed crystal. Furthermore there is a marked increase in the standard deviation at higher mixing. This was found to be caused by the vortex in the STC when no baffles were present as shown in Figure 4.4.

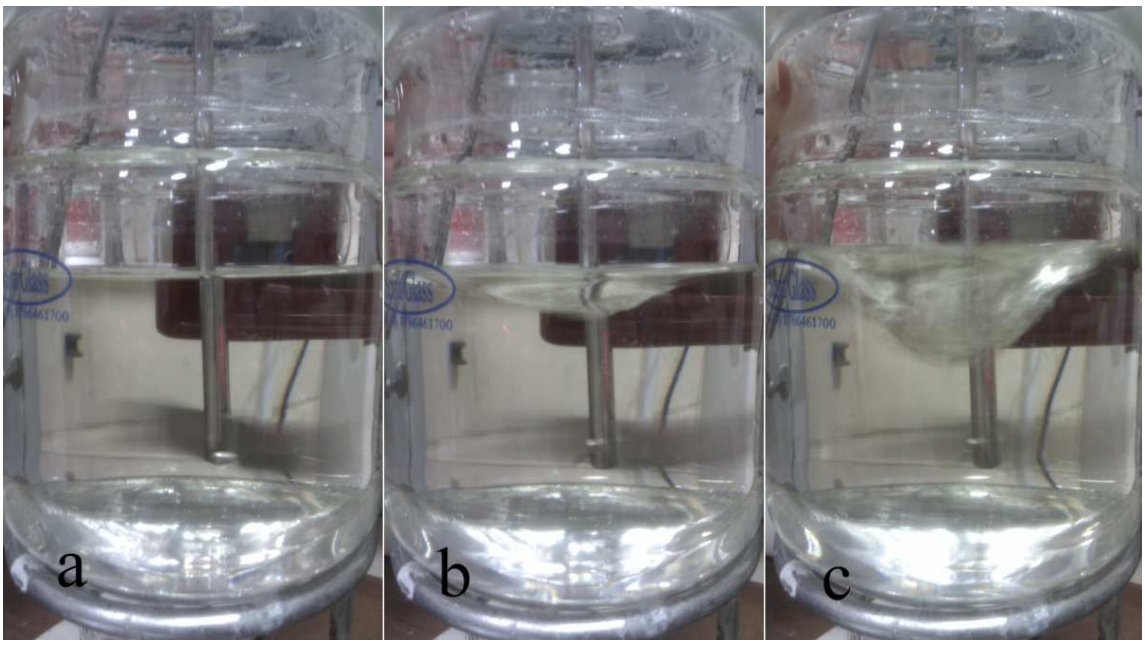

Figure 4.4 – Vortexing in the STC at 58 RPM (a), 145 RPM (b) and 232 RPM (c)

When baffles were placed in the STC [140], the vortexing was drastically improved as shown in Figure 4.5 and consistent data were then obtained (Tables 4.7 and 4.8).

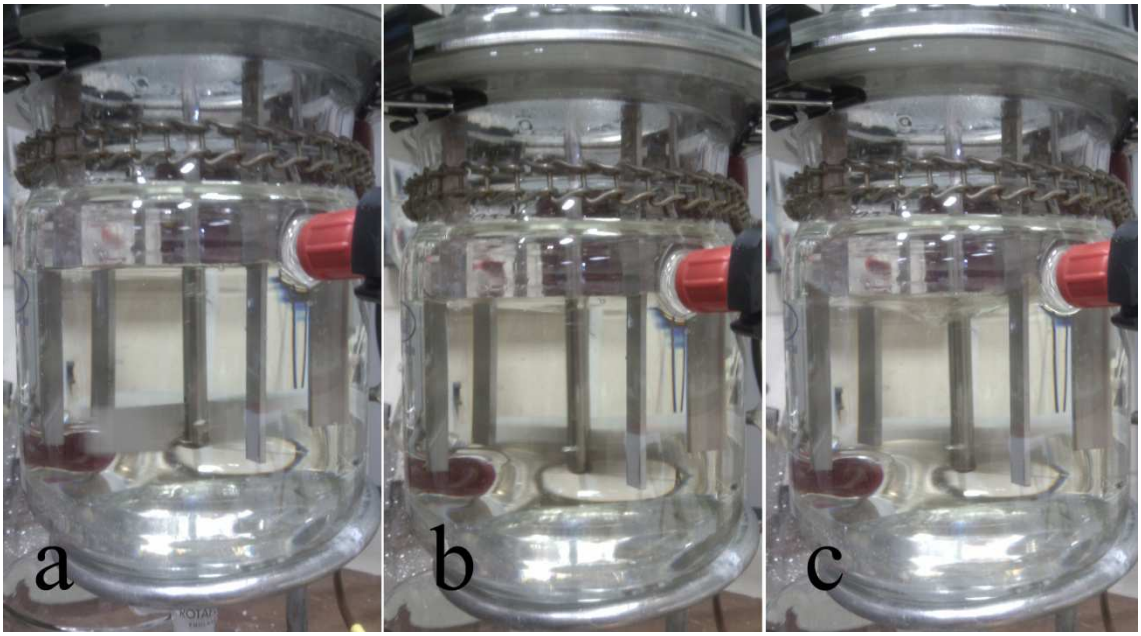

Figure 4.5 – Vortexing in the baffled STC at 58 RPM (a), 145 RPM (b) and 232 RPM (c)

Table 4.7 – The mass of the left and right handed sodium chlorate crystals obtained from the STC trials at a stirring speed of 160 RPM, corresponding to a power dissipation of approximately 180 Wm^{-3}. The shear rate was roughly 8.5 s^{-1}

Seed type	Trial	Mass right (g)	Mass left (g)	Total mass (g)	Percentage of products with same handedness as seed (%)
Left	1	0	7.817	7.817	100
	2	0	0.398	0.398	100
	3	0	9.866	9.866	100

Average similarity – 100 % S.D. – 0

Table 4.8 – The mass of the left and right handed sodium chlorate crystals obtained from the STC fitted with baffles at a stirring speed of 260 RPM, corresponding to a power dissipation of approximately 776 Wm^{-3}. The shear rate was roughly 13.8 s^{-1}

Seed type	Trial	Mass right (g)	Mass left (g)	Total mass (g)	Percentage of products with same handedness as seed (%)
Left	1	0	6.465	6.465	100
	2	0	8.366	8.366	100
	3	0	10.316	10.316	100

Average similarity – 100 % S.D. - 0

4.3 – Conclusions

In this chapter, the experimental setup and procedure was tested to ensure consistent temperature and fluid mechanical conditions in each apparatus as well as highly reproducible data and robust experimental procedures.

Chapter 5 – Influence of crystallizer type on nucleation mechanism

This chapter presents the results and discussion of the effect of crystallizer type on the nucleation mechanism. The content of this Chapter is largely based on the Publication 1 from the author's list given at the start of the thesis.

5.1 - Introduction

Two relevant investigations into nucleation mechanism were reported in 1972 by Denk and Botsaris[46, 47], where at a supercooling of 3 °C and 350 RPM stirring, a crop of product crystals had 100 % right handedness when seeded with a single right handed crystal (unfilled circles in Figure 2.3.1). The equivalent outcome was reported for seeding with a left handed crystal. This would indicate that secondary nucleation took place due to either dendrite coarsening or collision breeding within the crystallizer, i.e. the entire product crystals originated directly from the seed crystal. Again from Figure 2.3.1, it can be seen that without seeding and at higher supercoolings of greater than 7 °C, primary nucleation was observed. This was shown from a mixture of 50:50 left and right handed product crystals obtained (filled triangles in Figure 2.3.1). This would suggest that if spontaneous nucleation was occurring, a mixture of both left and right handed crystals would be the evidence. This outcome was also supported by Martin *et al.* (1996)[141].

Qian and Botsaris (1997)[48] cited the work of Sung (1973)[54], which suggested that fluid shear had an effect on the production of secondary nuclei. This phenomenon was also supported by Evans *et al*. (1974) who discussed that although crystal-crystallizer collisions and crystal-crystal collisions accounted for around 75% of the nucleation within an agitated crystallizer, the remaining 25 % of nucleation was controlled, speculatively, by fluid shear[142]. Ayazi Shamlou *et al*. (1990) showed how secondary nucleation of potassium sulphate crystals could occur due to "fluid-dynamic-induced breeding"[143]. A more recent investigation by Liang *et al.* (2004) on the crystallization of L-glutamic acid also highlighted the dependence of nucleation on crystallizer hydrodynamics[144]. What can be learnt from these previous studies is that by studying the product crystal handedness, it would be possible to probe into the nucleation mechanism when the hydrodynamic environment is changed in different crystallizers, provided that other process conditions, such as supersaturation,

temperature, mixing intensity, etc. are constants. This is the strategy for this investigative work.

5.2 – Conditions to be studied

Each crystallizer was filled with 500 mL of aqueous sodium chlorate solution saturated at 31 °C. This corresponded to 369 g $NaClO_3$ per 349 mL H_2O which was held at 40 °C for one hour as per the procedure outlined in Chapter 3, section 9.1.

The mixing conditions studied are shown in Table 5.1.

Table 5.1 – Mixing conditions for the STC and OBC. The STC would have a shear rate of approximately 3.5 s^{-1}, whilst the OBC would have a value of around 0.3 s^{-1}

	N_S (RPM)	f (Hz)	x_o (mm)	P/V (W m^{-3})
STC	65	--	--	12
OBC	--	0.4	32	12

5.3 – Benchmark testing

Before presenting the main results, a number of benchmark experiments were performed where no mixing at all was applied to the crystallizers. This was to verify the hypothesis that it was the mixing mechanism that had an effect on the secondary nucleation. The first set of benchmark tests were conducted with seeds, but in the absence of mixing.

When no mixing was applied before, during and after the seeding, it was seen that all product crystals bore the same handedness as the seed crystal in all experiments for both the OBC and STC. This indicates that secondary nucleation was the only mechanism in these tests and implies that primary nucleation did not take place. If primary nucleation had occurred, a mixture of left and right handed crystals would have been observed as primary nucleation yields both handed product crystals as shown by the triangles in the Figure 2.3.1 presented earlier, and some recent work presented by Vogl (2011) [145].

In order to further verify that no spontaneous nucleation could occur as a result of surface phenomena, the second set of benchmark experiments were conducted in the same manner as the first set, except no seeds were used. Only a blank wire that is used

to suspend the seed was suspended in the solution for three minutes. The crystallizers containing the supersaturated solutions were left overnight and it was found that no crystals can be seen in either system indicating that the possibility of entraining foreign particles to initiate heterogeneous primary nucleation was not possible and that seeds were the only necessary means to cause nucleation in both systems. The same outcome was observed three times in each system.

5.4 – Results and discussion – OBC I vs. STC

Following on from these benchmark experiments, mixing with identical power density was applied to the two systems (see Table 5.1). Tables 5.2 and 5.3 display the outcomes.

Table 5.2 – The mass of left and right handed crystals obtained and the resulting percentage similarity to a seed crystal for the fresh material in the OBC. The OBC was operated with a frequency of 0.4 Hz and an amplitude of 32 mm

Seed type	Trial	Mass right (g)	Mass left (g)	Total mass (g)	Percentage of products with same handedness as seed (%)
Left	1	0.4	6.3	6.7	94.0
	2	0.6	9.1	9.7	94.0
	3	0.3	5.6	5.9	95.0
Right	1	8.1	0.6	8.7	93.1
	2	5.4	0.4	5.8	93.1
	3	2.6	0.1	2.7	96.3

Average similarity – 94.25 % S.D. – 1.23

Table 5.3 - The mass of left and right handed crystals obtained and the resulting percentage similarity to a seed crystal for the fresh material in the STC. The STC was operated at a stirrer speed of 65 RPM

Seed type	Trial	Mass right (g)	Mass left (g)	Total mass (g)	Percentage of products with same handedness as seed (%)
Left	1	0	15.9	15.9	100
	2	0	0.9	0.9	100
	3	0	5.7	5.7	100
Right	1	1.4	0	1.4	100
	2	4.3	0	4.3	100
	3	8.9	0	8.9	100

Average similarity – 100 % S.D. – 0

From the results of three repeated runs, it is clear that under the conditions studied in this work, the STC consistently gave product crystals with 100 % similarity to the seed handedness. On the other hand, the OBC was always ≤ 96 %. As all of the product crystals from the STC bear the same handedness as the seed, it would appear that the nucleation mechanism was exclusively secondary. In the OBC, the secondary nucleation was still a dominant feature, but some sort of primary nucleation must have occurred in order to have the product crystals with the opposite handedness to the seed. This is a very interesting finding as it implies that the OBC could possess a means of creating primary nucleation without the need for an external stimulus such as ultrasonic [146] or laser [55]. Before examining how this could be possible, further tests were carried out to confirm the findings using some recycled material. In this investigation, the sodium chlorate was recovered from the previous experiments' mother liquors using a combination of evaporation and cooling to obtain a filterable crop of crystals. The crystals were dried and used in the place of the material purchased from Fisher Scientific. Further details of this material can be found in Appendix C and the following data was collected (Tables 5.4 and 5.5).

Table 5.4. - The mass of left and right handed crystals obtained and the resulting percentage similarity to a seed crystal for the recycled material in the OBC. The OBC was operated with a frequency of 0.4 Hz, and with an amplitude of 32 mm

Seed type	Trial	Mass right (g)	Mass left (g)	Total mass (g)	Percentage of products with same handedness as seed (%)
Left	1	0.4	7.2	7.6	94.7
	2	0.4	6.3	6.7	94.0
	3	1.3	6.9	8.2	84.1
Right	1	0.8	0.1	0.9	88.9
	2	6.9	0.2	7.1	97.2
	3	4.8	1.4	6.2	77.4

Average similarity – 89.38 % S.D. – 7.51

Table 5.5 - The mass of left and right handed crystals obtained and the resulting percentage similarity to a seed crystal for the recycled material in the STC. The STC was mixed using a stirrer speed of 65 RPM

Seed type	Trial	Mass right (g)	Mass left (g)	Total mass (g)	Percentage of products with same handedness as seed (%)
Left	1	0	0.3	0.3	100
	2	0	0.5	0.5	100
	3	0	0.4	0.4	100
Right	1	1.0	0	1.0	100
	2	0.5	0	0.5	100
	3	1.4	0	1.4	100

Average similarity – 100 % S.D. – 0

The results are clear that the STC produced crystals always of the same handedness as the seed while the OBC didn't, with the similarity to the seed being less with the recycled material (87.8 ± 9.9 %) than that with the fresh material (94.2 ±1.8 %). This indicates that the recycled material promoted more primary nucleation under the same conditions, a phenomenon was also observed in other crystallization processes [147]. Intuitively speaking, together with the UV-Vis analysis, the recycled material (produced by a re-crystallization process) has around 28 % fewer impurities in it than the fresh material of the identical compound. Fewer impurities would correspond to fewer opportunities for secondary nucleation and in turn, for more primary nucleation. However, deeper explanations on this are yet to be found. Nevertheless, the repeated data served the purpose of validating the findings.

So what has caused the primary nucleation in the OBC? There are a number of possibilities, e.g. microcrystalline dusts or the way the mixing is generated. A microcrystalline dust on the seed crystal could introduce either a seed of opposite handedness to that intended or by chance, a heterogeneous foreign body through which a crystal of opposite handedness to the seed could appear. This seems highly unlikely as not only was the single seed crystal thoroughly rinsed with distilled water prior to use, but this effect would have been seen in both the STC and OBC, not exclusively in the OBC.

5.5 – Results and discussion – OBC with gap vs. Scraped STC

On the examination of the way mixing is achieved in the two systems, i.e. stirring vs. oscillating, one unique feature in the OBC stands out: the likely scraping action on the wall of the column when the baffles are moving up and down the liquid phase. This interaction could cause sufficient friction to induce primary nucleation which has resulted in the mixture of left and right handed crystals in the product. Could the scraping action be the culprit for the primary nucleation?

In order to test this hypothesis, the STC and OBC were redesigned on purpose in that the stirrer in the STC was positioned to cause the scraping effect. Meanwhile, the baffle diameter is smaller than the tube diameter ensuring that the scraping effect would be eliminated in the OBC. If the hypothesis is correct, then the reverse results would prevail, i.e. 100 % of the product crystals from the OBC would bear the seed handedness whilst less than 100 % similarity to the seed would be seen in the STC. The results are now shown in Tables 5.6 and 5.7.

Table 5.6. - The mass of left and right handed crystals and the associated percentage similarity to the seed for the fresh material in the OBC with gap. The OBC was operated at a frequency of 0.8 Hz and an amplitude of 32 mm. In this case, the shear rate would be approximately equal to 0.65 s^{-1}

Seed type	Trial	Mass right (g)	Mass left (g)	Total mass (g)	Percentage of products with same handedness as seed (%)
Left	1	0.23	3.84	4.07	94.0
	2	0	3.95	3.95	100.0
	3	0	4.15	4.15	100.0
Right	1	2.49	0.01	2.5	99.6
	2	4.39	0	4.39	100.0
	3	4.73	0.07	4.8	98.5

Average similarity – 98.68 % S.D. – 2.37

Table 5.7 - The mass of left and right handed crystals and the associated percentage similarity to the seed for the fresh material in the scraped STC. The STC was stirred at a rate of 65 RPM

Seed type	Trial	Mass right (g)	Mass left (g)	Total mass (g)	Percentage of products with same handedness as seed (%)
Left	1	0.01	0.4	0.41	97.6
	2	0	5.9	5.9	100.0
	3	0	1	1	100.0
Right	1	0.2	0.01	0.21	95.2
	2	0.5	0.01	0.51	98.0
	3	5.1	0	5.1	100.0

Average similarity – 98.47 % S.D. – 1.93

From the above data, it can be seen that on the introduction of the scraping stirrer to the STC, there are now instances where the product crystals display less than 100 % similarity to the seed crystal (trials 1 and 2 in Table 5.6, trial 1 in Table 5.7), although there are still a few cases where a complete similarity to the seed has been maintained.

For the OBC where there was a gap between the baffle and the tube, the results did show a shift in similarity to seed towards the 100 % level, as seen with the un-scraped STC tests performed earlier. These initial data are encouraging. In order to further reinforce the outcomes, the experiments were again repeated utilising the recycled starting material. The results from these tests are shown in Tables 5.8 and 5.9.

Table 5.8. - The mass of left and right handed crystals and the associated percentage similarity to the seed for the recycled material in the OBC with gap. The OBC was mixed at a frequency of 0.4 Hz and with an amplitude of 32 mm. In this case, the shear rate would be approximately equal to 0.65 s^{-1}

Seed type	Trial	Mass right (g)	Mass left (g)	Total mass (g)	Percentage of products with same handedness as seed (%)
Left	1	0.1	2.0	2.1	95.3
	2	0.1	3.9	4.0	99.1
	3	0.1	2.1	2.2	95.0
Right	1	1.2	0.4	1.6	75.0
	2	3.4	0.5	3.9	87.2
	3	0.5	0.1	0.6	83.3

Average similarity – 89.15 % S.D. – 9.05

Table 5.9- The mass of left and right handed crystals and the associated percentage similarity to the seed for the recycled material in the scraped STC. The STC was agitated at a rate of 65 RPM

Seed type	Trial	Mass right (g)	Mass left (g)	Total mass (g)	Percentage of products with same handedness as seed (%)
Left	1	<0.1	0.5	<0.6	94.6
	2	0.6	3.7	4.3	86.1
	3	0.5	0.9	1.4	67.6
Right	1	0.1	<0.1	<0.2	71.5
	2	0.2	<0.1	<0.3	83.0
	3	2.0	0.2	2.2	90.8

Average similarity – 82.27 % S.D. – 10.69

The results partially verify the hypothesis, i.e. it is the scraping action in the OBC that was the means of generating the primary nucleation. It should be noted that it was difficult to source a stirrer that would generate an even scraping effect on the internal wall of the STC due to the uneven curvature. This may explain the smaller percentage shift than compared to the original OBC trials. In addition, increasing the gap between the baffles and the vessel wall in the OBC effectively reduced the overall mixing [108], this may explain why a full 100 % similarity was not achieved.

The data presented here is complementary to the recent work of Qian and Botsaris (2004). They investigated the effect of the morphology of the seed crystal on the observed nucleation mechanism. Using their proposed embryo coagulation secondary nucleation (ECSN) model, where embryos of both handedness can exist in the boundary layer of the seed crystal[48], they found that the percentage of the product crystals with the same handedness as the seed was highly sensitive to the crystal surface of the seed as well as depending on the supercooling. They concluded that the degree of supercooling required to switch from conventional secondary nucleation, i.e. by attrition, to the ECSN model was dependant on the seed preparation method[49]. While Qian and Botsaris studied the seeded crystallization of sodium chlorate with regards to the seed preparation and supercooling, this study has investigated the effect of hydrodynamic environment of crystallizers on the crystal similarity and observed a change in the nucleation mechanism.

The final set of three experiments that were performed involved no seeds, but kept the agitation running overnight in both STC and OBC. This is to further consolidate the findings. After agitating overnight at 30 °C, the STC had no product crystals present as would be expected. In the OBC, however, it was clear that nucleation had occurred; crystals were present in the system. In one instance out of the three, the OBC had not nucleated overnight; instead it occurred after two days. At such a low supercooling and the fairly gentle mixing, this result was reasonable. In addition, any primary nucleation would occur much more slowly than if seeds were used to initiate nucleation as described in Chapter 2, i.e. the seed crystal would act as a nuclei surface, effectively reducing the critical radius size to zero.

Analysis of the crystals' handedness revealed that there existed a combination of left and right handed crystals although the actual quantification was difficult and time consuming due to the small size of the crystals obtained. This result once again supports the hypothesis that the scraping is the cause of nucleation in the OBC, however some consideration must be made to the exact mechanism involved.

From the benchmark testing performed initially, no nucleation was seen in either system when the regular seed procedure was followed, but with no seed crystal present on the wire. Repeating this, but allowing agitation to continue as per the primary nucleation test performed here, resulted in product crystals only in the OBC. Why the

scraping action of the OBC allowed nucleation remains somewhat unclear, but some speculative hypotheses can be formed:

- The hydrodynamic environment in the high shearing region that is scraped may be responsible. There may be a relationship between the fluid hydrodynamic environment and the pre-nucleation embryos that may be present in the solution.
- The STC has a higher average shear rate than the OBC, as shown in the Tables given above. This shear rate does not consider the local shearing environment at the point of contact between the baffle edge and the vessel wall. Perhaps this region of extreme shear is a more important a consideration that that of the bulk shear rate, which is normally considered.
- The motion of the baffle against the glass may provide a tribological effect that may result in nano sized particles being sheared from the baffle edge into the bulk solution. These may act as heterogeneous nuclei and thus explain why the OBC nucleated whilst the STC did not.

Introduction of the seed resulted in product crystals being formed in both of the crystallizers. This is consistent with the secondary nucleation model described in Chapter 2. For the STC this appeared to be a mechanism that involved formation of product crystals directly from the seed crystal (all of the products were of the same form as the seed). For the OBC, the nucleation that occurred on the introduction of the seed resulted in product crystals of the opposite form to the seed. In this case, secondary nucleation appears to be the mechanism of product formation (in the benchmark test, no product crystals were formed when the seed was not present) but the exact mechanism is different to that seen in the STC. It now becomes necessary to expand on the existing nomenclature used to describe the nucleation mechanism. Three scenarios seem to be possible as opposed to simply primary or secondary nucleation:

- Primary nucleation can occur where the product crystals are formed without the necessity of a seed crystal, i.e. solute molecules assemble spontaneously into a stable nucleus and grow into discreet crystals.
- Secondary nucleation may occur directly from the seed crystal where the product crystals bear the same enantiomorphism as the seed. In such a mechanism, the solute molecules adsorb onto the crystal surface

and grow as either dendrites, or as additions to existing crystal faces. Once the dendrites, or the seed crystal grow to a certain minimum size, material can break away from the seed crystal, resulting in a crop of secondary crystals. This shall be termed as a seed similar secondary nucleation model.

- Secondary nucleation may occur wherein the product crystals do not form directly from the seed, but perhaps from the seed boundary layer. Perhaps in this type of mechanism, the solute molecules are attracted to the seed crystal and undergo some manner of self-assembly into stable nuclei prior to adhesion to the seed crystal surface. This nucleation due to attractive forces and molecular self-assembly combined shall be referred to as a seed dissimilar secondary nucleation mechanism.

5.6 – Results and discussion – Left handed vs. Right handed seeds

In order to identify any variance that may arise due to the type of seed utilised, the experiments were conducted using both left and right handed seeds. It would be short sighted to simply assume that there was no preference for the system to nucleate more readily with a left handed seed than a right handed seed or vice-versa. In order to confirm that the handedness of the seed has no impact on the outcome, statistical analysis of the data was performed comparing the left and right handed seed results.

For the STC experiments, all of the left handed seed runs and all of the right handed seed runs produced 100 % similarity to the seed crystal. In this case it is clear that there is no difference in the outcome of the experiment between a left and right handed seed. Looking at the data for the OBC reveals that any difference between the percentage similarity to a left handed seed and the percentage similarity to a right handed seed is most likely down to chance. The Kruskal-Wallis analysis of the data shows a high probability that there is an insignificant difference between the two seed enantiomorphs; $P = 0.5002$. Similar results from the statistical analysis can be found if the data from the scraped STC and non-scraped OBC is treated in the same way. P values of 0.4867 and 0.8166 respectively were obtained, indicating that there is likely no difference between using a left handed or right handed seed crystal for this experimental setup.

5.7 - Conclusions

The objective for this work was to seek scientific understanding as to why seeds were not necessary in some crystallization processes in the OBC, while seeds were essential in the STC for the same processes and at the same operational conditions. The starting point for this research was on the mixing mechanism while the chemistry (the model compound) and other conditions such as the procedures and operations remained unchanged. The experimental data showed that the STC produced crystals exclusively of the handedness of the seed crystal whether the mixing was applied or not. The OBC, however, produced crystals of mixed handedness when the mixing was applied. This indicates that a different nucleation mechanism must be present in the OBC as one would expect 100 % similarity to the seed crystal if the mechanism was the same.

By further hypothesizing that the way mixing is achieved in the system could be the cause for the primary nucleation; the presence of a scraping action was investigated in each crystallizer. The data generated so far are highly supportive of these theories. By adding scraping to the STC, there was a noticeable decrease in the percentage similarity to the seed crystal. Conversely, the removal of the scraping action in the OBC resulted in a significant increase in the percentage similarity to the seed crystal. This indicates scraping as being a key driver in altering the nucleation mechanism in a crystallization experiment; however the nature of this is still unknown. This will be investigated in more detail in the following chapters.

An interesting observation was made when utilising recycled starting materials. It is suspected that the material purity may play an important role in the nucleation mechanism (the effect of impurities on crystal nucleation and growth is well documented, see Chapter 2), however at this stage a thorough investigation into this is outwith the scope of this research into the effect of *mixing* on the nucleation mechanism. It was also seen that there was no effect of altering the seed crystal enantiomorphism. Equivalent results were seen for a left and right handed seed.

With the results obtained from this research, existing nomenclature used to define the nucleation mechanisms are insufficient. It is proposed that the secondary nucleation as seen with the STC is referred to as a seed similar nucleation mechanism. Furthermore, the secondary nucleation seen in the OBC will be referred to as a seed dissimilar nucleation mechanism.

Chapter 6 – Influence of mixing intensity on nucleation mechanism

Following on from the groundwork laid out in Chapter 5, the next area of investigation was the effect of mixing intensity on the nucleation mechanism. This research utilised all four types of crystallizer used in Chapter 5 and the general procedure was the same. The difference between the previous research and this work is that the mixing intensity was altered and the effect on nucleation mechanism recorded. The content of this Chapter is largely based on Publication number 2 from the list at the beginning of this thesis.

6.1 - Introduction

Over a hundred years ago, Young (1911) described how agitation would cause the onset of nucleation in a quiescent solution in which no crystallization would occur [148]. This has since been studied in more detail and it is now recognized that mixing influences the metastable zone width (MSZW) [149], an important scientific parameter of solution crystallization. Some early works by Mullin and Raven (1961, 1962) showed that for the batch cooling crystallization of some aqueous salts, increasing the agitation rate raised the nucleation temperature; further increasing the stirrer speed reduced the nucleation temperature slightly and further more intensifying the agitation rate resulted in enhanced nucleation with higher nucleation temperature once again. The suggested mechanism for this phenomenon was a highly complex combination of enhanced mass transfer due to reduced diffusion competing against disruption of pre-nuclei clusters due to fluid shear [35, 150].

Nývlt *et al.* (1968, 1970) investigated the relationship between stirrer speed and MSZW in order to probe the nucleation kinetics of aqueous solutions. They found that the higher the stirrer speed, the higher the nucleation rate constant, but the nucleation order was only dependant on the number of molecules required to form a critical nucleus, i.e. the nucleation order was independent of agitation rate [37, 40].

The relationship between nucleation and agitation rates investigated by Mullin and Nývlt were recently observed by Liang *et al.* (2004) in the study of L-glutamic acid crystallization. They hypothesised that reduction of boundary layer was observed at higher agitation rates, which caused the change in nucleation rates [144], although this parameter is difficult to observe and measure.

The mixing effect applies not only to primary nucleation, but also to secondary nucleation [3]. Melia and Moffitt (1964) presented data on the secondary nucleation of potassium chloride from aqueous solution. They suggested two possible mechanisms for the secondary nucleation process [151]. The first possibility was that in the vicinity of the seed crystal, weakly attracted solute molecules were somewhat ordered in the seed crystal boundary layer without actually being incorporated into the crystal structure. These clusters remained in the boundary layer, with increasing fluid shear, the boundary layer can be washed into the bulk solution and replaced with fresh solution. These clusters then developed into nuclei in the bulk solution away from the seed crystal. This type of nucleation was reported earlier by Powers (1963) in the study of sucrose crystallization [53].

The second mechanism was that the solute molecules were incorporated into the seed crystal structure as dendrites. Through the action of fluid shear, or by crystallizer-crystal collisions, these dendrites can be ripped from the seed crystal and carried into the bulk solution to further grow. Melia and Moffitt reported this type of mechanism for the crystallization of ammonium chloride [152]. It would be reasonable to assume that these mechanisms are dependent on agitation rate.

Min and Goldburg (1993) investigated the influence of fluid shear on droplet formation. In their experiments, the droplets appeared as temperature increased. Increasing the fluid shear resulted in a reduction of the embryo-type clusters and reduced the effective droplet nucleation rate [153].

The combined actions of collision breeding and the boundary layer models were discussed by Buhse *et al.* (2000) who concluded that secondary nucleation by either model was dependent on the crystallizer's hydrodynamics [38]. Chen *et al.* (2002) found that the sodium chlorate boundary layer thickness was dependant on the fluid dynamic conditions [39]. It seems likely that if the boundary layer bred nuclei and collision bred nuclei were the competing processes, the ratio of boundary layer nuclei to collision bred nuclei would depend on not only crystallizer hydrodynamics but also the mixing intensity.

In general it has been shown that by altering the crystallizer's fluid dynamics, it becomes possible to manipulate many important factors critical to nucleation. Increasing fluid agitation intensity and shear rates tends to reduce boundary layer thickness and would have measurable effects on what is happening in the vicinity of a

seed crystal. Fluid shear may also influence any pre-nucleation clusters that may exist in the system [154] and allow some degree of impact over nucleation rates.

Paul *et al.* (2005) stated that "crystallization may be the most difficult operation to scale-up – successfully" and highlighted the importance of mixing for control of nucleation and subsequent growth [32]. By understanding how nucleation changes with agitation, the scale up would become easier and can be done with confidence.

The previous chapter detailed how during seeded sodium chlorate crystallization at a supercooling of 1 °C, all of the product crystals bore the same handedness as the seed crystal in the STC, indicating that secondary nucleation directly from the seed was the source of product crystals. This will be referred to as "seed-similar" nucleation thereafter. For the OBC, on the other hand, the product crystals were never more than 96 % similar to the seed crystal, suggesting an alternative nucleation mechanism that facilitates a "seed-dissimilar" nucleation model. The scraping action of the baffle outer edge against the inner surface of the crystallizer wall was proposed as the cause of generation of the incorrect enantiomorph in the OBC. To test this hypothesis, the scraping was removed from the OBC, while it was introduced to the STC. The opposite results were obtained, i.e. the un-scraped OBC produced much more seed-similar crystals and the scraped STC produced seed-dissimilar crystals, which verified this hypothesis. The objective of this chapter is to investigate how the identified nucleation mechanism would vary with mixing intensity and local fluid flow mechanics, while at the same time shedding some light into the mechanism of nucleation as a result of scraping.

6.2 - Conditions to be studied

The mixing intensities are quantified by means of the power density as outlined in Chapter 3. In order to achieve the power density changes, the mixing conditions in Table 6.1 were applied.

Table 6.1 – Mixing conditions for each crystallizer. The mixing speed is given to the left and the approximate energy dissipation (Wm^{-3}) given in round brackets in the centre. The right hand value in each cell, given in square brackets, represents the approximate shear rate for each mixing condition. The OBC is oscillated at a centre to peak amplitude of 15 mm

Mixing condition	**STC (RPM)**	**OBC Tight baffles (Hz)**	**OBC Loose baffles (Hz)**
Low	65 (12) [3.5]	0.4 (9) [0.3]	0.8 (13) [0.6]
Medium	160 (180) [8.5]	1.0 (145) [0.6]	2.0 (216) [1.6]
High	260 (776) [13.9]	1.6 (595) [1.0]	3.0 (732) [2.4]
		2 (1162) [1.3]	

With the exception of the mixing intensities given in Table 6.1, the experimental procedure remained the same as in Chapter 4, with a single seed crystal being suspended for three minutes at 1 °C supercooling.

6.3 - Results and discussion

The results from the seeded crystallizations in the STC are now presented in Table 6.2.

Table 6.2 - Percentage similarity to the seed crystal for the seeded crystallization in both the un-scraped (left) and scraped (right) STC

un-scraped	**Mixing intensity**			**scraped**	**Mixing intensity**		
sample	**Low**	**Medium**	**High**	**sample**	**Low**	**Medium**	**High**
1	100.00	100.00	100.00	1	92.62	100.00	93.62
2	100.00	100.00	100.00	2	94.61	99.02	96.33
3	100.00	100.00	100.00	3	98.77	92.24	97.35
Average	100.00	100.00	100.00	Average	95.33	97.09	95.77
Standard Error	0.00	0.00	0.00	Standard Error	1.18	2.44	1.11

From the data of the un-scraped STC on the left of Table 6.2, it can be seen that the similarity to seed is consistently 100 % for all power dissipations. While no mechanism was expected in the un-scraped STC to promote seed dissimilar nucleation, increasing the power dissipated into the system would be expected to increase the rate of secondary nucleation by either crystal-crystal or crystal-crystallizer collisions [142, 155], without influencing the product crystal handedness.

When scraping was introduced to the STC by simply having the impeller tightly pressed against the bottom of the vessel, seed-dissimilar nucleation did occur (the right side of Table 6.2). This outcome was expected from the previous work [156]. It would seem reasonable to infer that as the mixing intensity increased in a system where a seed-dissimilar nucleation mechanism exists, one of three outcomes could be seen. The first possible scenario could be that the rate of seed-dissimilar nucleation because of the scraping mechanism would increase due to more scrapes per unit time (in this case rotations per second) resulting in a decrease in the percentage similarity to the seed of the crystals produced. The second possible outcome that may be observed could be the rate of seed-similar nucleation being enhanced due to either crystal-crystal or crystal-crystallizer collisions occurring more frequently because of the increased mixing. The third possible outcome is that both cases one and two would occur simultaneously. Should this be the case, then it is likely that the effects of each scenario would cancel each other out, resulting in no detectable change in the outcome of the experiment. The data in Table 6.2 suggest that it is likely that this third possibility was observed. Analysis of the data using the Kruskal-Wallis test suggests that there is no statistical significance in the differences between the results at various mixing intensities ($P=0.7326$). These experimental data explain that although scraping did cause the formation of product crystals of the opposite enantiomorphism to the seed crystal, the energy dissipation at which scraping is applied had little or no influence on the rate of this seed-dissimilar nucleation. This could perhaps be due to both seed-similar and seed-dissimilar nucleation rates increasing with mixing intensity, resulting in no net change in the average similarity.

The experiments conducted in the STC were then repeated in the OBC. The results of these tests are given in Table 6.3.

Table 6.3 - Percentage similarity to the seed crystal for the seeded crystallization in both the un-scraped (left) and scraped (right) OBC at a fixed centre to peak amplitude of 15 mm

un-scraped sample	**Mixing intensity**			**scraped sample**	**Mixing intensity**		
	Low	**Medium**	**High**		**Low**	**Medium**	**High**
1	100.00	98.86	99.58	1	94.02	99.00	93.09
2	96.99	99.49	99.83	2	94.89	93.43	93.20
3	99.88	98.69	99.01	3	96.31	92.90	90.49
Average	98.96	99.01	99.47	Average	95.07	95.11	92.26
Standard Error	0.98	0.24	0.24	Standard Error	0.67	1.95	0.89

Considering the scraped OBC first (the right side of Table 6.3), seed-dissimilar nucleation did occur, leading to the percentage of similarity to the seed being lower than 100 %. It appears, however, that there is no clear trend with the change in mixing intensity (frequency). Indeed, no statistical significance can be found in the difference between the outcomes under the three conditions (P=0.1479). Similarly, with the un-scraped OBC (the left side of Table 6.3), some seed-dissimilar nucleation also took place. Analysis of the data of the un-scraped set up suggests again that there is no significant difference between each mixing intensity (P=0.4298). In terms of trends found in both the scraped STC and scraped OBC, the effect of mixing (stirring vs. oscillation) had little impact. Statistical analysis of these data shows that there is no significant difference in the percentage similarity between the scraped OBC and the scraped STC (P=0.2004).

The seed-dissimilar mechanism took place in the un-scraped OBC, while it was not observed in the un-scraped STC. The statistical difference in the percentage similarity between the two un-scraped set ups is significant (P=0.0005). Why is this? Previous work on the numerical modelling of flow patterns in both tight fit and loose fit baffle arrangements in the OBC showed that more shear was predicted in the latter device than in the former [93] Liu *et al.* calculated the former to have an average wall

shear stress of around 2.5 Pa, whereas in the latter, a value of around 14 Pa was calculated [157]. The seed-dissimilar nucleation in the un-scraped OBC may be linked with the increased shear at the gap, even though it has previously been shown that the introduction of a gap in the OBC increased the mixing time, i.e. the larger the gap is, the poorer the mixing is [108]. This would suggest that the local fluid flow condition in the un-scraped OBC could have played a small but important role on the nucleation mechanism.

To put this hypothesis to the test, lower oscillation amplitudes of 3.5 and 7.5 mm were used at a fixed frequency, so that the amount of fluid shearing at the gap is effectively reduced as the shear (strain) rate is proportional to the change of oscillatory velocity ($x_o f$) at the gap as:

$$\dot{\gamma} \propto \frac{x_o f}{D} \tag{6.1}$$

Where $\dot{\gamma}$ is the fluid shear rate (s^{-1}) and D is the baffle diameter (m) [137].

Clearly, a reduction of the amplitude at a fixed frequency reduces the value of the oscillatory velocity, $x_o f$, and therefore the shear (strain) rate of the system. The results of the varied amplitude experiments in both the scraped and un-scraped OBC are presented in Table 6.4.

Table 6.4 – Percentage similarity to the seed crystal for the seeded crystallization in the scraped (left) and un-scraped (right) OBCs. These tests were conducted at a fixed frequency of 2 Hz, the approximate energy dissipation (Wm^{-3}) is given in brackets next to the amplitude

Un-scraped	**Amplitude, x_o (mm)**			**Scraped**	**Amplitude, x_o (mm)**		
Sample	**3.5 (3)**	**7.5 (27)**	**15 (216)**		**3.5 (14)**	**7.5 (145)**	**15 (1162)**
1	100.00	99.96	98.86		97.85	98.12	93.12
2	100.00	99.94	99.49		100.00	95.72	93.12
3	100.00	99.42	98.69		99.91	98.39	93.82
Average	100.00	99.77	99.01		99.25	97.41	93.35
Standard error	0.00	0.18	0.24		0.70	0.85	0.23

Examination of the data from the un-scraped OBC (the left side of Table 6.4) reveals that decreasing the amplitude, i.e. the shear (strain) effect, increased the similarity to the seed, and 100 % similarity to the seed was achieved at the lowest amplitude of 3.5 mm, where the shear effect was at its lowest. Increasing the amplitude gave a significant difference in the outcome of the experiment (P=0.0349). The data continue to suggest that the local fluid mechanical conditions could influence nucleation mechanisms. To further confirm this, the same conditions were tried in the scraped OBC as shown the right side of Table 6.4. A clear trend of the similarity to the seed increasing towards 100 % with reducing oscillation amplitude is evident here, with a significant statistical difference (P= 0.0496). It seems that by reducing the effective scraped area via the length of the scraping in the system, the local shearing effect was effectively reduced, leading to the significant reduction of the amount of seed-dissimilar nucleation. The results indicate that both the overall mixing intensity and the local fluid mechanical conditions during the seeding within a crystallizer are equally important in influencing nucleation. That said, it is important to note that although the power dissipation is comparable for each device, the shear rate in the STC was always much higher than that in the OBC. This raises the importance of local shear rates (in this case

the point of scraping of the baffle against the vessel wall) vs. that of bulk shear rates, which the shear rate equations consider.

The question remains as how exactly the seed-dissimilar crystals were formed in the scraped and un-scraped systems. It could be speculated that the seed boundary layer could be the key factor in deciding whether or not nucleation would be seed-similar or seed-dissimilar. In the OBC, the fluid flow regime could disrupt this boundary layer differently, giving different pre-nucleation conditions [68] to those seen in the STC. For the scraped systems, the results presented here resemble an undergraduate chemistry lab project using a spatula scraping the surface of a beaker containing supersaturated solution, but the exact mechanism becomes harder to elucidate, perhaps with a combined scraping and fluid flow regime model in effect. As Davey et al. pointed out, determination of the crystal nucleus characteristics (such as size, shape, and, particularly, the enantiomorph) will require technology and data that are as yet unavailable [158].

6.4 - Conclusions

In conclusion, it was previously found that when a scraping mechanism is introduced to either a stirred tank or oscillatory baffled crystallizer containing a supersaturated solution of sodium chlorate, nuclei of opposite enantiomorphism to the seed crystal are found in the crop of product crystals. The work undertaken in this chapter, somewhat surprisingly, finds that no real change in the percentage of similarity has been seen in the two systems when the mixing intensity (in terms of frequency and stirring rate) was altered. It has been further demonstrated that local fluid mechanical conditions (e.g. shearing effect due to the oscillatory amplitude) can also lead to the formation of seed-dissimilar crystals. By reducing such an effect, the un-scraped OBC gave 100 % similarity to the seed at the lowest amplitude (shear effect). The results of this work indicate that the action of scraping generates nuclei of the opposite enantiomorphism to the seed, so does the local mixing/shearing conditions in a crystallizer.

Chapter 7 – Effect of scraping – OBC I vs. OBC III

In the previous Chapters, the OBCs have all been the ones wherein the baffles are oscillated through the fluid. The focus of the work now shifts to the scenario where the fluid is oscillated around the stationary baffles. The content of this Chapter is based on the Publication number 3 from the list of work presented at the beginning of the thesis.

7.1 - Introduction

In Chapters 5 and 6, experiments were carried out using an aqueous solution of sodium chlorate in both the STC and OBC under comparable operating conditions (supersaturation, seed suspension time, solution concentration, curing times and power dissipation). It was found that the STC always produced crystals of the same enantiomorphism as the seed. This can be described as a "*seed-similar*" nucleation mechanism. In the OBC, however, the similarity to the seed was always less than 95 %. The five per cent or so of the opposite-to-seed crystals must have occurred due to an alternative "*seed-dissimilar*" nucleation mechanism. The influence of baffle scraping on the column wall in the OBC was investigated and identified as the source of the *seed-dissimilar* nucleation, i.e. nucleation of crystals with an opposite enantiomorphism to that of the seed crystal. By creating a gap between the outer edges of the baffles and the internal surface of the crystallizer, thereby eliminating the scraping action, the similarity increased towards 100 %. This was achieved by increasing the gap between the baffle and the crystallizer wall. By doing so, the value of α was dramatically altered (0.23 for the OBC I vs. 0.87 for the OBC with baffle gap). This resulted in the operational frequencies of the OBC II to greatly exceed that of the OBC I despite the power density remaining constant.

In order to further investigate this scraping effect, the OBC III described in Chapter 3, Figure 3.5, was used. The OBC III differs from the OBC I in that it is the fluid that is oscillated rather than the baffles. Not only does this remove the scraping effect of the baffles, but the value of α now remains similar to the OBC I (0.21 in OBC III). So far all experiments were performed in an OBC where the baffles are moving up and down through the fluid by a linear actuator at the top of the column. This chapter shall focus on an OBC where the baffles are stationary and the fluid is oscillated by a bellows at the base of the column. Although the uniform mixing can be achieved in both configurations, the purpose of this work is to identify and compare any difference

that may arise due to the different oscillation methods and any impact on nucleation mechanism, in particular, as the moving baffle arrangement is exclusively used in batch operation, while pulsing fluid in the presence of stationary baffles is employed in continuous operation [159]. It is the latter method that is used in lab, pilot and full scale continuous crystallizers, therefore the understanding, utilization and controlling of these differences, if any, could have profound influence on tailor-making crystal properties and also allow us to gain better knowledge on scale up of continuous crystallization processes.

In Chapter 6, the effect of increasing the power density on the nucleation mechanism was investigated in the OBC I/II and the STC. As the mixing intensity increased, no real trend was identified. In the STC where no scraping occurs, it was seen that the products bore 100 % similarity to the seed in each case. This suggests that collision breeding is the mechanism of secondary nucleation when no scraping is seen. The tests in the OBC III would either confirm the hypothesis that the scraping is the cause of primary nuclei or identify other primary nucleation mechanisms.

7.2 – Conditions to be studied

Continuing from the results obtained in the previous chapters, the experiments performed here utilise similar conditions and mixing intensities. The mixing conditions for the OBCs are given below in Table 7.1.

Table 7.1 – Mixing conditions of the OBCs with a centre to peak amplitude of 7.5 mm. The frequency of oscillation (Hz) gives an approximate power density that can be used as a basis of comparison between each system. The far right columns indicate the approximate shear rate for each type of OBC under the given conditions

Approximate *P/V* (Wm^{-3})	***f* (Hz)**	***$\dot{\gamma}$ Moving baffle* (s^{-1})**	***$\dot{\gamma}$ Moving fluid* (s^{-1})**
10	0.8	0.25	0.32
150	2.0	0.63	0.81
700	3.3	1.03	1.33

7.3 – Results and discussion – OBC III, seeded crystallization at ΔT = 1 °C

For the OBC with moving fluid, the results in Table 7.2 were obtained. The column, N'', denotes the number of seed-similar crystals, while the number of seed-dissimilar crystals is given in the column, N'. The total number of crystals obtained is presented in the 4th column, headed "N". Three tests were carried out for each condition as before.

Table 7.2 – Results from the moving fluid OBC at x_o = 7.5 mm and with various frequencies. The number of seed similar, N'', and seed dissimilar, N', crystals is determined allowing the percentage similarity to the seed crystal to be calculated

f **(Hz)**	**N''**	**N'**	**N**	**Similarity (%)**
0.8	1461	270	1731	84.40
0.8	614	143	757	81.11
0.8	580	133	713	81.35
2	1900	49	1949	97.49
2	772	34	806	95.78
2	698	38	736	94.84
3.3	1801	292	2093	86.05
3.3	820	106	926	88.55
3.3	907	201	1108	81.86

The tests using the moving baffle OBC were also performed at the same operating conditions and the results given in Table 7.3 obtained.

Table 7.3 – Results from the moving baffle OBC at xo = 7.5 mm and with various frequencies. The number of seed similar, N'', and seed dissimilar, N', crystals is determined allowing the percentage similarity to the seed crystal to be calculated

f **(Hz)**	**N''**	**N'**	**N**	**Similarity (%)**
0.8	757	43	800	94.63
0.8	1323	3	1326	99.77
0.8	1253	13	1266	98.97
2	1934	37	1971	98.12
2	939	42	981	95.72
2	1162	18	1180	98.47
3.3	835	61	896	93.19
3.3	3290	50	3340	98.50
3.3	1595	39	1634	97.61

Table 7.4 summarizes the averaged similarities to the seed for the OBC with both stationary and moving baffles.

Table 7.4 – Average percentage similarity to seed at various mixing intensities in both the OBC with moving fluid, and moving baffles. The ± value is the standard error and is based on the data from Tables 7.2 and 7.3

Approximate P/V (Wm^{-3})	**OBC (moving fluid) (OBC III)**	**OBC (moving baffles) (OBC I)**
10	82.24 ± 1.08	97.74 ± 1.61
150	96.00 ± 0.77	97.41 ± 0.87
700	85.44 ± 1.95	96.40 ± 1.67

It can be seen firstly that the percentage of the similarity to seed is higher in the OBC with moving baffle configuration than that in the OBC with moving fluid. The Kruskal-Wallis statistical analysis [160] gave a probability (P) of 0.0041, postulating that the difference in the percentages of product crystals with the same enantiomorphism as the seed between the two devices is statistically significant. This

confirms that more *seed-dissimilar* nucleation of the opposite-to-seed enantiomorphism occurred in the moving fluid OBC. As mentioned in the previous work [156] that the scraping action of the baffle outer edge on the internal surface of the column was identified and verified as the culprit for the unexpected nucleation in the OBC with the moving baffle system. How could even more *seed-dissimilar* nucleation have occurred in the OBC with moving fluid where there is no scraping action at all?

Secondly, the percentages of the similarity to the seed at each mixing intensity were more or less the same in the OBC with moving baffles (column 3 in Table 4 with P = 0.5611), but exhibited a "bell shape" trend in the moving fluid OBC (column 2 in Table 4 with P = 0.039). An increase in the percentage of the similarity to seed is expected with the increase of mixing intensity as more mixing brings about more *seed-similar* nucleation by the increased crystal-crystallizer collisions, however the decrease with further mixing was unexpected. Since various mixing intensities in the two OBCs are essentially related to different oscillation frequencies (Table 7.1), the observed results thus reflect the outcomes of the frequency effect. Could this be different when different oscillation amplitudes are used?

Back to the first observation, one possible explanation could lie with a recent paper by Manninen *et al.* (2012). They performed a series of CFD simulations using both Newtonian and non-Newtonian fluids and evaluated the axial dispersion coefficients in both the moving baffle and moving fluid OBCs for the production of polyaniline. They found that the moving baffle OBC had 4-11 % higher average shear rate and 10-17 % higher axial dispersion coefficient than the moving fluid OBC[161]. The axial dispersion coefficient indicates the extent of diffusion of a species under a given fluid dynamic environment with the higher the value of the axial dispersion coefficient, the greater the degree of mixing. Without considering other factors, for the low and high mixing intensities, the similarities to seed in the moving fluid OBC are 15.9 and 11.4 % lower than those in the moving baffle counterpart respectively. The reduced similarity in the moving fluid OBC coincides with the difference between axial dispersion coefficients in the two devices. It would appear without further scientific scrutiny that the lower the axial dispersion, the greater the rate of nucleation of the opposite to seed enantiomorph, but this seems counterintuitive as any increased nucleation rate would have been resulted from higher axial dispersion.

The attention now directs towards the internal liquid renewal due to fluid oscillation. Could the periodical liquid stretching and folding *within* the OBC for the moving baffles be somehow different than that for the moving fluid arrangement? A number of new experiments were constructed and conducted as before, except that the top baffle was removed in both OBCs as illustrated on the right in Figure 7.2. This would reduce the degree of internal renewal as well as the quality of the mixing in the vicinity where the seed crystal was immersed. These experiments were run under the same mixing conditions given in Table 7.1. The results from these tests are given in Table 7.5.

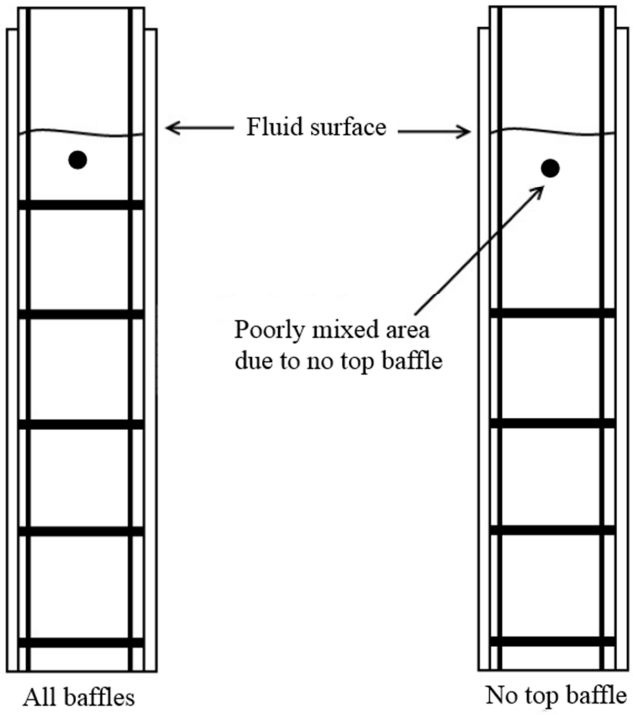

Figure 7.2 – OBCs with all baffles (left) and no top baffle (right). The seed was always immersed to the same depth indicated by the filled dot. Removing the top baffle would result in the mixing in the immediate vicinity of the seed crystal to be reduced

Table 7.5 – Removing the top baffle from each OBC yields a change in the outcome of the experiment. The average percentage similarities to the seed crystal in the two OBCs with and without the top baffle are shown ± the standard error. For each OBC, mixing was carried out with a centre to peak amplitude of 7.5 mm. The mixing intensity was varied by altering the frequency

	Scraping, moving baffle		**Non-scraping, moving fluid**	
Approximate P/V (Wm^{-3})	All baffles	No top baffle	All baffles	No top baffle
10	97.74 ± 1.61	99.53 ± 0.16	82.24 ± 1.08	96.48 ± 1.33
150	97.41 ± 0.87	99.49 ± 0.18	96.01 ± 0.77	98.15 ± 0.48
700	96.40 ± 1.67	99.45 ± 0.28	85.44 ± 1.95	94.67 ± 1.81

From the data in Table 7.5, it would appear that the presence or non-presence of the top baffle had a significant effect on the outcome of the experiment ($P = 0.0031$ and 0.0054 for the moving baffle and moving fluid OBCs respectively). It can be seen that the percentage of similarity increased for both setups when the top baffle was removed and the local mixing at the neighbourhood of the seed became poorer. In fact, when no mixing was applied to either system during the seeding process, 100 % similarity to the seed crystal was obtained. This indicates that the mixing conditions around the seed affected the nucleation mechanisms. Without the presence of the top baffle, the activities of eddies diminished in that area and the seed boundary region remained more or less unchanged. This finding points to the eddy size/length having an effect on the nucleation mechanism. As a direct consequence, a new series of experiments were designed and conducted (Table 7.6) where the amplitude of oscillation was altered at a fixed oscillation frequency of 2 Hz. For these experiments, both crystallizers were operated with all of the baffles present. The results for the moving fluid OBC are shown in Table 7.6 (a), while for the moving baffle system in Table 7.6 (b), the latter of which are imported from the earlier work [162].

By changing the magnitude of the oscillatory amplitude, it becomes possible to change the size of the eddies within the system with much more control than can be had by simply removing the top baffle of the system. Figure 7.3, below, gives an approximate representation of the various eddy sizes when the oscillatory amplitude is

changed. By altering the eddy size, the liquid mixing in the immediate vicinity of the seed crystal can be changed.

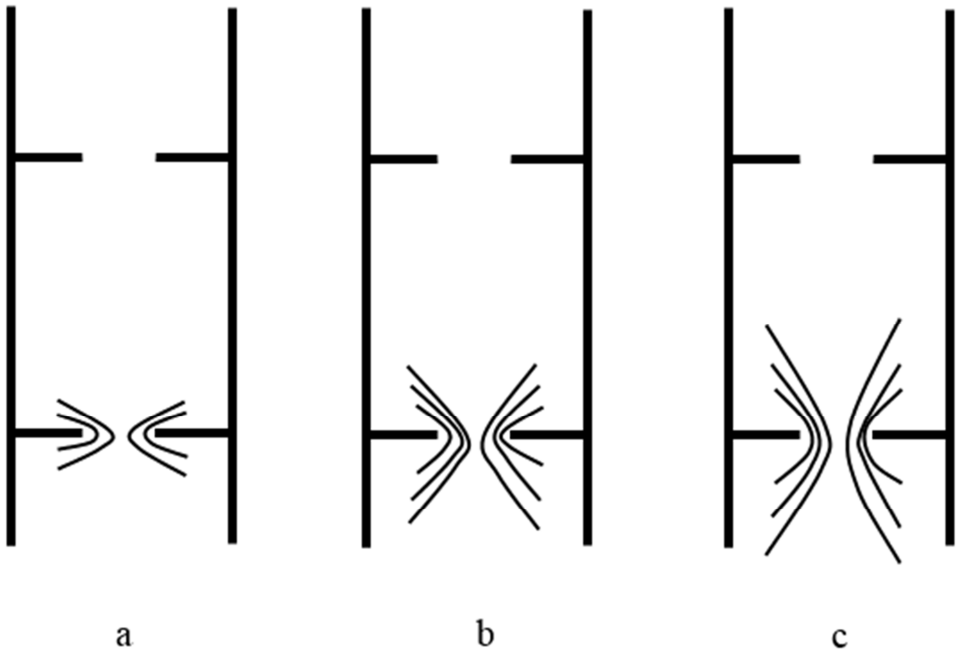

Figure 7.3 – Approximate size of the eddies at various amplitudes. There will be a distinct increase of eddy size when amplitude increases from (a) 3.5 mm to (b) 7.5 mm and to (c) 15 mm

Table 7.6 –The number of seed similar, N'', and seed dissimilar, N', crystals obtained from both types of OBC for varied centre to peak oscillation amplitudes (15, 7.5 and 3.5 mm) and a fixed frequency of 2 Hz. The percentage similarity to the seed crystal is also calculated

(a) – The moving fluid OBC with all baffles. The approximate shear rates at each amplitude were calculated to be approximately 1.62, 0.81 and 0.38 s^{-1} respectively.

x_o (mm)	P/V (Wm^{-3})	N''	N'	N	Similarity (%)
		491	36	527	93.17
15	1406	937	103	1040	90.10
		343	33	376	91.22
		1900	49	1949	97.49
7.5	175	772	34	806	95.78
		698	38	736	94.84
		520	10	530	98.11
3.5	18	831	37	868	95.74
		596	8	604	98.68

(b) – The moving baffle OBC with all baffles. The approximate shear rates at each amplitude were calculated to be approximately 1.25, 0.63 and 0.29 s^{-1} respectively.

x_o (mm)	P/V (Wm^{-3})	N''	N'	N	Similarity (%)
		2260	167	2427	93.12
15	1162	3020	223	3243	93.12
		6973	459	7432	93.82
		1934	37	1971	98.12
7.5	145	939	42	981	95.72
		1162	18	1180	98.47
		1817	40	1857	97.85
3.5	14	6567	0	6567	100.00
		3250	2	3252	99.94

From Table 7.6 above, it can be seen that changing the amplitude had a profound effect on the percentage similarity to the seed (P=0.0509 for both crystallizer

configurations) where a reduction in the amplitude yielded an increase in the percentage similarity to the seed, and 100 % similarity to the seed was achieved at the lowest amplitude in the moving baffle OBC. This is not the case with the moving fluid system. Looking closely at the configurations, unlike the moving baffle OBC, the fluid surface in the moving fluid OBC must rise and fall at the top of the liquid column. It could entirely be possible that this rising fluid in the moving fluid OBC could be deposited as a thin film on the vessel wall as depicted in Figure 7.4.

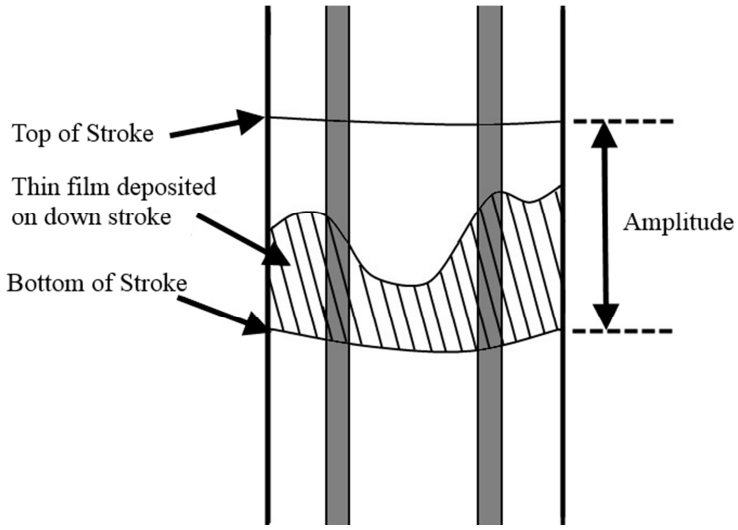

Figure 7.4 – Thin film deposited in moving fluid OBC between the bottom and top of the oscillation stroke (not to scale)

This film could then be evaporated, leading to either potential nuclei or, more likely, localised areas of high supersaturation that may be washed back into the bulk solution on the next pulse of the oscillation. Following Denk and Botsaris' works [46], this would effectively lead to *seed-dissimilar* nucleation and give a mixture of levo- and dextrorotatory product crystals. This may also account for the earlier observation of the bell-shaped trends with the varied frequency tests. An alternative mechanism that may be taking place could be splashing of the solution onto the curved vessel wall. The splashed droplets themselves could evaporate due to a high vapour pressure as a result of the small droplet sitting on the curved vessel surface. If this was the case, sealing the column top could prevent evaporation from taking place and reduce or eliminate the *seed-dissimilar* crystals. Furthermore, in the setup of a continuous crystallizer, the external surface renewal will be at the end of the COBC, as shown in Figure 7.5. At this point of the crystallizer, the product crystals should have fully grown (at any rate, no nucleation should be occurring), and any effect of the liquid/air interface would not affect nucleation any more.

The column was sealed at the top by replacing the splash cap with a PTFE gasket and a PTFE lid, which was clamped onto the glass column. The seed crystal was mounted to a moveable magnetic holder prior to the apparatus being sealed. The seed was held well above the solution initially, and lowered into it when required. Early attempts at this experiment involved the internal pressure of the crystallizer being increased by means of a hand pump to around 1 bar_g, however this pressure was too high to allow the bellows to physically oscillate the fluid. The experiment was eventually performed as intended after being sealed the equilibrium was reached by holding the quiescent solution for one hour at 40 °C, preventing or minimizing any evaporation from occurring. The data to test this hypothesis is given in Table 7.7

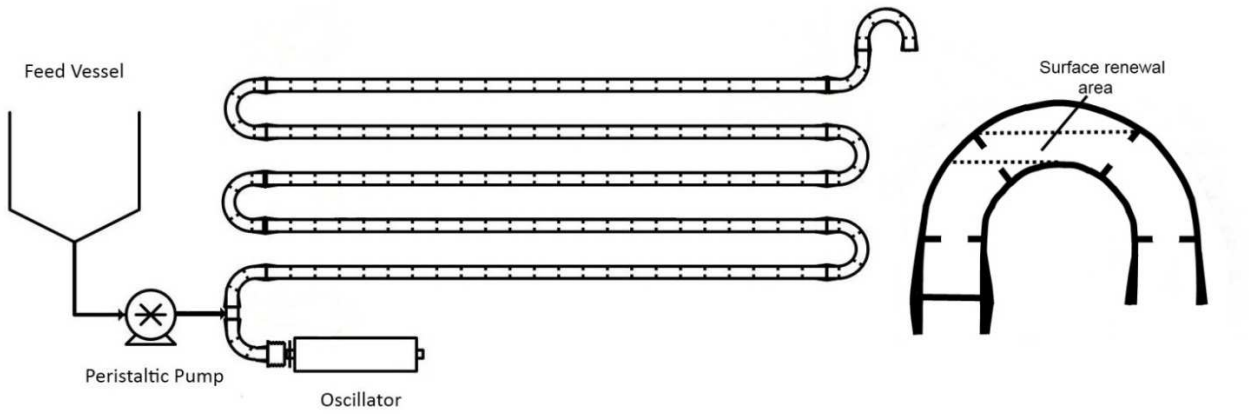

Figure 7.5 – Typical configuration of a COBC. The fluid oscillation is achieved by the bellows unit and a linear motor at the front end of the vessel. This results in the surface renewal occurring approximately between the two dashed lines at the end of the system

Table 7.7 – The number of seed similar and seed dissimilar crystals obtained from the moving fluid OBC after being sealed and operated at a vapour pressure equilibrium. The number of crystals obtained allowed the percentage similarity to be determined. The system was tested at various oscillatory amplitudes and frequencies as shown in the Table

x_o (mm)	f(Hz)	P/V (Wm^{-3})	N''	N'	N	Similarity (%)
3.5	2	18	5	0	5	100.00
			34	0	34	100.00
			69	0	69	100.00
7.5	0.8	11	10	0	10	100.00
			266	0	266	100.00
			374	0	374	100.00
	2	175	487	0	487	100.00
			358	0	358	100.00
			819	0	819	100.00
	3.3	790	162	0	162	100.00
			557	0	557	100.00
			10	0	10	100.00
15	2	1406	97	15	112	86.61
			531	54	585	90.77
			214	29	243	88.07

On sealing the moving fluid OBC, all the product crystals bore the same enantiomorphism as the seed crystal regardless of frequency at a fixed centre to peak oscillatory amplitude of 7.5 mm. 100 % similarity to the seed were also obtained for varying the amplitude at a fixed frequency of 2 Hz, except one condition at an oscillatory amplitude of 15 mm. It was unexpected to see that more *seed dissimilar* nucleation took place in the sealed setup than that in the unsealed system under these same conditions (P=0.0495). The dissimilarity to the seed crystal may be a result of the high amount of splashing that exists in the moving fluid OBC at this amplitude if more splashing results in more small droplets, then evaporation may exist despite operating with a sealed vessel. When compared to the results in Table 7.5, the data in Table 7.7 imply that the external surface renewal, i.e. the effects of splashing or evaporation, is a mechanism of initiating *seed-dissimilar* nucleation in the OBC with moving fluid. This

is in addition to the scraping action in the OBC with moving baffles that was identified in the previous work [156]. The findings also suggest that the amplitude of the mixing is not as important for the moving fluid OBC as it is for the moving baffle OBC. In the sealed moving fluid system, 100 % similarity to the seed was obtained at low and medium amplitudes suggesting that the splashing and/or evaporation is a more important consideration than the amplitude as previously considered in Table 7.6. This may be due to the fact that no scraping is present in the moving fluid OBC.

Although no thin film effect would be expected in the moving baffle OBC as the surface movement is restricted, a few experiments were performed in a sealed moving baffle system and the data indicated that no significant difference was found between the sealed and unsealed moving baffle OBCs (P=0.1797, 0.1797 and 0.6547 for the 3.5, 7.5, and 15 mm amplitude experiments respectively). This result indicates yet again that the scraping action of the baffle against the vessel wall is a significant influence on seed-dissimilar nucleation. Whether this is the outcome of the tribological action of scraping itself or an increase in the fluid shear at the vicinity of the baffle edge is yet to be seen.

What can be learnt from these experiments? It has been found that for both the moving baffle and moving fluid OBCs, the internal fluid mechanics is critical in whether or not *seed similar*, or *seed-dissimilar* secondary nucleation takes place. The data here demonstrates that the percentage similarity to the seed increases as the amplitude is reduced, and *seed dissimilar* nucleation can be eliminated. A speculative explanation is that this could be down to the disruption of the fluid in the immediate vicinity of the seed crystal with the greater the amplitude (the eddy size), the greater the extent of disturbance to this boundary layer. Furthermore, this research has demonstrated that there is a substantial issue surrounding thin film evaporation with the moving fluid OBC as the liquid surface moves within the column. This was eliminated by sealing the system albeit *seed dissimilar* nucleation was only observed with the highest operating amplitude. The reasons for this are still unknown, but may be attributed to droplet evaporation due to splashing in the moving fluid OBC at high amplitude.

7.4 – Conclusion

In this Chapter, it was found that even more *seed-dissimilar* nucleation took place in the OBC with moving fluid where the previously identified scraping action was avoided.

Through different hypotheses, the conditions that favour *seed-dissimilar* secondary nucleation have been identified. Depositing/evaporating supersaturated solution as either thin film, or as splashed droplets due to the oscillatory motion in the moving fluid system appears to be the largest cause of seed-dissimilar nucleation. Altering mixing conditions, i.e. the amplitude, at the vicinity of the seed crystal at first glance appears to have a large effect for the unsealed moving fluid and moving baffle OBCs. This effect is also seen in the sealed moving baffle OBC. For the sealed moving fluid OBC, the effects of altering the amplitude are negligible. This suggests that the presence of splashing has been the true source of the *seed-dissimilar* nucleation. With this knowledge gained, it should be possible to utilize these conditions, i.e. avoiding splashing by using a low oscillatory amplitude and sealing the system to minimize any effect of evaporation, to promote or avoid *seed dissimilar* crystals, and allow secondary nucleation directly from the seed crystal to prevail in continuous crystallization.

Chapter 8 – Effect of Material of Construction – PTFE vs. SS

In the previous chapters, all of the crystallizers have been operated with PTFE agitators (baffles and impellers). The purpose of this chapter is to investigate how a change in agitator material of construction may affect the outcome of the seeded nucleation of sodium chlorate in both the STC and OBC. The content of this Chapter is based on the publication number 4 from the list given at the start of the thesis.

8.1 - Introduction

The material of construction of components has long been recognized as a fundamental consideration when designing a crystallization system. Shah *et al.* (1972) studied seeded crystallization of magnesium sulphate heptahydrate with a polyethylene and a stainless steel impeller, and found that the stainless steel impeller resulted in, on average, four times more product crystals than when a polyethylene impeller was used [163]. They attributed this difference to the changes in contact energy when the material of construction was varied [164]. Evans *at al.* (1974) revealed that the rate of secondary nucleation by crystal-crystallizer collisions could be reduced by coating the crystallizer internal surfaces with polymer [142]. Liang *et al.* (2004) investigated the contact angle between the solution and the material of impeller construction (an acrylic and a stainless steel impeller) in the cooling crystallization of L-glutamic acid and found that the contact angle was much smaller and, in turn, the nucleation rate on the surface was much higher in the stainless steel impeller than that in the acrylic stirrer [8]. More recently, Page and Sear (2009) reported that the surface geometry could be used to control the nucleation of a desired polymorph via a relationship between the contact angle and an angle specific to the crystal lattice of the target polymorph[165]. The material surface directly affected the contact angle, which in turn influenced the free energy (ΔG_{crit}) of the system according to [5]:

$$\Delta G'_{crit} = \phi \Delta G_{crit} \tag{2.1.13}$$

Where ΔG_{crit} is the critical free energy of the system (J), $\Delta G'_{crit}$ the reduced free energy due to the contact angle (J) and ϕ a function of the contact angle, defined by Volmer [30]as:

$$\phi = \frac{(2+cos\theta)(1-cos\theta)^2}{4} \tag{2.1.15}$$

Where θ is the contact angle (°).

Relevant to this work, Ni *et al.* (2010) investigated the effect of baffle material for the crystallization of L-glutamic acid in an oscillatory baffled crystallizer and reported that the baffle material played a role in the polymorph formed, with a smoother surface favouring the formation of the α polymorph [20]. The motivation of this work was therefore to investigate if there is any difference in the nucleation mechanism in an OBC when PTFE baffles and stainless steel baffles are employed. There are two reasons for carrying out this work. Firstly, the contact angle could be different, resulting in the baffle acting as a substrate for nucleation [166]. In the PTFE system, it would be expected that any pits or irregularities in the surface could result in a large contact angle, denoted by θ_P in Figure 8.1. In the case of the stainless steel baffle, larger surface pits could lead to a much smaller contact angle, denoted by θ_S in Figure 8.1.

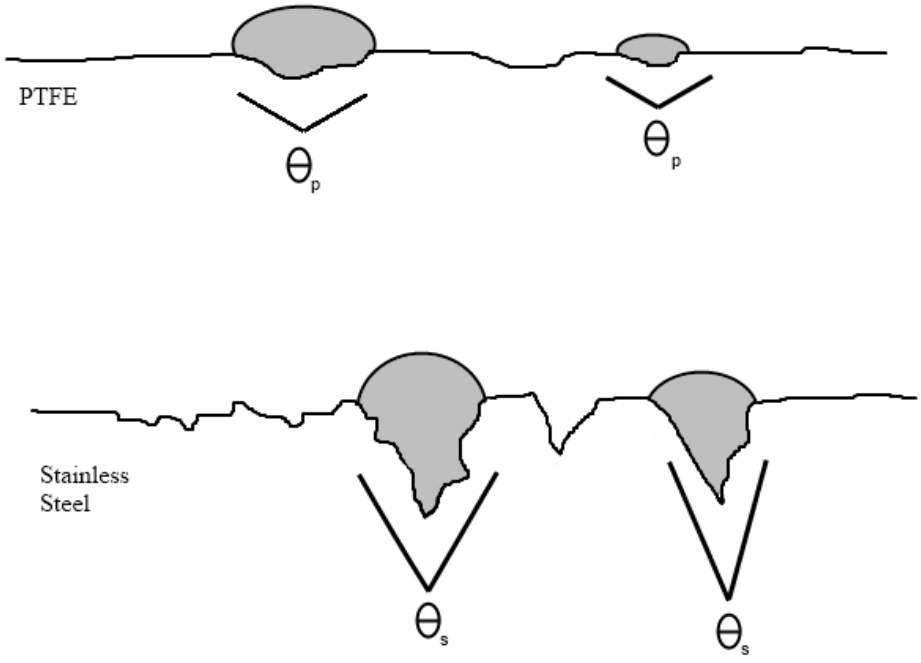

Figure 8.1 – Representation of surface roughness in PTFE (top) and Stainless Steel (bottom). The stainless steel surface could have a greater chance of retaining material in the deeper crevices than those seen in the PTFE surface

Secondly, stainless steel has a much higher Rockwell hardness (~90) [167] compared to PTFE (~58) [168]. As the scraping motion within the OBC played a vital role in initiating different nucleation mechanisms, a harder material could favour more vigorous mechanical scraping compared to a softer one.

In order to quantify the surface roughness in each system, PTFE and stainless steel baffles were subjected to atomic force microscopy (AFM) analysis. Figures 8.2 and 8.3 show the respective AFM images.

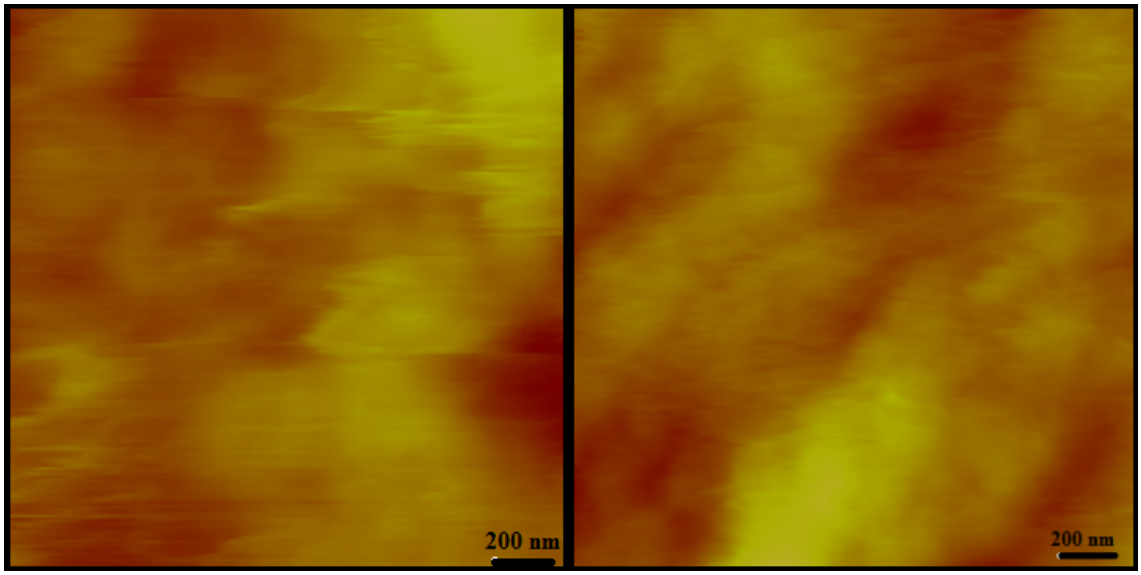

Figure 8.2 – AFM imaging of the smooth PTFE baffle surface

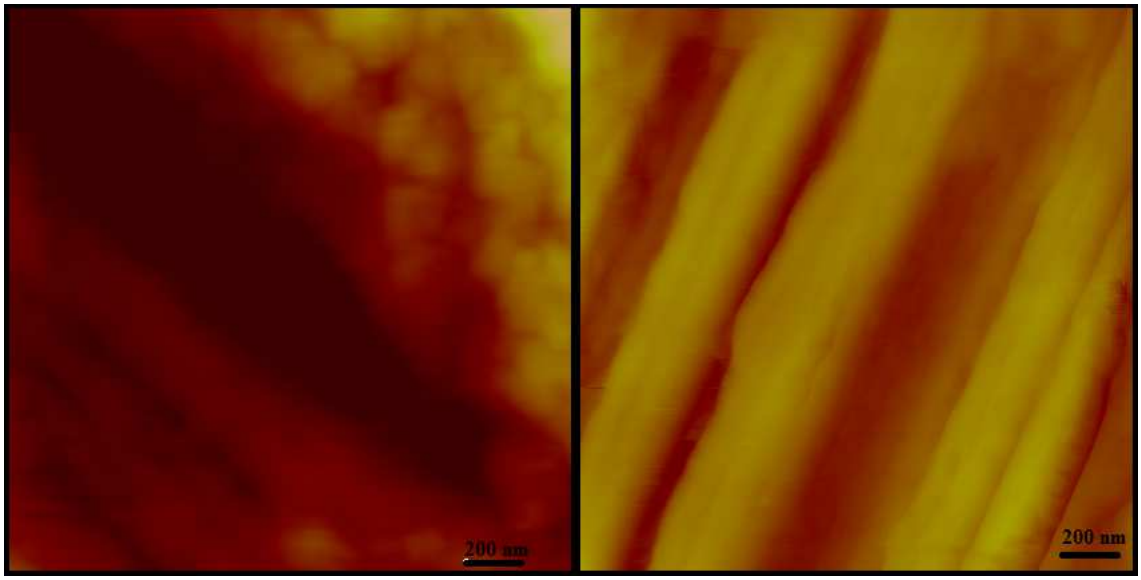

Figure 8.3 – AFM imaging of the much rougher stainless steel baffle surface

As can be seen in the Figures 8.2 and 8.3, the stainless steel surface is rougher than the PTFE counterpart. The PTFE surface shown in Figure 8.2 has a somewhat smooth appearance, whilst the stainless steel surface shown in Figure 8.3 has well defined ridges and crevices. In order to quantify this observation, the surface roughness was then measured by AFM for each material. The results are given in Table 8.1.

Table 8.1 – Surface roughness of the baffles as recorded by AFM

Material	Roughness / nm	Error / nm
PTFE 1	28	±6
PTFE 2	29	±11
S.S. 1	67	±11
S.S. 2	49	±10

Clearly the stainless steel proves a rougher surface than PTFE as shown in the second column of Table 8.1. It is also worth noting that the stainless steel has a much more irregular surface compared to the PTFE. This is reflected by the large difference between the repeat measurements of the surface roughness in Table 8.1.

8.2 - Results and discussion

8.2.1 Stirred tank crystallizer

For the STC with the stainless steel impeller, the results in Table 8.2 were obtained. The data for the PTFE impeller were taken from the previous Chapters.

Table 8.2 – The number of crystals obtained (N_T) and the percentage similarity to the seed in the STC with a stainless steel and PTFE impeller at various stirrer speeds (Ns)

	Stainless Steel		**PTFE**	
Ns (RPM)	**N_T**	**Similarity (%)**	**N_T**	**Similarity (%)**
65	827	100	1089	100
65	757	100	569	100
65	495	100	1162	100
145	1777	100	2594	100
145	1933	100	331	100
145	1097	100	816	100
258	2580	100	1860	100
258	5799	100	2690	100
258	2908	100	854	100
MEAN	2019	100	1329	100

Considering the stainless steel impeller first, no difference in the percentage similarity to the seed was seen when the stirrer speed was changed. As the stirring speed increased, the number of crystals (N_T) obtained was also increased. The Kruskal-Wallis test shows this to be significant (P=0.0273). This outcome is expected as higher stirring speeds lead to greater secondary nucleation rates due to crystal/crystallizer collisions, hence more crystals.

The same similarity figures were obtained for the PTFE impeller (right hand side of Table 8.2). This suggests that the impeller surface played no role in dictating the nucleation mechanism. In terms of the number of crystals, there was no trend with respect to the impeller speed; however, the overall average number of crystals produced appears to be higher for the stainless steel (2019) than for the PTFE (1329). Intuitively the harder material of stirrer would produce more crystals via a crystal/crystallizer collision than the relatively soft PTFE stirrer under the same RPM, however the Kruskal-Wallis test for each pair at the same stirring speed reveals that any difference between the materials is statistically insignificant (P=0.2752, 0.5127 and 0.1266 for 65, 145, and 258 RPM respectively). Consequently, the material of construction has negligible impact on the nucleation mechanism for this crystallization process in the stirred tank crystallizer. This could perhaps be due to the fact that seeding was only present for a fixed period of three minutes before agitation was stopped.

8.2.2 Moving baffle OBC with tight fitting baffles

Similar tests were repeated in the OBC with the moving baffle setup, the data are summarised in Tables 8.3 to 8.5.

Table 8.3 – The number of crystals produced (N_T) and the percentage similarity to the seed in the OBC with stainless steel and PTFE baffles at the various oscillatory frequencies (0.4, 1, and 2 Hz) and at a trough to peak amplitude of 30 mm

	Stainless Steel		**PTFE**	
f(Hz)	**N_T**	**Similarity (%)**	**N_T**	**Similarity (%)**
0.4	4077	86.51	1421	94.02
0.4	1413	97.24	1567	94.89
0.4	1222	81.83	1191	96.31
1	2872	100.00	4198	99.00
1	4559	100.00	4519	93.43
1	5422	99.78	4746	92.90
2	2035	74.50	5025	93.09
2	1167	89.29	4008	90.49
2	3606	93.32	4768	93.20
MEAN	2930	91.39	3493	94.15

Although there appears to be a maximum in the similarity data with the increase of the oscillatory frequency, while no particular trend in the crystal number data for the stainless steel baffles, the Kruskal Wallis test reveals the difference between each frequency to be insignificant (P = 0.065 and 0.1931 for the percentage similarity and the crystal number respectively). The same Kruskal Wallis outcome applies to the similarity and the crystal number data for the PTFE baffles. When cross comparing the data of the stainless steel with the PTFE baffles, the Kruskal Wallis test delivered P = 0.8946 for the similarity and P = 0.3538 for the number of crystals, indicating again that that no significant difference between the data is noticeable.

More experiments were carried out at a fixed amplitude of 15 mm while varying the oscillatory frequencies (Table 8.4) as well as at a fixed frequency of 2 Hz with various oscillatory amplitudes (Table 8.5). Insignificant differences in all the data between the steel and PTFE baffles were returned by the same Kruskal Wallis tests.

Table 8.4 – The number of crystals produced (N_T) and the percentage similarity to the seed in the OBC with stainless steel and PTFE baffles. The OBC was mixed at the various oscillatory frequencies shown in the Table (0.8, 2, and 3.3 Hz) and at a trough to peak amplitude of 15 mm

	Stainless Steel		**PTFE**	
f(Hz)	**N_T**	**Similarity (%)**	**N_T**	**Similarity (%)**
0.8	757	90.09	800	94.63
0.8	2015	100.00	1326	99.77
0.8	1109	97.02	1266	98.97
2	2031	97.24	1971	98.12
2	1728	98.44	981	95.72
2	680	97.06	1180	98.47
3.3	1961	100.00	896	93.19
3.3	944	95.87	3340	98.50
3.3	1278	95.15	1634	97.61
MEAN	1389	96.76	1488	97.22

Table 8.5 – The number of crystals produced (N_T) and the percentage similarity to the seed in the OBC with stainless steel and PTFE baffles operated at a fixed frequency of 2 Hz and with the various trough to peak amplitudes of 7, 15, and 30 mm

	Stainless steel		**PTFE**	
X (mm)	**N_T**	**Similarity (%)**	**N_T**	**Similarity (%)**
7	1363	97.73	1857	97.85
7	1346	99.33	6567	100.00
7	1514	98.41	3252	99.94
15	2031	97.24	1971	98.12
15	1728	98.44	981	95.72
15	680	97.06	1180	98.47
30	2035	74.50	5025	93.09
30	1167	89.29	4008	90.49
30	3606	93.32	4768	93.20
MEAN	1718	93.92	3289	96.32

One thing to note is that the mean number of crystals produced from the stainless steel baffles (Tables 8.3 to 8.5) is always lower than that produced by the PTFE counterpart. This finding is unusual considering that the stainless steel is much harder than PTFE and a larger number of crystals would be produced in the former due to more energetic crystal/crystallizer collisions. A plausible explanation for this finding remains elusive.

8.2.3 Moving baffle OBC with loose fitting baffles

In the previous Chapters, the seed-dissimilar nucleation mechanism was minimised and eventually eliminated by increasing the gap between the baffle edge and the vessel wall. This same type of experimental work was repeated with loose fitted stainless steel and PTFE baffles giving the results shown in Tables 8.6 and 8.7. Applying the Kruskal-Wallis tests to all data, no significant difference could be detected for both the percentage similarity and the number of crystals produced.

Table 8.6 – The number of crystals produced (N_T) and the percentage similarity to the seed in the OBC with loose fitting stainless steel and PTFE baffles at the various oscillatory frequencies (0.8, 2, and 3 Hz) and at a trough to peak amplitude of 30 mm

	Stainless steel		**PTFE**	
f(Hz)	**N_T**	**Similarity (%)**	**N_T**	**Similarity (%)**
0.8	8606	96.22	1660	100.00
0.8	967	96.79	1459	97.05
0.8	1561	99.62	10407	99.88
2	2875	100.00	4797	99.60
2	2504	100.00	587	99.83
2	1066	99.16	14169	99.01
3	878	100.00	1056	98.86
3	1356	98.60	3309	99.52
3	1629	98.83	1990	98.74
MEAN	2382	98.80	4381	99.17

Table 8.7 - The number of crystals produced (N_T) and the percentage similarity to the seed in the OBC with loose fitting stainless steel and PTFE baffles operated at a frequency of 2 Hz and with varying trough to peak amplitudes of 7, 15 and 30 mm

	Stainless steel		PTFE	
X (mm)	**N_T**	**Similarity (%)**	**N_T**	**Similarity (%)**
7	3458	100.00	4517	100.00
7	1443	99.79	988	100.00
7	364	93.13	2851	100.00
15	1924	100.00	5364	99.96
15	211	99.53	1605	99.94
15	1005	99.90	1558	99.42
30	2875	100.00	1056	98.86
30	2504	100.00	3309	99.52
30	1066	99.16	1990	98.74
MEAN	1650	99.06	2582	99.60

Comparing the tight-fit and loose-fit stainless steel baffle arrangements (the left hand sides of Tables 8.3 and 8.6 respectively), the average similarity to the seed was higher in the loose fit baffle system than in the tight-fit one. This result is consistent with what has been presented in the previous Chapters, however the difference between the two systems was deemed insignificant, P=0.1184. Analysing the number of crystals produced, the Kruskal-Wallis difference was again insignificant (P=0.2004). A significant difference (P = 0.0009) was retuned for the PTFE similarity data, whilst an insignificant difference (P = 0.7573) for the PTFE number of crystals data (the right hand sides of Tables 8.3 and 8.6). Nevertheless, the effect of the materials on the nucleation mechanism is small.

8.2.4 The moving fluid OBC

The effect of materials on the nucleation mechanism was further tested in the OBC with the moving fluid configuration. Tables 8.8 and 8.9 show the results as well as the experimental conditions.

Table 8.8 – The number of crystals produced (N_T) and the percentage similarity to the seed in the moving fluid OBC with stainless steel and PTFE baffles at various oscillatory frequencies of 0.8, 2 and 3.3 Hz, and at a trough to peak amplitude of 30 mm

	Stainless Steel		**PTFE**	
f(Hz)	**N_T**	**Similarity (%)**	**N_T**	**Similarity (%)**
0.8	729	94.38	1731	84.40
0.8	721	95.01	757	81.11
0.8	564	98.40	713	81.35
2	1137	95.87	1949	97.49
2	245	98.78	806	95.78
2	315	91.11	736	94.84
3.3	593	92.24	2093	86.05
3.3	574	95.82	926	88.55
3.3	179	98.32	1108	81.86
MEAN	561	95.55	1202	87.94

Table 8.9 – The number of crystals produced (N_T) and the percentage similarity to the seed in the sealed OBC with moving fluid and utilizing stationary, stainless steel and PTFE baffles operated at 2 Hz. Trough to peak amplitudes of 7, 15 and 30 mm were tested

	Stainless steel		**PTFE**	
X (mm)	**N_T**	**Similarity (%)**	**N_T**	**Similarity (%)**
7	1166	100.00	50	100
7	332	100.00	34	100
7	366	100.00	69	100
15	224	100.00	487	100
15	1340	100.00	358	100
15	1367	100.00	819	100
30	393	100.00	112	86.60
30	958	89.04	585	90.77
30	182	100.00	243	88.07
MEAN	703	98.78	306	96.16

Once again, there were no statistically significant differences in both the percentage similarity and the number of crystal data in the moving fluid OBC. When cross comparing the two sets of data between the moving baffle (Table 8.5) and the moving fluids OBC (Table 8.9) with the equivalent systems with PTFE baffles, the Kruskal-Wallis difference was again negligible.

8.4 - Conclusions

After extensive and vigorous testing on the effect of the materials of baffles and impellers on the nucleation mechanisms, no significant difference was discovered for all experimental conditions and configurations. This indicates that the materials of the moving parts within the crystallizers had no influence on the nucleation mechanism for the seeded crystallization of sodium chlorate. The outcomes are in contrast to others in this field, perhaps due to the facts that a very short period of seeding time was used in all tests, in conjunction with the mixing being stopped after the seeding. There would be insufficient fluid motion in the crystallizers to cause any noticeable differences after the controlled introduction of the seed crystal.

Chapter 9 – Primary nucleation

In the previous Chapters, the nucleation mechanisms via secondary nucleation were investigated. The motivation of this Chapter is to examine the nucleation mechanism via primary nucleation in both the STC and OBC. The content of this Chapter is based on the Publication number 5 from the list given at the start of the thesis.

9.1 – Introduction

Kondepudi *et al.* (1990) described non-stirred spontaneous nucleation of sodium chlorate [169] in evaporation crystallisation, in agreement with the work of Kipping and Pope (1898) [170], and found that equal numbers of left and right handed crystals were obtained. On the introduction of stirring, however, the crystals were almost always exclusively of a single enantiomorphism (100 % in most cases). They suggested that secondary nucleation from a spontaneous nucleus coupled with rapid depletion of solute concentration was the likely nucleation mechanism [169]. As the process of secondary nucleation alone cannot result in a single enantiomer, there must be some means of suppressing the crystals of opposite handedness to the original primary nuclei. Kondepudi *et al.* postulated that the rate of secondary nucleation could be high enough such that the solute concentration became sufficiently low to reduce the rate of primary nucleation to essentially zero [169]. Kondepudi *et al.* (1993) monitored the solute concentration during the course of stirred and non-stirred crystallizations where the solute concentration in the stirred case was much lower with time due to enhanced secondary nucleation [171]. How would the likely secondary nucleation be initiated with and without stirring? Kondepudi *et al.* (1995) studied the effect of stirring speed on the observed enantiomeric excess (ee), and found that the stirring rate was proportional to the ee and the value of ee would tend, logarithmically, towards ±1 with increasing the mixing rate [172].

The observations reported by Kondepudi *et al* [169, 171, 172] seems to point out that the chiral symmetry breaking, i.e. the transformation from a symmetric to asymmetric state, could be realised by simply applying mixing to the solution. Martin *et al.* (1996) questioned the origin of the secondary nuclei, and by designing some experiments in which mixing was achieved in different ways, they found that the chiral symmetry breaking was possible due to crystal/mixer collisions. When the mixing created no collisions, e.g. applying fluid flow rather than mechanical stirring, the chiral

symmetry breaking was not seen [141]. In contrast to the previous works (where the driving force for crystallization was evaporation), Qian and Botsaris (1998) investigated cooling crystallization of sodium chlorate and found that their results were consistent with the data from evaporative crystallization, i.e. the individual crystallizations produced exclusively one enantiomer [50]. Botsaris *et al.* (1999) related this outcome with that of Kondepudi's work where a single "mother crystal" underwent secondary nucleation resulting in a single enantiomer in the product crystal crop[173]. Furthermore, Botsaris performed the same experiments but with bubbling applied to the system. The introduction of bubbles created multiple nucleation sites for both handedness crystals and let to both enantiomers in the product crystals where only a single enantiomer was seen before without bubbles [173]. This again supports the hypothesis that a single crystal forms spontaneously before growing into products via secondary nucleation. When more primary nucleation sites are added, multiple mother crystals are formed giving chiral symmetry in the product crystals.

Buhse *et al.* (2000) conducted some clever experiments wherein a solution of sodium chlorate was forced to flow over a seed crystal of sodium bromate to heteroepitaxially nucleate product crystals. The outcome of these trials was that fluid flow was the sole generator of secondary nuclei as no seed crystal/crystallizer collisions were possible [38]. This is a good answer to the previous report by Martin *et al.* (1996) who suggested that contact nucleation due to mechanical stirring was necessary to generate secondary nuclei from a seed crystal and that hydrodynamics were of questionable importance [141].

The findings of Buhse *et al.* (2000) are complementary to the earlier work of Qian and Botsaris (1997, 1998). They proposed an embryo coagulation secondary nucleation (ECSN) model, where embryos of both handedness crystals could exist in the boundary layer of the seed. They also found that the percentage of the product crystals with the same handedness as the seed was highly sensitive to the supercooling. When supercooling passed a threshold of 6 °C, the similarity was decreased with increasing variations between individual experiments [48, 50].

All the cited research in cooling crystallization was carried out in stirred tank crystallizers. Furthermore, the chiral symmetry breaking is associated with the extent of the competition between primary and secondary nucleation rates that are mixing dependent. The motivation of this research is to investigate the chiral symmetry

breaking in the crystallization of sodium chlorate in an oscillatory baffled crystallizer at high supercooling where spontaneous, primary nucleation is allowed to take place. The previous work on seeded, secondary nucleation experiments has demonstrated that different nucleation mechanisms were resulted by different methods of mixing generation, e.g. stirring vs. oscillating. This current work on primary nucleation would support and extend these previous studies on the nucleation mechanism of a chiral crystallization.

9.2 – Experimental setup and procedure

For this investigation, two types of crystallizer were investigated: the stirred tank crystallizer (STC) and oscillatory baffled crystallizer (OBC). In order to minimize any difference due to crystallizer geometries, the glass vessel was common to both devices and the agitator was changed to suit. Figure 9.1 below shows the general apparatus setup for the STC (left) and OBC (right).

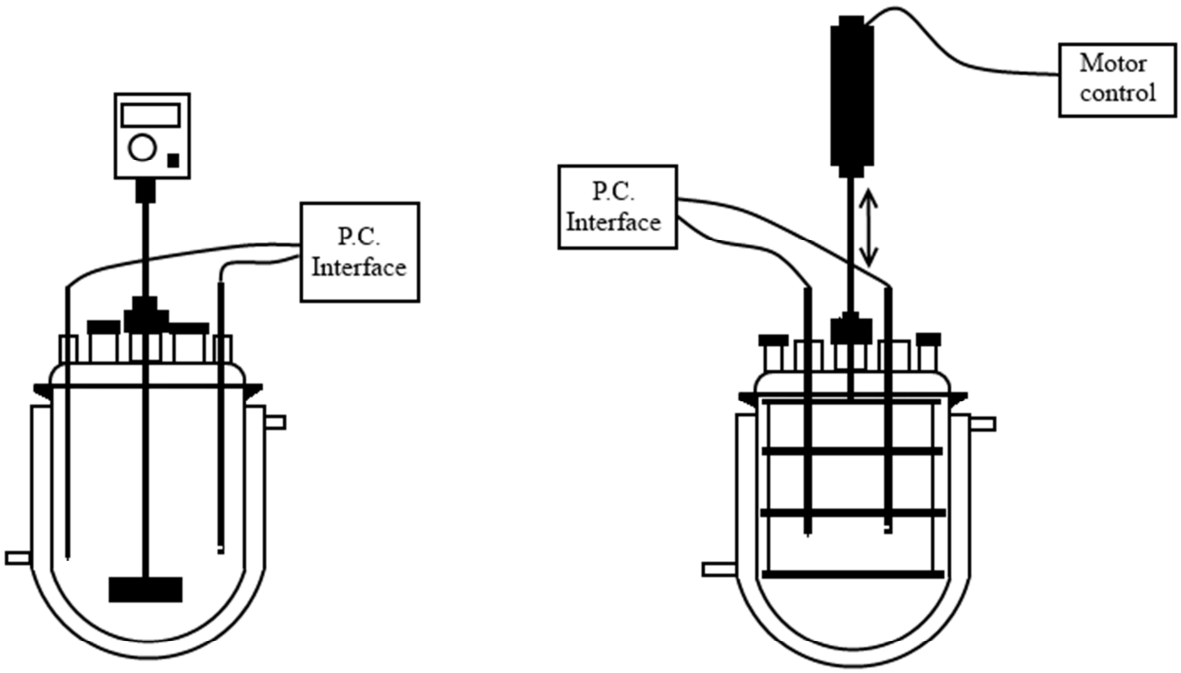

Figure 9.1 – The STC (left) and OBC (right) used in this study. The glass vessel is the same in each case, whilst the method of agitation is altered. The solution turbidity and temperature were logged by P.C. interface

The vessel consisted of an 80 mm diameter, 600 mL jacketed glass vessel that was clamped beneath either an overhead stirrer in the STC or under a linear actuator in the OBC. The vessel was sealed with a six-neck glass lid, which allowed material to be added and extracted from the vessel, the input of the PAT probes, and either a rotary bearing or a linear bearing to provide a good seal for the agitator. For the use as a STC, the vessel was fitted with a 52 mm diameter, PTFE, twin paddle type impeller; with the PAT probes acting as wall baffles to assist with the mixing in the system. In the STC mode of operation, the vessel had a surface to volume ratio of 68.21. For the OBC, the vessel contained 3 PTFE annular baffles of outer diameter 74 mm and an orifice diameter of 36 mm. The baffles were spaced at 30 mm using stainless steel spacers. The baffles were oscillated in the fluid by means of a Copley Motion Ltd. Linear actuator (Model number STA2504S-55-S-S03X) that was controlled by a PC. In the OBC, the PAT probes were moved to a central port on the vessel lid to avoid interfering with the motion of the baffles. For the OBC mode of operation, a surface to volume ratio of 121.29 was determined.

Mixing conditions for both types of vessel were selected that the power density was approximately equal. The mixing conditions for each crystallizer are outlined below in Table 9.1.

Table 9.1 – The mixing conditions for the STC (RPM) and the OBC (frequency and trough to peak amplitude). Under these conditions, the STC would have a shear rate of approximately 10.7 s^{-1}, and the OBC would have a shear rate of approximately 0.59 s^{-1}

	STC	**OBC**
Frequency	-	2.8 Hz
Amplitude	-	15 mm
Stirrer speed	250 RPM	-

Heating and cooling was provided to the crystallizers by a Grant GP200/R2 water heater/chiller. The water bath had a programmable heating element, which allowed good control of the cooling rate applied to the crystallizer. The cooling rates investigated in this work were 0.04, 0.1, 0.2 and 0.4 °C/min. The temperature of the solution was monitored using a stainless steel PT100 temperature probe that was connected to a P.C. interface for data logging. Similarly, the solution turbidity was monitored using a stainless steel turbidity probe with a Hastelloy mirror. The turbidity

was logged using the same P.C. interface as the PT100 probe (HEL Crystaleyes DMS-2).

For each experiment, 446.8 g $NaClO_3$ was added to a separate dissolution vessel along with 400 g of distilled water. Sodium chlorate was sourced from Fisher Scientific and the distilled water was generated in the laboratory. The dissolution vessel was set to 50 °C and a PTFE anchor shaped stirrer agitated the solution for one hour to ensure that the solid had completely dissolved. After dissolution, the solution was filtered using a 1.2 micron Whatman GF/C glass fibre filter to remove any impurities, if any. The filtered solution was then added to the crystallizer and held at 50 °C for a further hour prior to the experiment. The agitator was set to the conditions outlined in Table 9.1, and the cooling profile, which was pre-set on the water bath, started. The data logger for the temperature and turbidity data was switched on and remained so for the course of the experiment. After nucleation, samples of the slurry were taken every hour for three hours and the crystal enantiomorphism analysed by polarised light microscopy. Three runs were undertaken at each cooling rate under the conditions listed in Table 9.1, ensuring good repeatability.

9.3 – Results and discussion

9.3.1 Stirred tank crystallizer

Based on the research set out earlier by Kondepudi et al. it can be envisaged that the STC *should* produce crystals of exclusively one enantiomer. The polarised light microscopy (PLM) of the product crystals from the STC are shown in Figures 9.2-9.5.

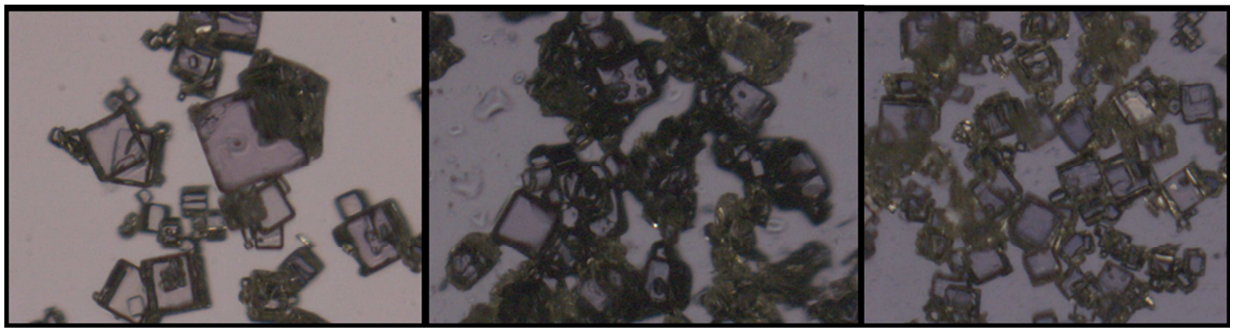

Figure 9.2 – PLM images of the crystals produced at a cooling rate of 0.4°C/min in the STC at 250 RPM. All of the crystals bore the same enantiomorphism (in this case dextrorotatory) except for one sample (far right) where a single levorotatory crystal was detected in the crystal crop

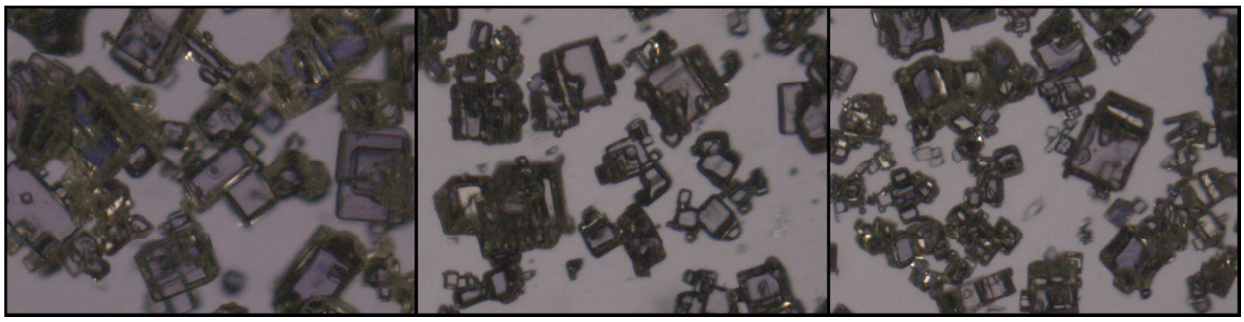

Figure 9.3 – PLM images of the crystals obtained at a cooling rate of 0.2°C/min in the STC at 250 RPM. Almost all of the crystals obtained were levorotatory. Only a small number of dextrorotatory crystals were detected from the three repeated experiments

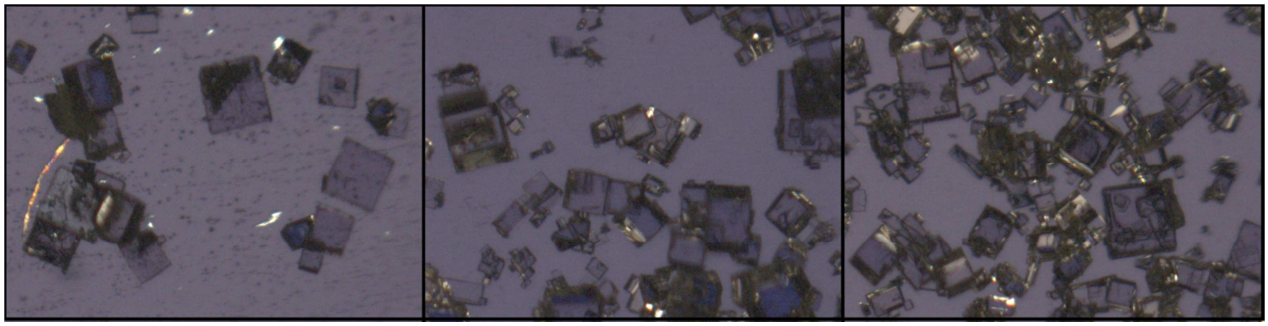

Figure 9.4 – PLM images of the product crystals from the STC at a cooling rate of 0.1°C/min and agitation rate of 250 RPM. Although the majority of the crystals were of a single enantiomorph, a small number of crystals of the opposite form to the bulk existed in all the samples

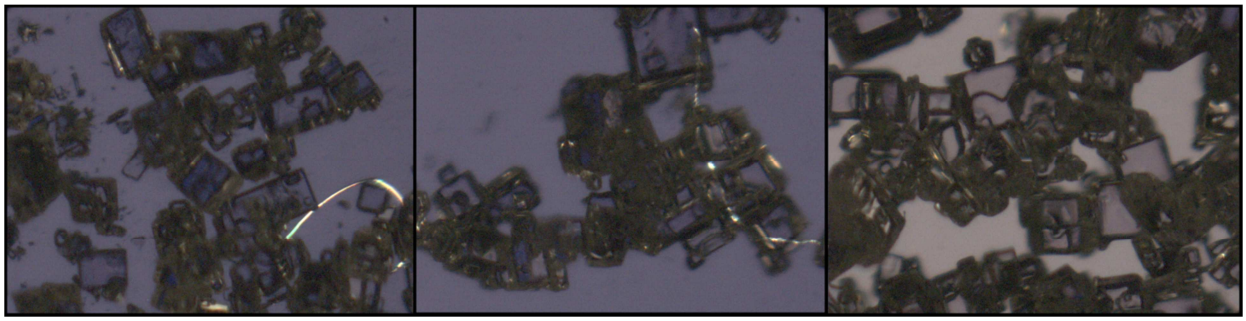

Figure 9.5 – PLM images of the product crystals obtained using a cooling rate of 0.04°C/min in the STC at 250 RPM. Almost all of the product crystals obtained were of a single enantiomorph. Very few crystals of the "minority form" were detected

From Figures 9.2 to 9.5 above, it can be seen that the majority of the crystals from each experiment were of a single enantiomorph. This is in line with the expected outcome. The exact percentage can be quantified by counting the number of crystals of

each enantiomorph in the samples and determining the ee of the sample, which are given below in Table 9.2.

Table 9.2 – The average enantiomeric excess from the STC experiments at a mixing rate of 250 RPM and at cooling rates of 0.4, 0.2, 0.1 and 0.04 °C/min

Cooling rate (°C/min)	Average ee (absolute)	±Std. Error
0.4	0.999	0.000673
0.2	0.995	0.004191
0.1	0.988	0.006953
0.04	0.961	0.03072

The data presented in Table 9.2 together with the images in Figures 9.2 to 9.5 strongly support the previous work by Kondepudi *et al.* who suggested that the primary nucleation of sodium chlorate in a crystallizer would occur via a single "mother crystal", which gives rise to product crystals of the same form. Because the ee was slightly less than 1, this may be due to the hypothesis that a few nuclei of the opposite enantiomorph would have been produced; the mechanism for this is currently unclear.

9.3.2 Oscillatory baffled crystallizer

The identical experiments were performed in the OBC and the results are shown below in Figures 9.6 to 9.9.

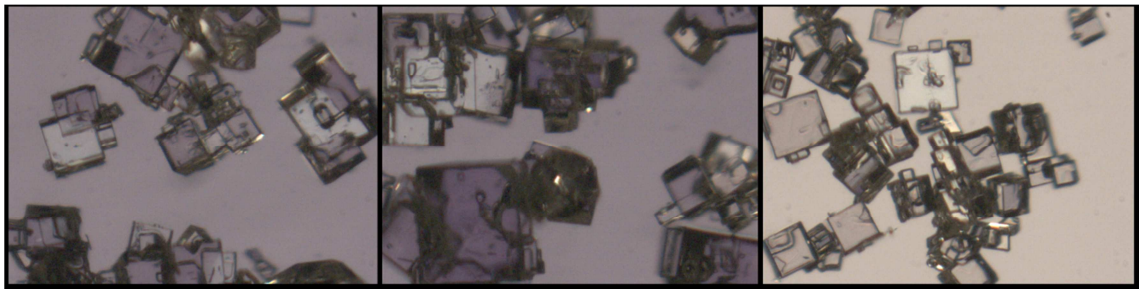

Figure 9.6 – PLM images of the crystals produced at a cooling rate of 0.4°C/min in the OBC with an oscillatory frequency of 2.8 Hz and trough to peak amplitude of 15 mm. There is a mixture of dextro- and levorotatory crystals present in the product crystal crop

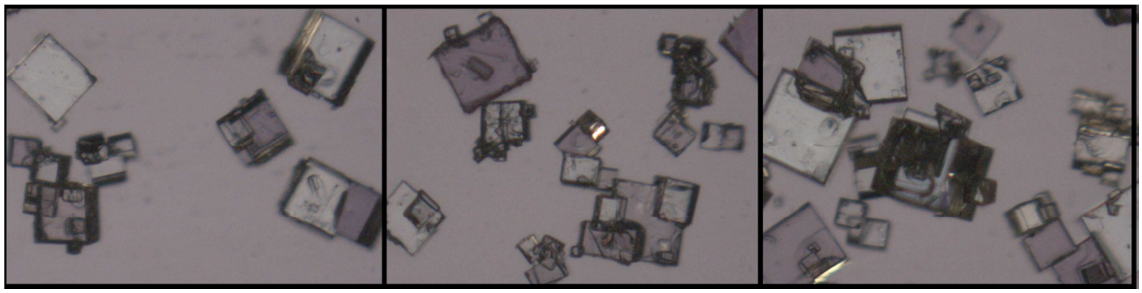

Figure 9.7 – PLM images of the crystals formed at a cooling rate of 0.2°C/min in the OBC. The mixing conditions were a frequency of 2.8 Hz, and an amplitude of 15 mm. Both enantiomorphs are present in the product crystals

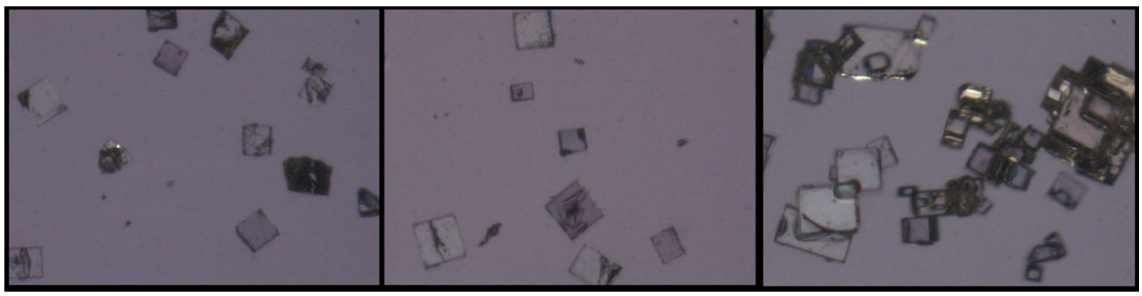

Figure 9.8 – PLM images of the crystals obtained with an oscillatory frequency of 2.8 Hz, an amplitude of 15 mm, and at a cooling rate of 0.1°C/min in the OBC. Both enantiomorphs are produced in almost equal measure

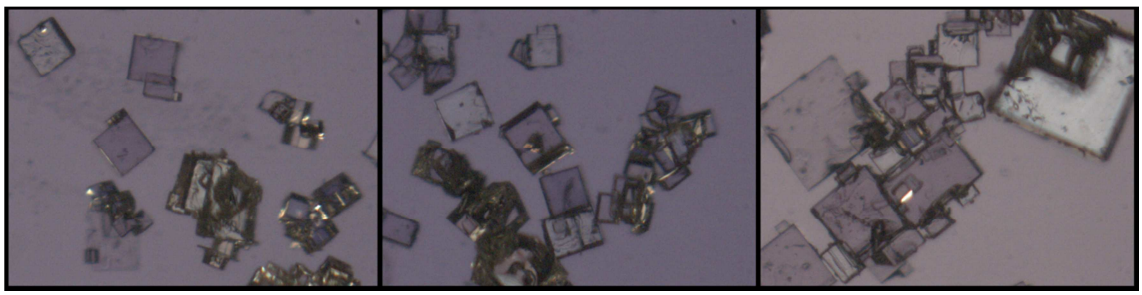

Figure 9.9 – PLM images taken of the crystals made from cooling at a rate of 0.04°C/min in the OBC with a frequency of 2.8 Hz and an amplitude of 15 mm. There is a mixture of dextro- and levorotatory crystals present in the product crop

Both enantiomorphs are visible in all of the images in Figures 9.6 to 9.9. The ee values were determined in the same way as before and summaries in Table 9.3.

Table 9.3 – The average enantiomeric excess from the OBC experiments. In each case the frequency was 2.8 Hz and the amplitude was 15 mm. Cooling rates of 0.4, 0.2, 0.1 and 0.04 °C were investigated as shown in the Table below

Cooling rate (°C/min)	Average E.E. (absolute)	±Std. Error
0.4	0.488	0.132147
0.2	0.158	0.099379
0.1	0.312	0.117157
0.04	0.594	0.170199

The data in Table 9.3 are in clear contrast to the outcome of the STC experiments, with both enantiomeric identities detected. This could suggest that either two parent crystals were generated initially and competed for secondary nucleation; or multiple nuclei were formed as opposed to a single original crystal. This outcome provides evidence that the nucleation mechanism in the OBC would have been different to that seen in the STC. Producing product crystals of both dextro- and levorotatory enantiomorphism would imply that the OBC could have a stronger preference for primary nucleation than for secondary nucleation, but what could be the real cause for this? Could the supersaturation generation and/or depletion rates be different in the two systems, which have affected the nucleation mechanism?

The STC and OBC experiments were repeated with the crystallizer fitted with the FTIR probe and the changes in relative absorbance with time are shown in Figures 9.11 and 9.12 for each cooling rate in the two devices. Note that the y axis, relative absorbance, is directly associated with the solution concentration. In this case, the relative absorbance refers to the absorbance at a given time, t, minus the value of absorbance at the start of the experiment, t=0. Generally, the absorbance increased as the solution became supersaturated, and then decreased in various degrees as the direct result of nucleation. Visibly the rate of the increase and the rate of de-crease of absorbance are somewhat different for the two systems.

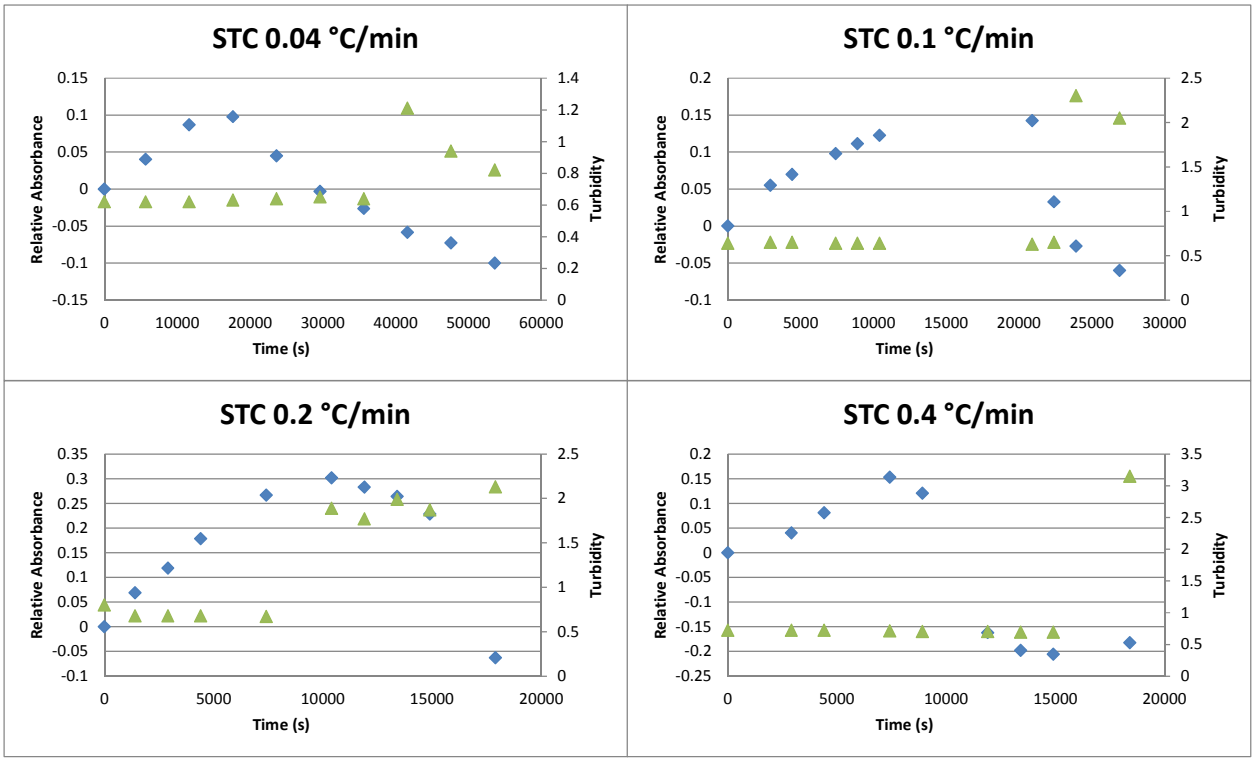

Figure 9.11 – The absorbance indicated by the blue data points and the solution turbidity indicated by the green data points as a function of time in the STC at various cooling rates

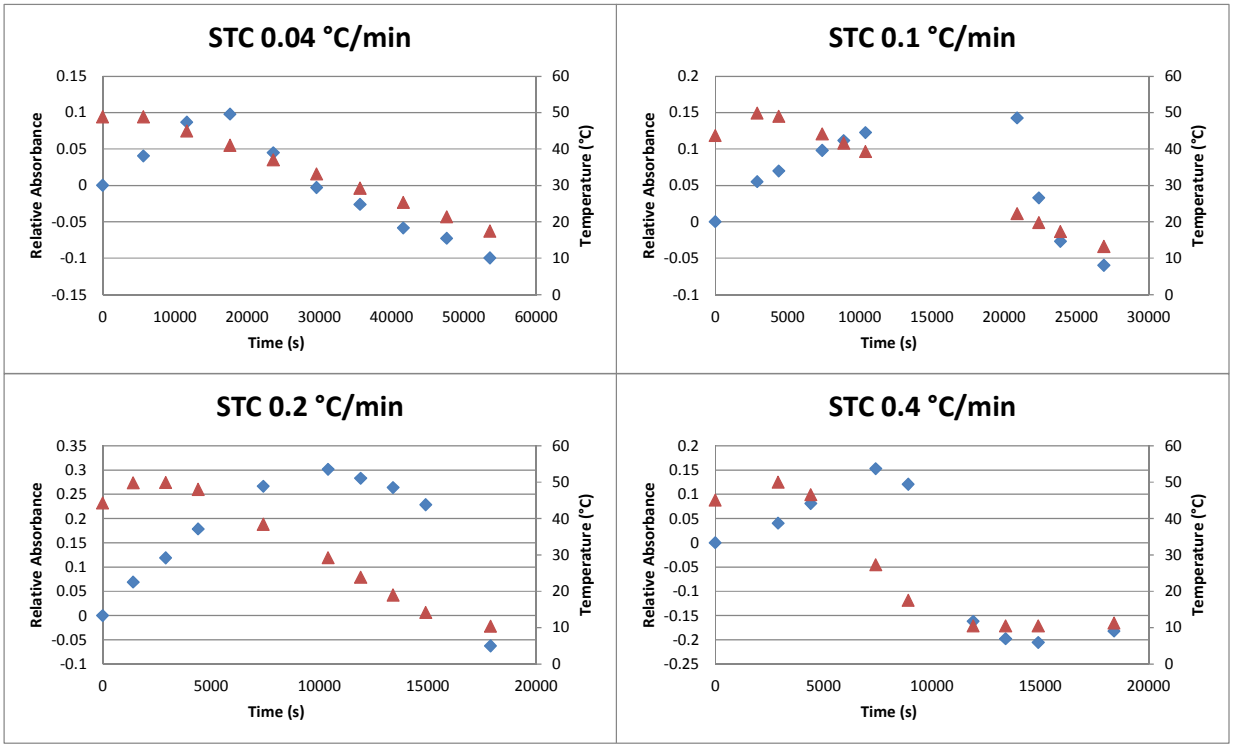

Figure 9.12 – The absorbance (blue data points) and temperature of the solution (red data points) for the STC at varied cooling rates

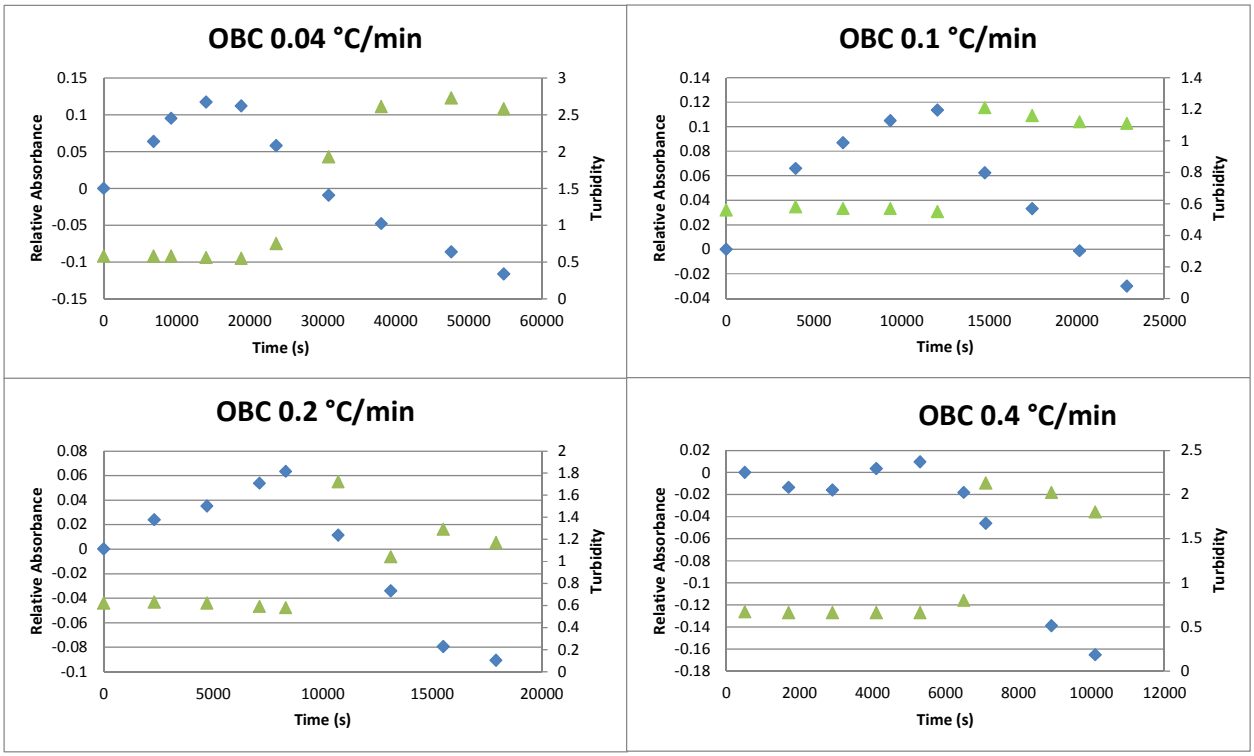

Figure 9.13 – The absorbance indicated by the blue data points and the solution turbidity indicated by the green data points as a function of time in the OBC at various cooling rates

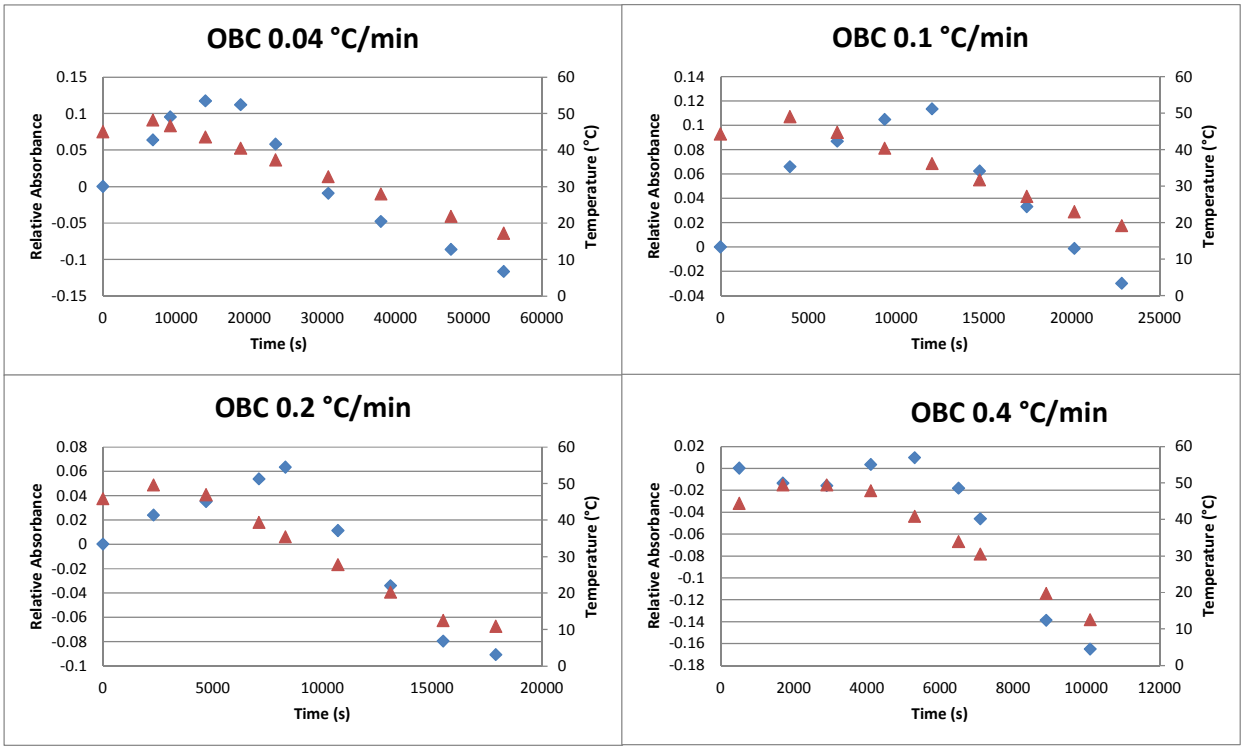

Figure 9.14 – The absorbance (blue data points) and temperature of solution (red data points) for the OBC at varied cooling rates

In Figures 9.11 and 9.13, the points at which the solution absorbance began to decrease indicate the onset of nucleation, which always occured earlier in the OBC than in the STC at the same cooling rate. For each case, the nucleation point by solution absorbance coincides with the onset of nucleation as indicated by a sharp increase in solution turbidity. Reusing the free energy diagram of Figure 2.1.4, the lower supersaturation required to nucleate in the OBC would mean the lower critical free energy barrier (ΔG_{crit}) and in turn, the smaller critical nuclei radius (r_{crit}). This would be consistent with the earlier occurrence of nucleation in the OBC than that in the STC. The question now is what has lowered the energy barier for nucleation in the OBC?

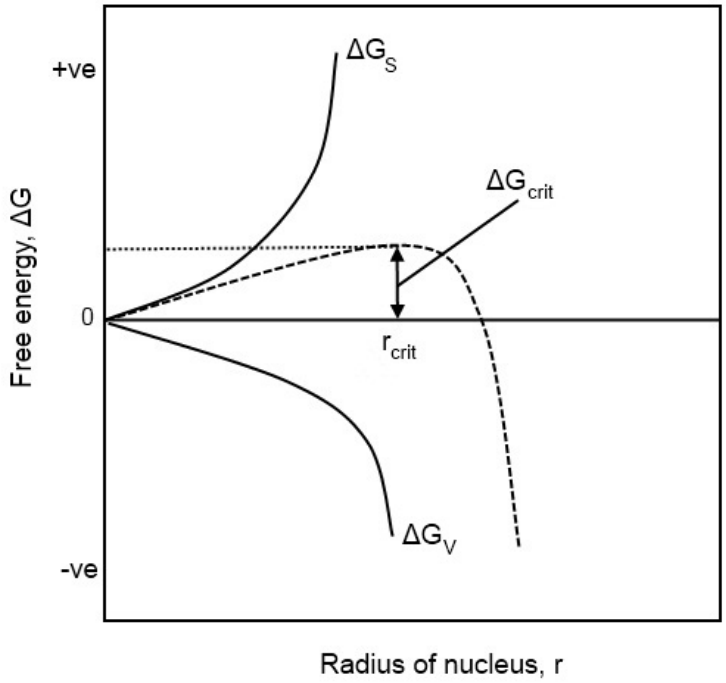

Figure 2.1.4 – Critical free energy (ΔG_{crit}) and critical radius (r_{crit}) of nucleation, derived from [29]

Could it be possible that the mixing in the OBC results in a much more homogenous distribution of solute concentration? Could the mixing in the OBC dissipate more energy into the solution than the STC?

In order to probe this further, the regions of Figures 9.11 and 9.13 that relate to the de-supersaturation (the right hand side of the maxima) were focused upon and the gradient of the lines determined in MatLab, as shown in Table 9.4.

Table 9.4 – The gradients (x 10^{-6}) of the generation of and depletion of supersaturation at various cooling rates in the STC and OBC

	Supersaturation depletion	
cooling rate (°C/min)	**STC**	**OBC**
0.04	5.26	6.12
0.1	31.66	12.35
0.2	59.21	16.63
0.4	65.97	39.49

The data in Table 9.4 clearly indicate that the STC had substantially faster rates of depletion of solute concentration with time compared to the OBC under identical operating conditions.

These findings are significant and the first of this kind in the OBC, as such, this would have profound ramifications on the understanding of the nucleaiton mechanism in the two types of crystallizers. In the OBC, the rates of supersaturation depletion were much slower than that in the STC, while it nucleated earlier and at lower supersaturation in the former than the latter. The faster depletion rates of supersaturation in the STC lead to almost exclusively a single enantiomorph, while the slower rates generated crystals of both handedness. It seems that the faster de-supersaturation rate suppressed primary nucleaiton of the opposite-handed crystal to those initially formed, while the slower rate favoured both.

Previous research showed that a product crystal crop of a single enantiomorph was resulted when there was no mixing, while both enantiomorphs were harvested when mixing was applied. This would confirm the hypothesis that the mixing in the OBC is somewhat stronger, or more uniform than the STC at the equivalent conditions. It is the degree and the uniformity of mixing generation that has influenced the nucleation mechanism.

Although at first glance, these findings are exciting, it must be noted that no plausible explanation is in place as of yet to describe why in Figures 9.11 and 9.13, the left hand side of the graphs show an increase in absorbance with time. An increase in absorbance would be expected to be associated with an increase in solution concentration. As no material is added to the vessel after dissolution, i.e. the

concentration is at a maximum at time = 0 s, explanations must be sought to explain why the absorbance increases initially prior to falling at the onset of nucleation.

It could be that there is evaporation of water from the system, but given the construction of the vessel, and the robust sealing protocol that was put in place, this seems unlikely. Another possibility could be that the FTIR probe tip is detecting a local concentration of solute molecules that must be treated seperately from the bulk solution. Perhaps the probe tip (a crystalline structure in its own right) is acting as a nucleation site; attracting solute molecules to the immediate vicinity in a manner similar to that of a seed crystal. The most likely cause of the increase of relative absorbance could be due to a temperature dependance of the absorbance reading. Considering the Figures 9.12 and 9.14, this seems complex, as in each case, the absorbance increases slightly before decreasing. This is despite the temperature constantly decreasing. A robust calibration of the FTIR system with both the sodium chlorate : water system and the IR background at varied temperatures therefore becomes necessary to draw valid conclusions with respect to the solution concentration.

9.4 - Conclusions

From this work, it can be seen that the STC generally nucleated via a mechanism similar to that proposed in the earlier works; a single mother crystal nucleated first and a generation of product crystals was created with almost identical enantiomorphism to that of the mother crystal due to crystal/crystallizer collisions, dendrite breakage, or some other common secondary nucleation mechanism.

The OBC continues to present results which are indicative of an alternative mechanism through which nucleation took place, where the enantiomeric excess was strongly suggestive of many of these “mother crystals” being formed prior to secondary nucleation taking place. By analysing the concentration measurements, the single enantiomorph mechanism was associated with faster rates of supersaturation depletion, while the dual enantiomorph mechanism was related to the slower rates, indicating that the OBC nucleated via a mechanism less dominated by secondary nucleation.

Chapter 10 – Conclusions and Further Research

This ultimate chapter presents the conclusions reached as a result of the research undertaken in the previous chapters. Some suggestions for future research are also put forward.

10.1 – Conclusions

For seeded nucleation in the OBC, the product crystals obtained were of a different enantiomorphic profile to those obtained in the STC, where the product crystals were always of the same enantiomorphism as the seed crystal. This indicates that a seed-similar nucleation mechanism dominated the nucleation process in the STC and a seed-dissimilar nucleation process was present in the OBC. This work was the first of its kind.

In both devices, the presence of a scraping action was found to affect the nucleation mechanism. For the STC, an introduction of scraping promoted the formation of seed-dissimilar product crystals. Conversely, the removal of scraping from the OBC increased the percentage similarity to the seed crystal. In both the STC and the OBC, enhancing the mixing intensity by raising the stirrer speed or oscillatory frequency resulted in no significant change in the outcome of the experiment. The scraping action appeared to have a more significant effect on the nucleation mechanism than the rate of scraping.

For the moving baffle OBC, the internal fluid mechanical environment was altered by reducing the oscillatory amplitude. This decreased the sizes of mixing eddies within the fluid and changed the surface renewal in the boundary layer of the seed crystal. The lower the amplitude, the greater the similarity to the seed was obtained. At the lowest amplitude of 7 mm, the product crystals were exclusively via a seed-similar nucleation mechanism, whereas at the highest amplitude of 30 mm, the product crystal crop displayed a seed-dissimilar nucleation mechanism.

In the OBC, the removal of any scraping was achieved by using a moving fluid setup wherein the fluid was pulsed around stationary baffles. This resulted in product crystals of exclusively the same enantiomorphism as the seed crystal, except at the highest amplitude, where some seed-dissimilar nucleation was observed. This outcome further validates the earlier observation that the scraping action influenced the

nucleation mechanism in the crystallizing vessel. A second outcome of the moving fluid OBC work was that splashing and evaporation were found to cause seed-dissimilar nucleation. When splashing was allowed in an unsealed moving fluid OBC, strong evidence of seed-dissimilar nucleation was found in the product crystal crop. Furthermore, in the sealed moving fluid OBC, the amplitude and frequency was found to have very little effect on the nucleation mechanism, with no seed-dissimilar nucleation observed unless a high amplitude was utilised.

Seeded crystallization experiments were performed in OBCs and STCs that utilised either PTFE or stainless steel agitators. It was found that under the conditions investigated in this work, no significant change in the outcome of the experiment (in terms of both the percentage similarity to the seed and the number of crystals produced in each test) could be detected. It was concluded that the scraping action and the internal fluid mechanical environment around the seed were more important in deciding the nucleation mechanism than the materials of construction of the agitators.

When the crystallization tests were performed without the addition of seeds, more differences between the OBC and STC were revealed. Analysis of the product crystals from the STC revealed an enantiomeric excess of approximately 1 for each cooling rate investigated. This was consistent with previous research, which suggested that such an outcome was evidence of a single “mother crystal” forming first and generating a secondary crop of product crystals due to rapid secondary nucleation. The OBC, on the other hand, yielded a product crop with an enantiomeric excess closer to 0 due to the presence of both enantiomorphic forms of sodium chlorate being produced in almost equal measure. This would imply that the OBC would have had the capability of producing multiple “mother crystals” before undergoing further nucleation.

The solution absorbance as recorded by FTIR spectrophotometry provided some limited, but nonetheless useful data on the rates of supersaturation depletion in both devices. The STC was found to have much faster rates of de-supersaturation than the OBC. This is consistent with spontaneous primary nucleation of a single crystal followed by rapid secondary nucleation, as indicated by the steep gradient in the concentration profile [171]. Much slower rates of supersaturation depletion in the OBC would mean more time for primary nucleation to take place, possibly explaining the presence of both dextro- and levo-rotatory crystals being produced.

This final observation may form part of the answers to the question as to why the OBC nucleated without seeding whereas seeds were essential in the STC for the same process. The effective mixing in the OBC could reduce the critical free energy/nucleus radius size, allowing nucleation to occur at lower concentrations than that in the STC. How the mixing allows such a reduced free energy barrier is yet to be determined.

It must be noted that the tentative answers to the above fundamental questions should be treated separately from the outcomes of this thesis work, where the scraping and the local mixing environment around the seed crystal have shown to initiate unexpected nucleation whether desirable or not in the OBC. This nucleation has been termed as seed-dissimilar secondary nucleation. With this knowledge, it should become possible to avoid such conditions in continuous crystallization, resulting in more straightforward experiments and product crystals of a desired specification.

10.2 – Future research

Based on this research, the following recommendations are outlined:

- The scraping action may act as a result of high fluid shear forces at the baffle edge – some experiments could be performed to quantify this fuller by using varied baffle gaps (similar to those performed by Ni et al.[108]). By doing so, the true nature of scraping may be elucidated. This work would also shed some light into why the OBC
- The work conducted so far involved batch devices, a logical next step would be to implement the unique features of scraping into the COBC and to examine how effectively the nucleation events could be measured, controlled and utilized.
- Assuming the different nucleation mechanism in the OBC proceeds via a two-step mechanism, it could be expected that the nucleation could occur via a dense liquid state prior to crystalline nuclei forming. The mixing conditions of the OBC should have a strong influence on this mechanism and by utilizing a technology such as Nanoparticles Tracking Analysis, this effect may be quantified. Some initial investigations into this were conducted with the OBC and sodium chlorate solutions; these are presented in the Appendix E.
- The results from the IR experiments should be repeated and expanded upon. The concentration analysis by FTIR has provided interesting, but very much limited information on the rates of local supersaturation generation and

depletion. Further work is recommended to examine the effects of mixing, cooling and crystallizer configurations on these rates. In addition, the concentration measurements should also be applied to the seeded nucleation work to investigate how these rates could affect the crystal handedness.

Appendix A - Determination of power dissipation in the crystallizers

The basis of comparison between the various crystallizing devices has been the power dissipation. This appendix contains the graphs used to determine the operating conditions of the crystallizers used in this thesis work..

The stirred tank crystallizers

Power density in the STCs is calculated using the following equation:

$$\frac{P}{V} = \frac{P_O \rho N_s^3 D_S^5}{V_L} \qquad (A1)$$

Where P/V is the power density (W m^{-3}), ρ the fluid density (1456 kg m^{-3} at 40 °C), N_s the speed of the stirrer (rps), D_S the diameter of the stirrer (m), V_L the volume of liquid in the STC (0.0005m^3) and P_O the dimensionless power number of the agitator.

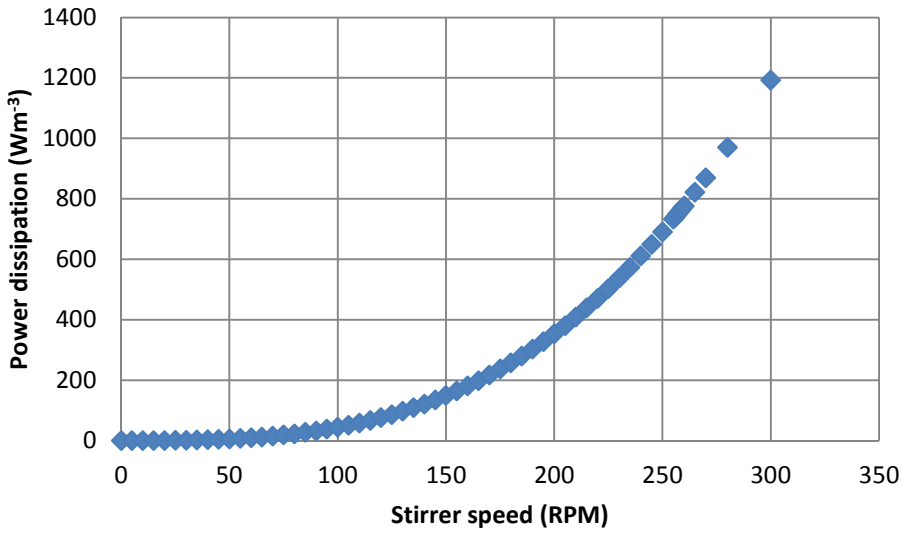

Figure A1 – Power dissipation of the STC with varied stirring speed

The oscillatory baffled crystallizers

The power density of the OBC is estimated using the quasi steady flow model proposed by Baird and Stonestreet (1995):

$$\frac{P}{V} = \frac{2\rho N_b}{3\pi C_D^2}\left(\frac{1-\alpha^2}{\alpha^2}\right) x_o^3 (2\pi f)^3 \qquad (A2)$$

Where N_b the number of baffles per unit length of OBC (m^{-1}), C_D the discharge coefficient of the baffles (taken as 0.7), x_o the centre to peak amplitude of oscillation (m), f the oscillation frequency (Hz) and α the baffle free area ratio. The free area ratio, α is defined by the area of the orifice divided by the total baffle area.

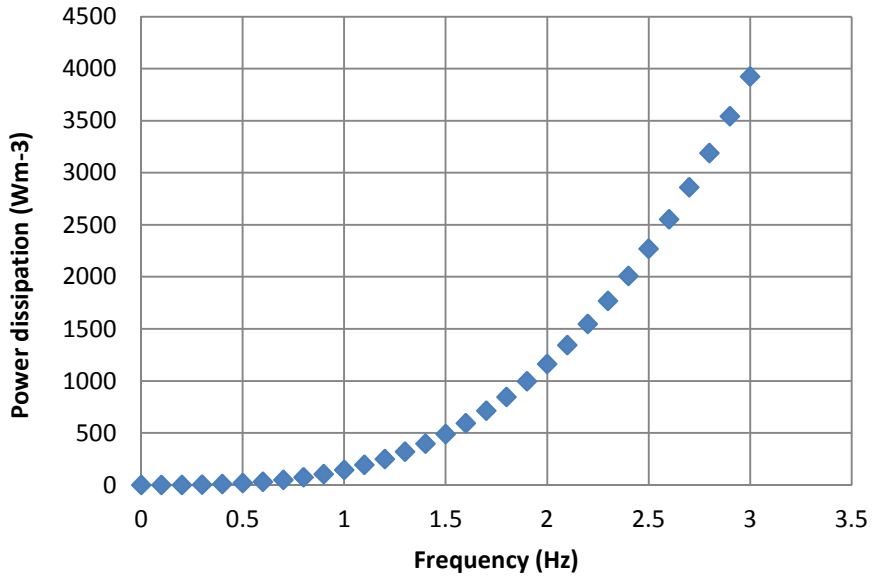

Figure A2 – The power dissipation of the moving, tight fit baffle OBC with varied frequencies

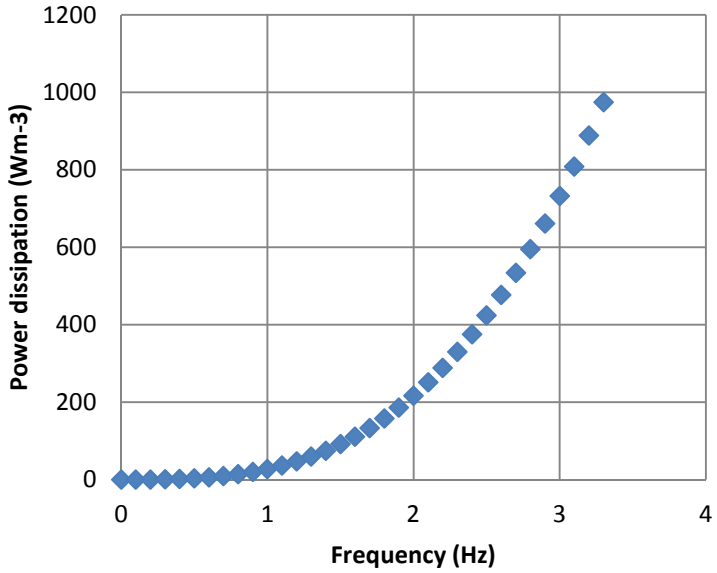

Figure A3 – The power dissipation of the OBC with loose fitting baffles with varied frequencies

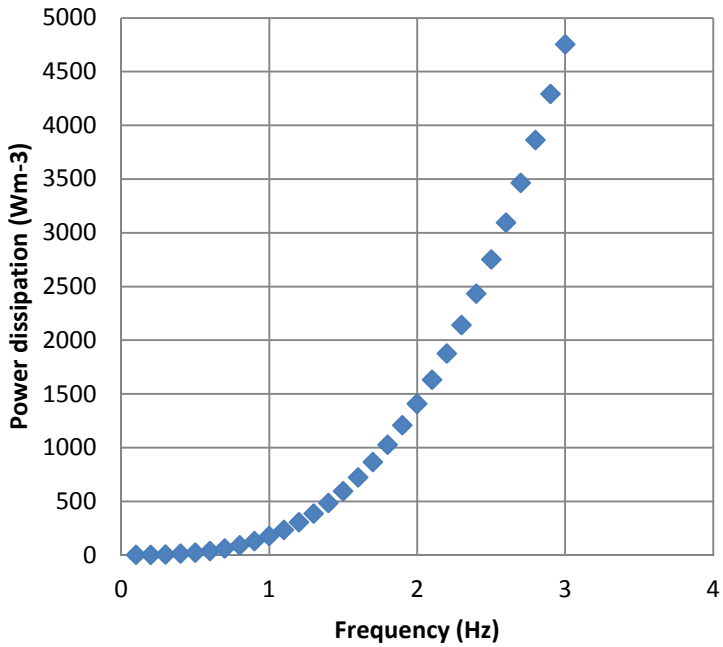

Figure A4 – The power dissipation of the moving fluid OBC with varied frequencies

From the graphs presented here, it can be seen that the power dissipation is sensitive to small changes in the frequency or stirring speed of the crystallizer. It should also be noted that while the overhead stirrer used for the STC could be varied in approximately 1 RPM increments, the OBC was limited to increments of 0.1 Hz. This prevents the power density being matched, particularly at high oscillatory frequencies.

Appendix B – Determination of supersaturation

Mullin describes in detail how supersaturation can be calculated. A number of values must be defined in order to do so:

The concentration driving force is defined as:

$$\Delta C = C - C^*$$

Where C is the saturation concentration and C^* is the concentration at the supersaturation temperature.

The supersaturation ratio is defined as:

$$S = \frac{C}{C^*}$$

Relative supersaturation can be defined by:

$$\sigma = \frac{\Delta C}{C^*} = S - 1$$

Note that in Denk's thesis, the term σ is replaced with the term S and C^* by the term C_O.

C is taken at the temperature that the solution is made up at. For example, at 42 °C, C=78.66 g/100 mL sat. sol.

C^* is the temperature that the solution is cooled to. In each of Denk's experiments, this was 30 °C. So C^* would be equal to 73.37 g/100 mL sat. sol.

The term sat. sol. refers to the fact that the concentrations are based on a saturated solution.

Based on the above equations, the supersaturation can be calculated for each temperature, or, initial concentration. The results are shown in table 4.

Table B1 – Supersaturation for different supercoolings

T_{sat}/ °C	**C**	T_{sup}/ °C	**C***	ΔC	σ	ΔT / °C
30	73.37	30	73.37	0	0	0
30.5	73.58	30	73.37	0.21	0.002862	0.5
31	73.79	30	73.37	0.42	0.005724	1
32	74.26	30	73.37	0.89	0.01213	2
33	74.68	30	73.37	1.31	0.017855	3
34	75.1	30	73.37	1.73	0.023579	4
35	75.52	30	73.37	2.15	0.029304	5
36	76	30	73.37	2.63	0.035846	6
37	76.42	30	73.37	3.05	0.04157	7
38	76.84	30	73.37	3.47	0.047295	8
39	77.32	30	73.37	3.95	0.053837	9
40	77.75	30	73.37	4.38	0.059697	10
41	78.18	30	73.37	4.81	0.065558	11
42	78.66	30	73.37	5.29	0.0721	12
43	79.1	30	73.37	5.73	0.078097	13
44	79.57	30	73.37	6.2	0.084503	14
45	80.01	30	73.37	6.64	0.0905	15

Supersaturation

For a solution saturated at 40 °C and cooled to 30 °C, the supersaturation is calculated as follows:

$$C = 77.75\ g/100\ mL \quad C^* = 73.37\ g/100\ mL.$$

$$\Delta C = C - C^* = 77.75 - 73.37 = 4.38\ g/100\ mL$$

$$\sigma = \frac{\Delta C}{C^*} = \frac{4.38 g/100 mL}{73.37 g/100 mL} = 0.0597$$

Multiplying by 100% gives the percentage supersaturation:

$$\sigma_{\%} = 100\ x\ \sigma = 100\%\ x\ 0.0597 = 5.97\%$$

The supercooling is simply the starting temperature minus the final temperature:

$$\Delta T = T_1 - T_2 = 40°C - 30°C = 10°C$$

Determination of supersaturation for a supercooling of 1 °C

$\Delta T = 31\text{-}30°C = 1\ °C$

C* = solution concentration at supersaturation (30 °C) = 73.37 g$NaClO_3$/100mL sat. sol.

C = solution concentration at saturation (31 °C) = 73.79 g$NaClO_3$/100mL sat. sol.

$$S = \sigma + 1$$

$$S = \left(\frac{C - C^*}{C^*}\right) + 1$$

$$S = \left(\frac{73.79 - 73.37}{73.37}\right) + 1$$

$$S = \left(\frac{0.42}{73.37}\right) + 1$$

$$S = 1.0057$$

Appendix C - Comparison of recycled and fresh starting material

The material used for these trials comes in three forms:

1) The material purchased from Fisher Scientific. This is termed the "fresh" material

2) The mother liquor that was completely dried using a rotary evaporator. The resulting dry powder is the "recycled A" material.

3) The mother liquor that was evaporated to make a very concentrated solution. The solution yielded material on cooling. This filtered material is termed the "recycled B" material.

The recycled sodium chlorate must be compared to the fresh sodium chlorate delivered from Fisher. We suspect that there is a difference in the purity of the starting materials. A qualitative analysis was performed using a Hach DR/4000 spectrophotometer in the wavelength range 276 – 650 nm as presented in Figure C1.

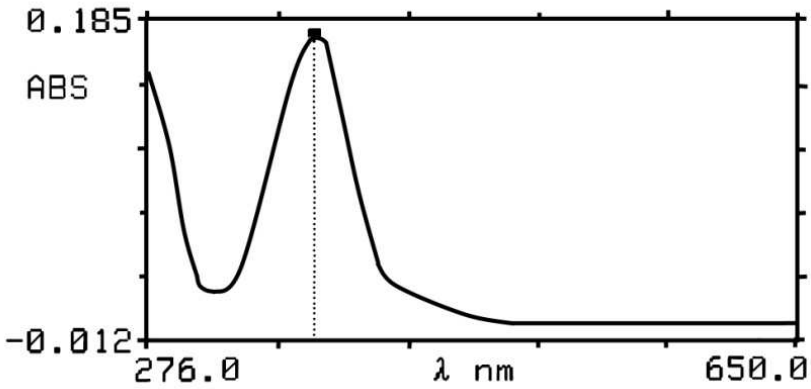

Figure C1 – Analysis of fresh material

From Figure C1 above, it can be seen that there is a clear peak around the 370 nm region. In order to investigate the purity of the materials further, analyses were performed in the range of 360 – 380 nm. Figures C2-C4 show the traces for the fresh material, recycled A, and recycled B material.

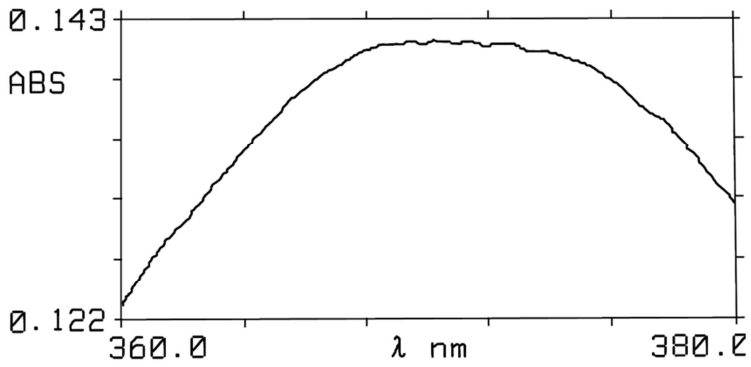

Figure C2 – UV-Vis analysis of fresh material

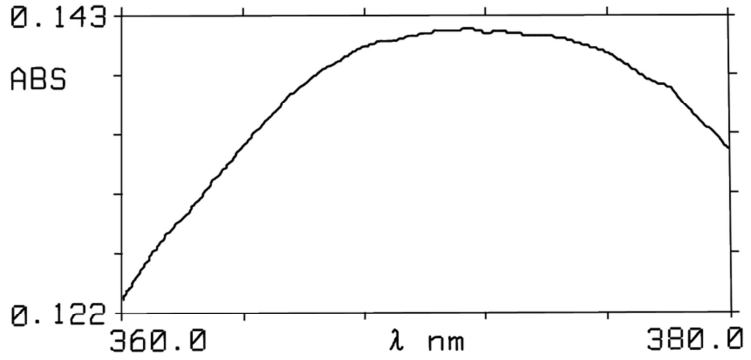

Figure C3 – UV-Vis analysis of recycled A material

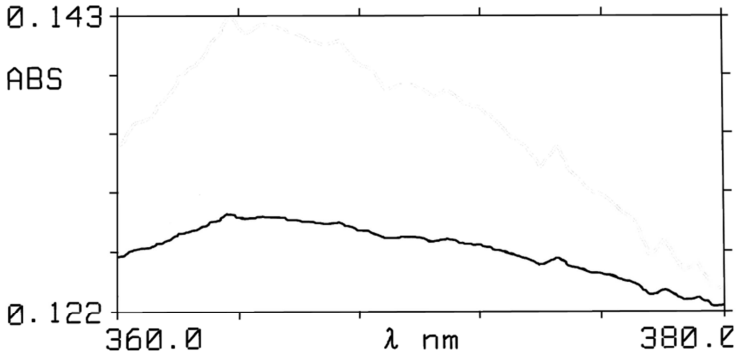

Figure C4 – UV-Vis analysis of recycled B material

From The above analysis, it can be seen that the purity profiles of Figures C2 and C3 are almost the same. There is only a slight change in the width of the peak seen to the right hand side of the chart. It would be reasonable to assume that the purity of the fresh material is similar to that of the material obtained by completely drying the mother liquor in the rotary evaporator.

Looking at Figure C4, it is apparent that the material purity is vastly different to the other materials. The trace is much more jagged in appearance and the absorbance is much less when compared to the other material.

Based on the similarity in the purity profiles for the fresh and recycled A material, we consider the material to be interchangeable. When the mother liquor is not evaporated to complete dryness, but instead concentrated, cooled and filtered, the material adopts a purity profile unlike that of the fresh material. The recycled B material is therefore unsuitable for use in crystallization experiments.

A final test of the material suitability can be made by performing some of the earlier experiments with the recycled A material. Seeded crystallizations in the STC and the OBC I at 12 Wm^{-3} mixing were performed with a left handed seed in each case. The OBC yielded crystals with 95.15 % similarity to the seed (compared to 94.3 ± 0.6 % from the fresh material with left handed seeds). The STC yielded crystals with 100 % similarity to the seed crystal, an identical outcome to the fresh material work. It would seem that using a rotary evaporator to completely dry the mother liquor is a suitable method of recovering material for use in further experimental work.

Appendix D – The number of crystals of each enantiomorph obtained in the seeded work

This Appendix collects all of the experimental data from this thesis work and defines the number of seed-similar and seed-dissimilar crystals obtained in each test.

The number of crystals produced by PTFE agitators

Table D1 – The number of crystals obtained from the STC

Ns (RPM)	N''	N'	N_T	Similarity
65	1089	0	1089	100
65	569	0	569	100
65	1161	0	1161	100
145	2594	0	2594	100
145	330	0	330	100
145	815	0	815	100
258	1860	0	1860	100
258	2690	0	2690	100
258	853	0	853	100

Table D2 – The number of crystals obtained from the scraped STC

Ns (RPM)	N''	N'	N_T	similarity
65	2521	200	2721	92.65
65	3351	190	3541	94.63
65	79	1	80	98.75
145	7213	0	7213	100.00
145	3943	38	3981	99.05
145	5988	503	6491	92.25
258	5904	161	6065	97.35
258	3610	246	3856	93.62
258	4801	183	4984	96.33

Table D3 – The number of crystals obtained from the scraped OBC

X=	**30mm**	**St=**	**0.26525824**	
f(Hz)	**N''**	**N'**	**N_T**	**similarity**
0.4	1335	84	1419	94.08
0.4	1486	79	1565	94.95
0.4	1147	44	1191	96.31
1	4155	42	4197	99.00
1	4221	297	4518	93.43
1	4409	336	4745	92.92
2	4678	346	5024	93.11
2	3626	380	4006	90.51
2	4444	324	4768	93.20

X=	15mm	St=	0.53051648	
f(Hz)	**N''**	**N'**	**N_T**	**similarity**
0.8	757	43	800	94.63
0.8	1323	3	1326	99.77
0.8	1253	13	1266	98.97
2	1934	37	1971	98.12
2	939	42	981	95.72
2	1162	18	1180	98.47
3.3	835	61	896	93.19
3.3	3290	50	3340	98.50
3.3	1595	39	1634	97.61

X=	7mm	St=	1.13682102	
f(Hz)	**N''**	**N'**	**N_T**	**similarity**
2	1817	40	1857	97.85
2	6567	0	6567	100.00
2	3250	2	3252	99.94

Table D4 – The number of crystals obtained from the unscraped OBC

X=	**30mm**	**St=**	**0.26525824**	
f(Hz)	**N''**	**N'**	**N_T**	**Similarity**
0.8	1660	0	1660	100.00
0.8	1416	43	1459	97.05
0.8	10394	13	10407	99.88
3	4778	19	4797	99.60
3	586	1	587	99.83
3	14029	140	14169	99.01
2	1044	12	1056	98.86
2	3293	16	3309	99.52
2	1965	25	1990	98.74
X=	15mm	St=	0.53051648	
f(Hz)	**N''**	**N'**	**N_T**	**Similarity**
2	5362	2	5364	99.96
2	1604	1	1605	99.94
2	1549	9	1558	99.42
X=	7mm	St=	1.13682102	
f(Hz)	**N''**	**N'**	**N_T**	**Similarity**
2	4517	0	4517	100.00
2	988	0	988	100.00
2	2851	0	2851	100.00

Table D5 – The number of crystals obtained from the moving fluid OBC

X=	**30mm**	**St=**	**0.265258**	
f(Hz)	**N''**	**N'**	**N_T**	**similarity**
2	491	36	527	93.17
2	937	103	1040	90.10
2	343	33	376	91.22
X=	15mm	St=	0.530516	
f(Hz)	**N''**	**N'**	**N_T**	**similarity**
0.8	1461	270	1731	84.40
0.8	614	143	757	81.11
0.8	580	133	713	81.35
2	1900	49	1949	97.49
2	772	34	806	95.78
2	698	38	736	94.84
3.3	1801	292	2093	86.05
3.3	820	106	926	88.55
3.3	907	201	1108	81.86
X=	7mm	St=	1.136821	
f(Hz)	**N''**	**N'**	**N_T**	**similarity**
2	520	10	530	98.11
2	831	37	868	95.74
2	596	8	604	98.68

Table D6 – The number of crystals obtained from the sealed, moving fluid OBC

X=	**30mm**	**St=**	**0.265258**	
f(Hz)	**N''**	**N'**	**N_T**	**similarity**
2	97	15	112	86.60714
2	531	54	585	90.76923
2	214	29	243	88.06584
X=	15mm	St=	0.530516	
f(Hz)	**N''**	**N'**	**N_T**	**similarity**
0.8	10	0	10	100
0.8	266	0	266	100
0.8	374	0	374	100
2	487	0	487	100
2	358	0	358	100
2	819	0	819	100
3.3	162	0	162	100
3.3	557	0	557	100
3.3	10	0	10	100
X=	7mm	St=	1.136821	
f(Hz)	**N''**	**N'**	**N_T**	**similarity**
2	5	0	5	100
2	34	0	34	100
2	69	0	69	100

Table D7 – The number of crystals obtained from the sealed, moving baffle OBC

X=	**30mm**	**St=**	**0.26525824**	
f(Hz)	**N''**	**N'**	**N_T**	**similarity**
2	1217	93	1310	92.90
X=	15mm	St=	0.53051648	
f(Hz)	**N''**	**N'**	**N_T**	**similarity**
2	1921	116	2037	94.31
X=	7mm	St=	1.13682102	
f(Hz)	**N''**	**N'**	**N_T**	**similarity**
2	2187	63	2250	97.20

Table D8 – The number of crystals obtained from the moving baffle OBC with no top baffle

X= 15mm		St= 0.53051648		
f(Hz)	**N''**	**N'**	**N_T**	**Similarity**
0.8	4203	31	4234	99.27
0.8	1854	8	1862	99.57
0.8	1684	3	1687	99.82
2	3555	10	3565	99.72
2	799	3	802	99.63
2	1543	13	1556	99.16
3.3	1067	9	1076	99.16
3.3	1886	14	1900	99.26
3.3	1057	0	1057	100.00

Table D9 – The number of crystals obtained from the moving fluid OBC with no top baffle

X= 15mm		St= 0.530516		
f(Hz)	**N''**	**N'**	**N_T**	**similarity**
0.8	694	68	762	91.08
0.8	294	12	306	96.08
0.8	991	9	1000	99.10
2	541	13	554	97.65
2	549	4	553	99.28
2	1367	32	1399	97.71
3.3	702	24	726	96.69
3.3	1492	65	1557	95.83
3.3	543	20	563	96.45

The number of crystals produced by stainless steel agitators

Table D10 – The number of crystals obtained from the STC with steel impeller

Ns (RPM)	**N''**	**N'**	**N_T**	**similarity**
65	827	0	827	100
65	757	0	757	100
65	495	0	495	100
145	1777	0	1777	100
145	1933	0	1933	100
145	1097	0	1097	100
258	2580	0	2580	100
258	5799	0	5799	100
258	2908	0	2908	100

Table D11 – The number of crystals obtained from the scraped moving baffle OBC with stainless steel baffles

X=	**30mm**	**St=**	**0.26525824**	
f(Hz)	**N''**	**N'**	**N_T**	**Similarity**
0.4	3527	550	4077	86.51
0.4	1374	39	1413	97.24
0.4	1000	222	1222	81.83
1	2872	0	2872	100.00
1	4559	0	4559	100.00
1	5410	12	5422	99.78
1.6	1516	519	2035	74.50
1.6	1042	125	1167	89.29
1.6	3365	241	3606	93.32
X=	15mm	St=	0.53051648	
f(Hz)	**N''**	**N'**	**N_T**	**Similarity**
0.8	682	75	757	90.09
0.8	2015	0	2015	100.00
0.8	1076	33	1109	97.02
2	1975	56	2031	97.24
2	1701	27	1728	98.44
2	660	20	680	97.06
3.3	1961	0	1961	100.00
3.3	905	39	944	95.87
3.3	1216	62	1278	95.15
X=	7mm	St=	1.13682102	
f(Hz)	**N''**	**N'**	**N_T**	**Similarity**
2	1332	31	1363	97.73
2	1337	9	1346	99.33
2	1490	24	1514	98.41

Table D12 – The number of crystals obtained from the unscraped moving baffle OBC with stainless steel baffles

X= 30mm			**St= 0.26525824**	
f(Hz)	**N''**	**N'**	**N_T**	**similarity**
0.8	8281	325	8606	96.22
0.8	936	31	967	96.79
0.8	1555	6	1561	99.62
2	2875	0	2875	100.00
2	2504	0	2504	100.00
2	1057	9	1066	99.16
3	878	0	878	100.00
3	1337	19	1356	98.60
3	1610	19	1629	98.83
X= 15mm			St= 0.53051648	
f(Hz)	**N''**	**N'**	**N_T**	**similarity**
2	1924	0	1924	100.00
2	210	1	211	99.53
2	1004	1	1005	99.90
X= 7mm			St= 1.13682102	
f(Hz)	**N''**	**N'**	**N_T**	**similarity**
2	3458	0	3458	100.00
2	1440	3	1443	99.79
2	339	25	364	93.13

Table D13 – The number of crystals obtained from the moving fluid OBC with stainless steel baffles

X= 15mm			**St= 0.530516**	
f(Hz)	**N''**	**N'**	**N_T**	**Similarity**
0.8	688	41	729	94.38
0.8	685	36	721	95.01
0.8	555	9	564	98.40
2	1090	47	1137	95.87
2	242	3	245	98.78
2	287	28	315	91.11
3.3	547	46	593	92.24
3.3	550	24	574	95.82
3.3	176	3	179	98.32

Table D14 – The number of crystals obtained from the sealed, moving fluid OBC with stainless steel baffles

X=	**30mm**		**St=**	**0.265258**
f(Hz)	**N''**	**N'**	**N_T**	**similarity**
2	393	0	393	100.00
2	182	0	182	100.00
2	853	105	958	89.04
X=	15mm		St=	0.530516
f(Hz)	**N''**	**N'**	**N_T**	**similarity**
2	224	0	224	100.00
2	1340	0	1340	100.00
2	1367	0	1367	100.00
X=	7mm		St=	1.136821
f(Hz)	**N''**	**N'**	**N_T**	**similarity**
2	1166	0	1166	100.00
2	332	0	332	100.00
2	366	0	366	100.00

Appendix E – Preliminary results from Nanosight investigation

Previous work has shown the OBC to nucleate sodium chlorate crystals via a different mechanism to that seen in the STC. One possible hypotheses is that a two-step nucleation model may be responsible for this. In order to provide some scientific insight into these phenomena, the same apparatus was utilised in order to investigate the presence of nanostructures, an indicator of a precursor to nucleation, in the system.

The OBC was filled with water initially to determine the background for which the sodium chlorate solution can be compared to. The OBC was run at varied amplitudes (30, 15, and 7 mm) at fixed amplitude of 1 Hz. Samples were then taken at various times under each mixing condition and at varied stage temperatures at the nanosight apparatus: 40, 30 and 20 °C.

Looking at Figures E1 and E2 below, it appears that some nano-structures exist in the solvent under oscillatory flow conditions. It would appear that the average size reduces slightly with a reduction in temperature (Figure E1) but no real change in the average size is seen with varied amplitudes.

Table E1 – The mean nano-structure size (nm) for various amplitudes and temperatures in the OBC

30 mm amplitude	**Mean size (nm)**		
	40°C	30°C	20°C
Sample 1	251.45	233.16	159.96
Sample 2	222.18	167.7	134.94
Average	236.815	200.43	147.45

15 mm amplitude	Mean size (nm)
	40°C
Sample 1	197.49
Sample2	306.58
Average	252.035

7 mm amplitude	Mean size (nm)
	40°C
Sample 1	155.26
Sample 2	221.84
Average	188.55

Based on Table E1, it would seem that structures up to approximately 300 nm could exist due to the water used for making up the sodium chlorate solutions. It would be reasonable to "subtract" particles of <300 nm from the PSD obtained for the nanostructures seen in the sodium chlorate solutions. If the particles less than 300 nm are disregarded, it is clear that larger structures are present in the system under these conditions.

Considering the plots in Figures E3-E5, there seems to be little variation in the mean particle size with varied amplitudes and temperatures, however it is important to notice that the concentration of the nano-structures reduces somewhat with a reduction of the temperature at which the samples are taken from the OBC.

Table E2 – The average particle size of the nano structures detected by nanosight in the OBC under various amplitudes and temperatures

Amplitude	**30 mm**				**15 mm**				**7 mm**		
Temp (°C)	**40**	**30**	**20**		**40**	**30**	**20**		**40**	**30**	**20**
Sample 1	251	534	590	**Sample 1**	441	564	444	**Sample 1**	556	295	432
Sample 2	222	471	533	**Sample 2**	580	569	399	**Sample 2**	460	466	424
				Sample 3	392	467	377				
				Sample 4	286	437	501				
Ave.	236	502	562		425	509	430		508	380	428

The fact that the mean particle size doesn't seem to change much with varied crystallizer conditions is somewhat disappointing. It would make sense to envisage that the number of nano structures and their size would vary greatly with the operating conditions of the OBC, particularly amplitude/frequency variations (Ni et al. investigated droplet size distribution with varied frequencies and amplitudes [107]). One possible reason for this could lie with the fact that crystallizing solutions have been recognised as having a memory effect [174], which may affect the outcome of such an experiment. In order to investigate this, a fresh solution was generated and the 7 mm tests repeated.

Table E3 – The mean particle size for the OBC at 7 mm amplitude and various temperatures for a fresh batch of solution

7 mm	**Mean size**		
	40	30	20
1	776.71	426.65	491.42
2	506.84	548.75	439.84
Average	641.775	487.7	465.63

From the data in Table E3, it would appear that the average mean particle size is larger in each case when a fresh solution was prepared. A statistical test on the data reveals, however, that this may be an insignificant difference (Kruskal-Wallis P=0.2, 95 % confidence). That said, limited experimental time resulted in only two tests at each condition being performed. Repeating the investigation, but with a fresh batch of

material each time the conditions are changed should minimize any effect of the influence of a solution memory phenomenon.

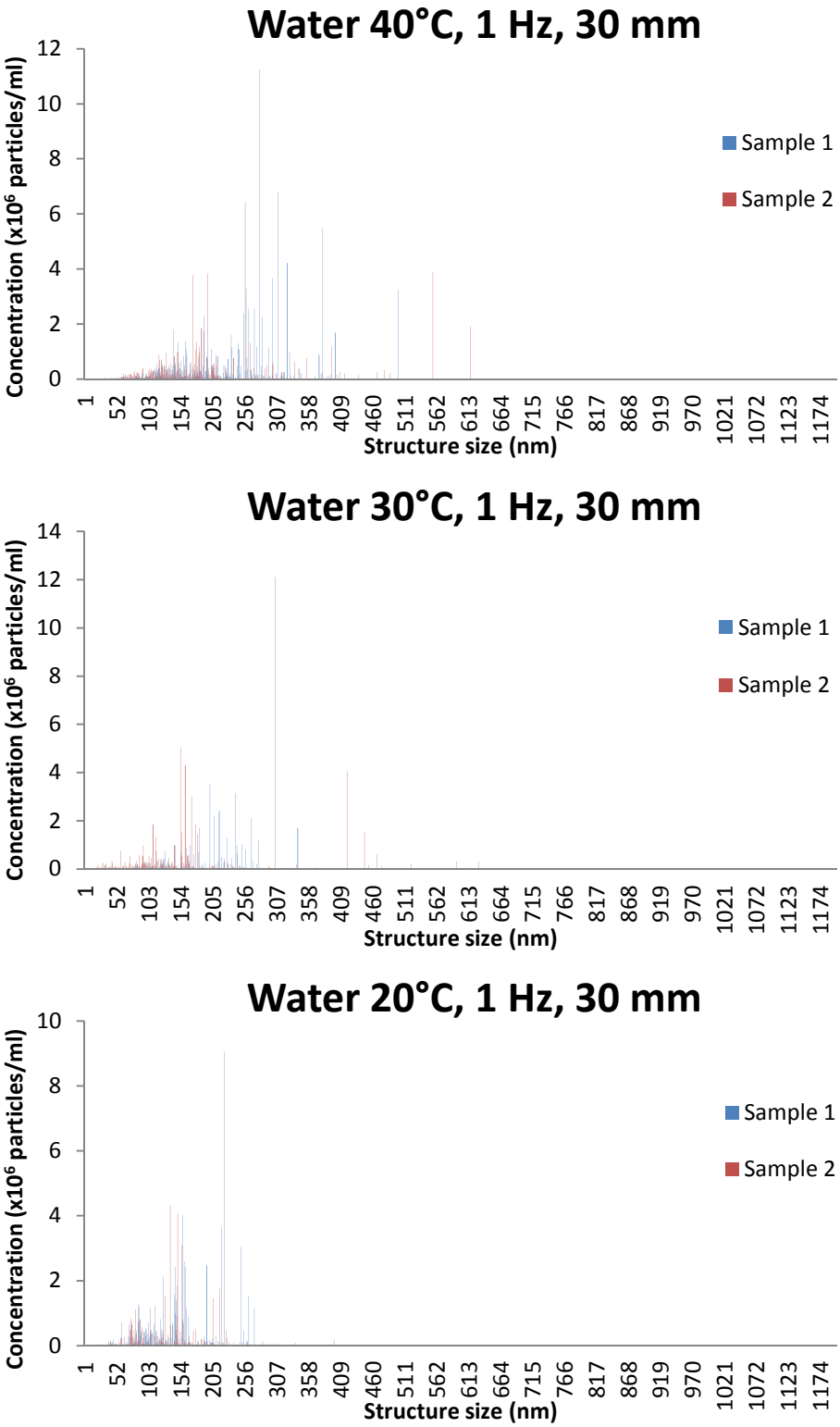

Figure E1 - The particle size distributions for filtered, distilled water in the OBC operating at 1 Hz and 30 mm. The particle size was determined by nanosight at 40 °C (top), 30 °C (middle) and 20 °C (bottom)

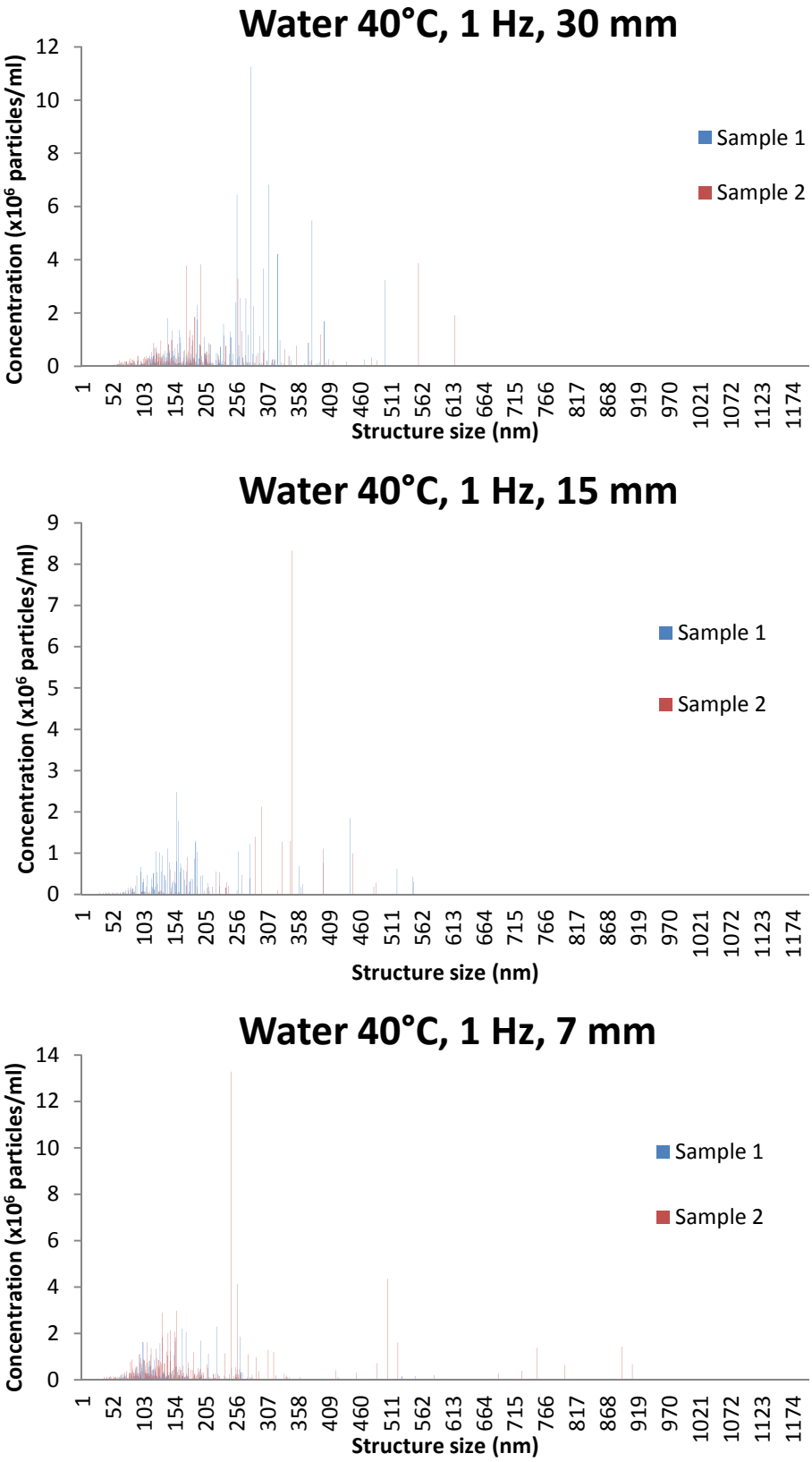

Figure E2 - The particle size distributions for filtered, distilled water at 40 °C in the OBC operating at 1 Hz and various amplitudes. The particle size was determined by nanosight at 30 mm (top), 15 mm (middle) and 7 mm (bottom) amplitudes

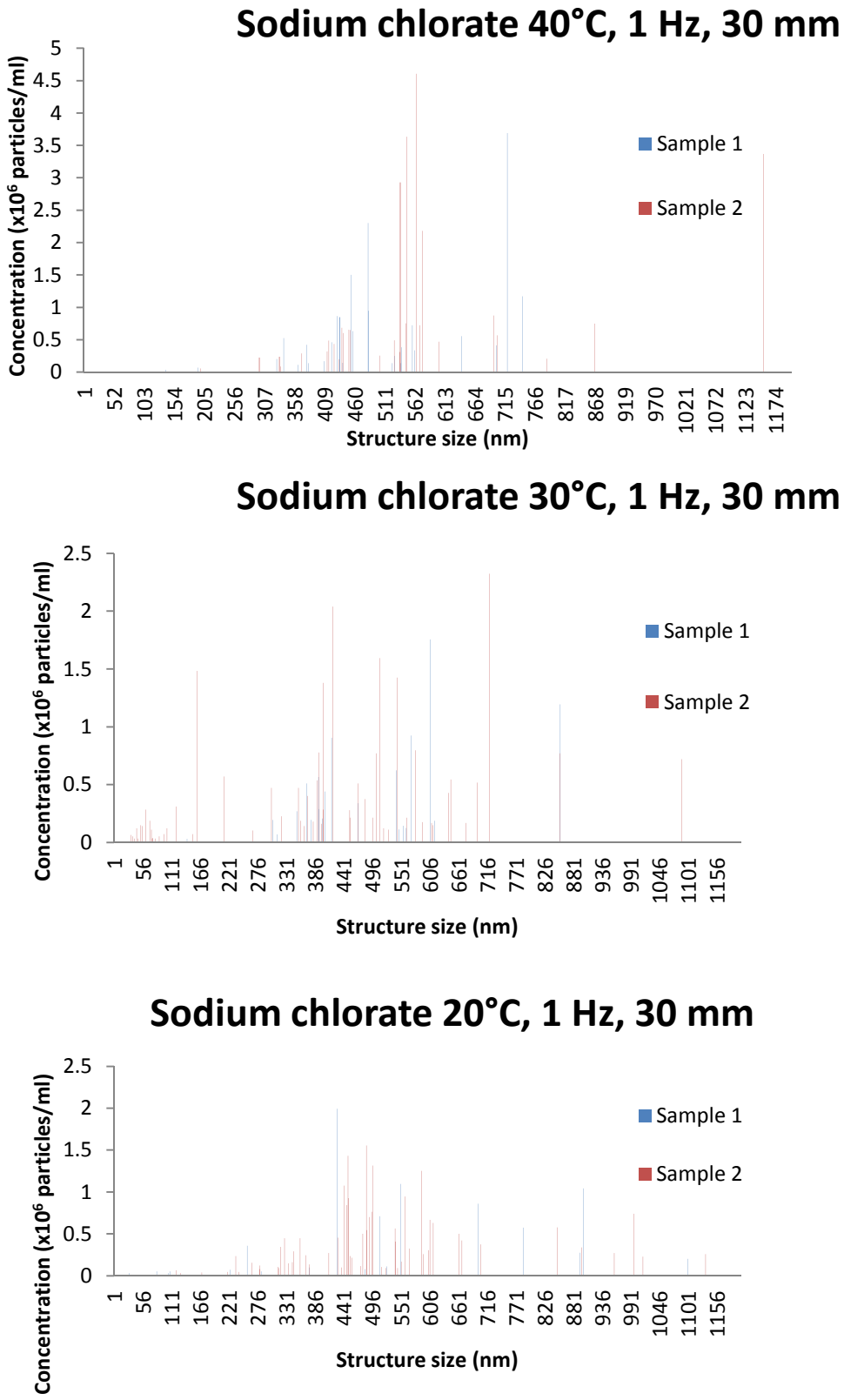

Figure E3 - The particle size distributions for filtered, sodium chlorate solution in the OBC operating at 1 Hz and 30 mm. The particle size was determined by nanosight at 40 °C (top), 30 °C (middle) and 20 °C (bottom)

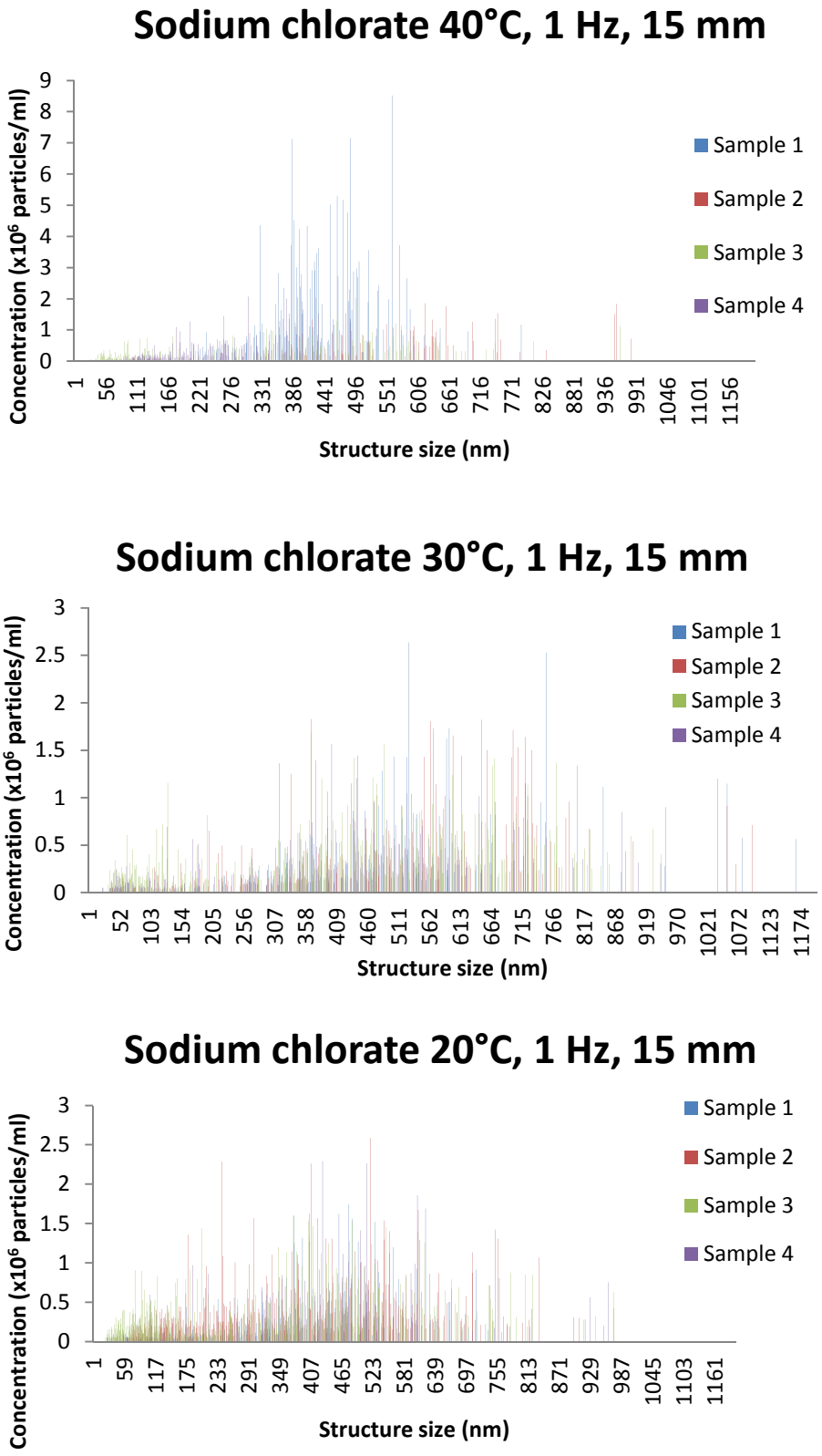

Figure E4 - The particle size distributions for filtered, sodium chlorate solution in the OBC operating at 1 Hz and 15 mm. The particle size was determined by nanosight at 40 °C (top), 30 °C (middle) and 20 °C (bottom)

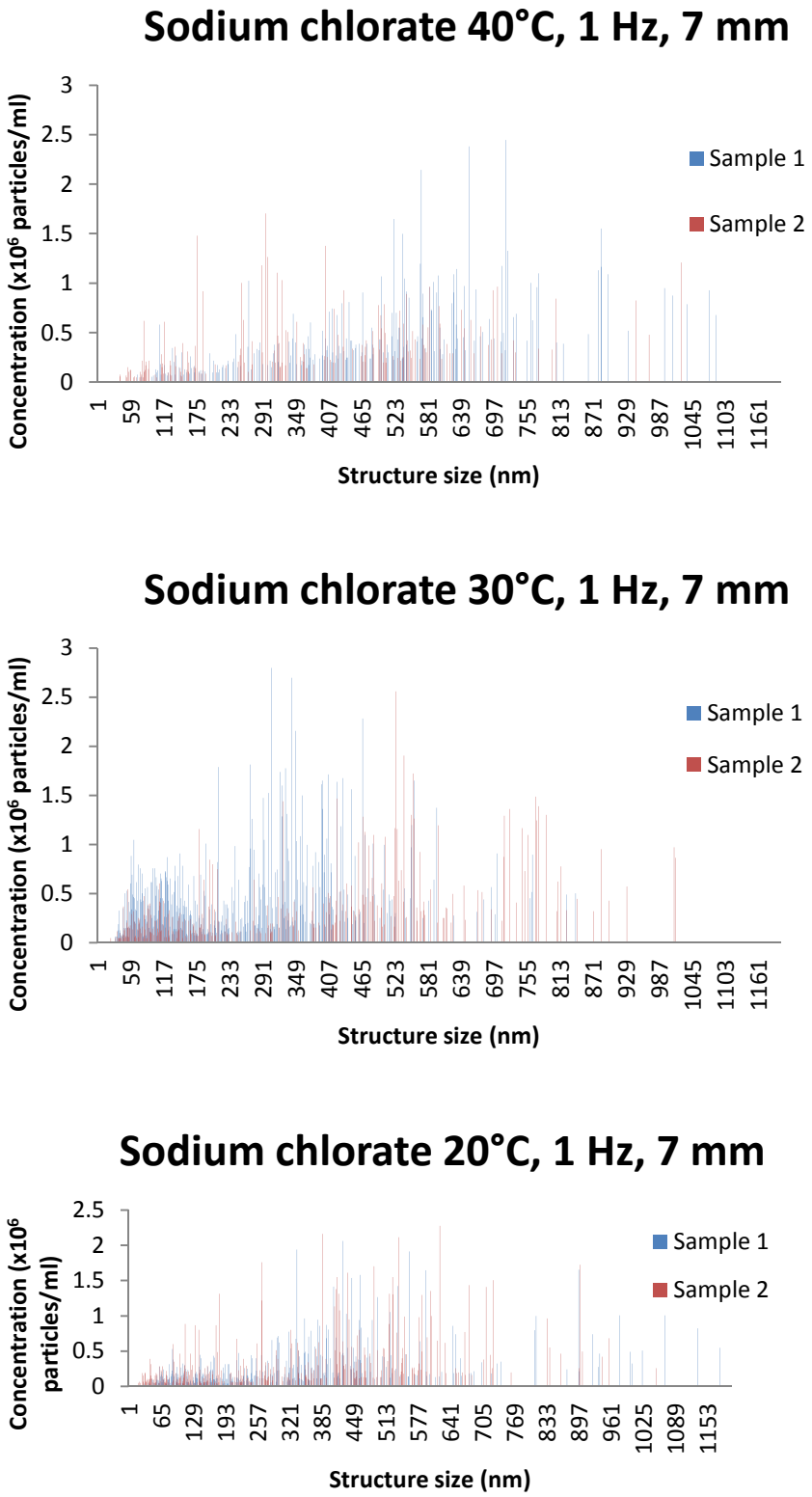

Figure E5 - The particle size distributions for filtered, sodium chlorate solution in the OBC operating at 1 Hz and 7 mm. The particle size was determined by nanosight at 40 °C (top), 30 °C (middle) and 20 °C (bottom)

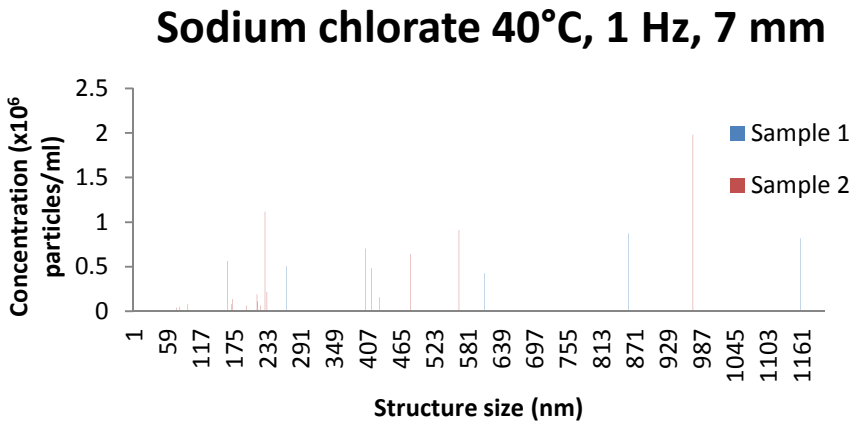

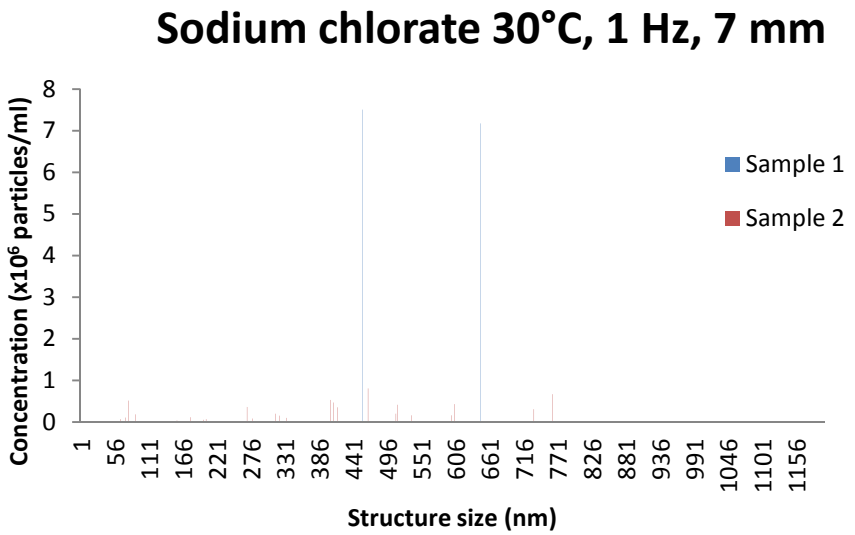

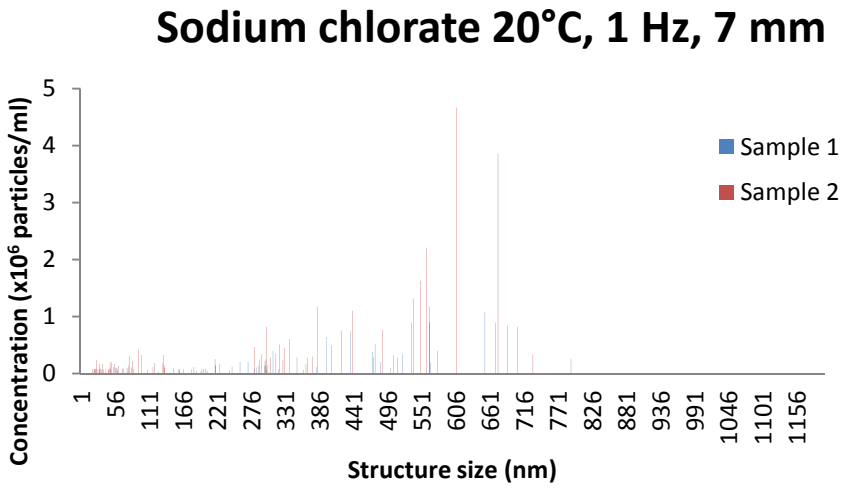

Figure E6 - The particle size distributions for filtered, sodium chlorate solution in the OBC operating at 1 Hz and 7 mm and with a fresh solution. The particle size was determined by nanosight at 40 °C (top), 30 °C (middle) and 20 °C (bottom)

Although there does not appear to be a significant change in the average nanostructure size with varied crystallizer conditions, there does appear to be a marked change in the concentration of the detected particles when the mixing conditions are altered. At first glance of Figure E3, the concentration of the particles seems to be higher at the 30 mm test compared to those at 15 and 7 mm amplitudes (Figures E4 and E5 respectively). This is consistent with the dissimilarity to the seed crystal in the work presented in this thesis, where a greater dissimilarity is seen at 30 mm amplitude than at 7 mm amplitude. The total number of tracked particles (Table E4) can then be examined and the above effect quantified.

Table E4 – The number of detected structures in the OBC at varied amplitudes and temperatures

	Temperature (°C)		
X (mm)	**40**	**30**	**20**
7	183	783	475
	253	412	394
15	102	147	143
	179	221	169
	223	400	562
	180	185	650
30	26	21	18
	29	59	58

It would seem from the data in Table E4 that there may be a relationship between the oscillatory amplitude and the number of structures that exist in the solution, with a much larger number of structures present in the samples taken when the amplitude is low compared to when it is high. It is important to remember that in this case the solution was recycled for each of the amplitudes studied, and a memory effect may influence these findings. Coupling the OBC with a sophisticated method of analysis such as the NTA and a sound experimental design may provide the opportunity to build upon the findings of this thesis.

References

1. Garside, J. and R.J. Davey, *Secondary contact nucleation: Kinetics, growth and scale up.* Chem. Eng. Comm., 1980. **4**: p. 393-424.
2. Vekilov, P.G., *Nucleation.* Cryst. Growth Des., 2010. **10**(12): p. 5007-5019.
3. Myerson, A., *Handbook of Industrial Crystallization*. Second ed. 2002: Butterworth Heinemann.
4. Mersmann, A., *Crystallization Technology Handbook*. Second ed. 2001, New York: Marcel Dekker.
5. Mullin, J.W., *Crystallization*. Third ed. 1992, Oxford: Butterworth-Heinemann.
6. Tung, H., et al., *Mixing Effects on Crystal Growth*, in *Crystallization of Organic Compounds, An Industrial Perspective*. 2009, John Wiley & Sons: New Jersey. p. 122-123.
7. Ni, X. and A. Liao, *Effects of cooling rate and solution concentration on solution crystallization of L-glutamic acid in an oscillatory baffled crystallizer.* Cryst. Growth Des., 2008. **8**(8): p. 2875-2881.
8. Liang, K., et al., *An Examination into the Effect of Stirrer Material and Agitation Rate on the Nucleation of l-Glutamic Acid Batch Crystallized from Supersaturated Aqueous Solutions.* Cryst. Growth Des., 2003. **4**(5): p. 1039-1044.
9. O'Grady, D., et al., *The Effect of Mixing on the Metastable Zone Width and Nucleation Kinetics in the Anti-Solvent Crystallization of Benzoic Acid.* Chem. Eng. Res. Des., 2007. **85**(7): p. 945-952.
10. Chen, P.-C., et al., *Nucleation and morphology of barium carbonate crystals in a semi-batch crystallizer.* J. Cryst. Growth, 2001. **226**(4): p. 458-472.
11. Ni, X., *Continuous oscillatory baffled reactor technology.* Innovat. Pharm. Tech., 2006. **20**: p. 90-96.
12. NiTech Solutions Ltd. *Company website*, Cited 18th March 2011, Available from: http://www.nitechsolutions.co.uk.
13. Ni, X., et al., *Mixing through oscillations and pulsations: A guide to achieving process enhancements in the chemical and process industries.* Trans. IChemE, 2003. **81**(A): p. 373-383.
14. Ni, X., H. Jian, and A. Fitch, *Evaluation of turbulent integral length scale in an oscillatory baffled column using large eddy simulation and digital particle image velocimetry.* Trans. IChemE, 2003. **81**(A): p. 842-853.
15. Hewgill, M.R., et al., *Enhancement of gas-liquid mass transfer using oscillatory flow in a baffled tube.* Chem. Eng. Sci., 1993. **48**(4): p. 799-809.
16. Mackley, M.R., G.M. Tweedle, and I.D. Wyatt, *Experimental heat transfer measurements for pulsatile flow in baffled tubes.* Chem. Eng. Sci., 1990. **45**(5): p. 1237-1242.
17. Chew, C.M., et al., *Crystallization of Paracetamol under Oscillatory Flow Mixing Conditions.* Cryst. Growth Des., 2004. **4**(5): p. 1045-1052.
18. Lawton, S., et al., *Continuous crystallization of pharmaceuticals using a continuous oscillatory baffled reactor.* Org. Process Res. Dev., 2009. **13**: p. 1357-1363.
19. Ni, X., et al., *Scale up of single phase axial dispersion coefficients in batch and continuous oscillatory baffled tubes.* Can. J. Chem. Eng., 2001. **79**(3): p. 444-448.

20. Ni, X. and A. Liao, *Effects of mixing, seeding, material of baffles and final temperature on solution crystallization of L-glutamic acid in an oscilaltory baffled crystallizer.* Chem. Eng. J., 2010. **156**: p. 226-233.
21. Chew, C.M. and R.I. Ristic, *Crystallization by oscillatory and conventional mixing at constant power density.* AIChE J., 2005. **51**(5): p. 1576-1579.
22. *NiTech Solutions Ltd. Clients' Data, Private Communication*. 2010.
23. Stapley, A., H. Tewkesbury, and P. Fryer, *The effects of shear and temperature history on the crystallization of chocolate.* Journal of the American Oil Chemists' Society, 1999. **76**(6): p. 677-685.
24. Hartel, R.W., *Ice crystallization during the manufacture of ice cream.* Trends in Food Science and Technology, 1996. **7**(10): p. 315-321.
25. Davey, R.J. and J. Garside, *From Molecules to Crystallizers*. Oxford Chemistry Primers, ed. L.F. Gladden. 2000, New York: Oxford University Press.
26. Nash, J.F., et al., *The relationship between particle size of dicumarol and its bioavailability in dogs part 1. capsules.* Drug development and industrial pharmacy, 1974. **1**(5): p. 443-457.
27. Nash, J.F., et al., *The relationship between the particle size of dicumarol and its bioavailablity in dogs part 2. drug substance.* Drug development and industrial pharmacy, 1974. **1**(5): p. 459-470.
28. Ridolfo, A.S., et al., *Benoxaprofen, a new anti-inflammatory agent: particle-size effect on dissolution rate and oral absorption in humans.* J. Pharm. Sci., 1979. **68**(7): p. 850-852.
29. Hodgen, S., *An Introduction to Crystallisation*. 2006, The University of Strathclyde: Glasgow.
30. Volmer, M., *Kinetic der Phasenbildung*. 1939, Dresden: Steinkopff.
31. Lundheim, R., *Physiological and ecological significance of biological ice nucleators.* Philosophical Transactions of the Royal Society of London. Series B, Biological Sciences, 2002. **357**(1423): p. 937-943.
32. Paul, E.L., H.-H. Tung, and M. Midler, *Organic crystallization processes.* Powder Technol., 2005. **150**(2): p. 133-143.
33. Metcalfe, G. and J.M. Ottino, *Autocatalytic processes in mixing flows.* Physical Review Letters, 1994. **72**(18): p. 2875-2878.
34. Borchert, C., et al., *On the prediction of crystal shape distributions in a steady-state continuous crystallizer.* Chemical Engineering Science, 2009. **64**(4): p. 686-696.
35. Mullin, J.W. and K.D. Raven, *Influence of Mechanical Agitation on the Nucleation of Some Aqueous Salt Solutions.* Nature, 1962. **195**(4836): p. 35-38.
36. Mitchell, N.A. and P.J. Frawley, *Nucleation kinetics of paracetamol–ethanol solutions from metastable zone widths.* Journal of Crystal Growth, 2010. **312**(19): p. 2740-2746.
37. Nývlt, J., et al., *Metastable zone-width of some aqueous solutions.* J. Cryst. Growth, 1970. **6**(2): p. 151-162.
38. Buhse, T., et al., *Chiral Symmetry Breaking in Crystallization: The Role of Convection.* Phys. Rev. Lett., 2000. **84**(19): p. 4405-4408.
39. Chen, W.C., et al., *The determination of solute distribution during growth and dissolution of NaClO3 crystals: the growth of large crystals.* J. Cryst. Growth, 2002. **236**(1–3): p. 413-419.
40. Nývlt, J., *Kinetics of nucleation in solutions.* J. Cryst. Growth, 1968. **3–4**(0): p. 377-383.
41. Simon, L.L., Z.K. Nagy, and K. Hungerbuhler, *Comparison of external bulk video imaging with focused beam reflectance measurement and ultra-violet visible spectroscopy for metastable zone identification in food and*

pharmaceutical crystallization processes. Chemical Engineering Science, 2009. **64**(14): p. 3344-3351.
42. Simon, L.L., Z.K. Nagy, and K. Hungerbuhler, *Endoscopy-Based in Situ Bulk Video Imaging of Batch Crystallization Processes.* Organic Process Research & Development, Special Issue on Crystallization and Polymorphism, 2009. **13**(6): p. 1254-1261.
43. Lakerveld, R., et al., *Application of generic principles of process intensification to solution crystallization enabled by a task-based design approach.* Chemical Engineering and Processing: Process Intensification, 2010. **49**(9): p. 979-991.
44. Soos, M., et al., *Effect of shear rate on aggregate size and morphology investigated under turbulent conditions in stirred tank.* Journal of Colloid and Interface Science, 2008. **319**(2): p. 577-589.
45. Strickland-Constanble, R.F., *Kinetics and Mechanism of Crystallization*, ed. R.F. Strickland-Constable. 1968, London: Academic Press.
46. Denk, E.G. and G.D. Botsaris, *Fundamental studies in secondary nucleation from solution.* J. Cryst. Growth, 1972. **13/14**: p. 493-499.
47. Denk, E.G. and G.D. Botsaris, *Mechanism of contact nucleation.* J. Cryst. Growth, 1972. **15**: p. 57-60.
48. Qian, R. and G.D. Botsaris, *A new mechanism of nuclei formation in suspension crystallzers: the role of interparticle forces.* Chem. Eng. Sci., 1997. **52**(20): p. 3429-3440.
49. Qian, R.-Y. and G.D. Botsaris, *The effect of seed preparation on the chirality of the secondary nuclei.* Chemical Engineering Science, 2004. **59**(14): p. 2841-2852.
50. Qian, R.-Y. and G.D. Botsaris, *Nuclei breeding from a chiral crystal seed of NaClO3.* Chemical Engineering Science, 1998. **53**(9): p. 1745-1756.
51. Garside, J., *Industrial crystallization from solution.* Chemical Engineering Science, 1985. **40**(1): p. 3-26.
52. Nývlt, J., *The Kinetics of industrial crystallization*. 1985, Amsterdam; New York; New York: Elsevier ; Elsevier Science Pub. Co., Inc. [distributor].
53. Powers, H.E.C., *Nucleation and Early Crystal Growth.* Ind. Chem., 1963. **39**: p. 351.
54. Sung, C.Y., J. Estrin, and G.R. Youngquist, *Secondary nucleation of magnesium sulfate by fluid shear.* AIChE J., 1973. **19**: p. 957-962.
55. Alexander, A.J. and P.J. Camp, *Single pulse, single crystal laser-induced nucleation of potassium chloride.* Cryst. Growth Des., 2008. **9**(2): p. 958-963.
56. Miyasaka, E., et al., *Effect of ultrasonic irradiation on nucleation phenomena in a Na2HPO4 · 12H2O melt being used as a heat storage material.* Ultrasonics Sonochemistry, 2006. **13**(4): p. 308-312.
57. Davey, R.J., et al., *The chiral purity of a triazolylketone crystallised from racemic solutions.* Journal of Crystal Growth, 1990. **102**(1–2): p. 97-102.
58. Yokota, M. and K. Toyokura. *Heterogeneous nucleation of d-SCMC on the surface of l-SCMC crystal*. in *AIChE Annual Meeting*. 1992. Miami Beach, FL.
59. Vekilov, P.G., *Two-step mechanism for the nucleation of crystals from solution.* Journal of Crystal Growth, 2005. **275**(1–2): p. 65-76.
60. Myerson, A.S. and B.L. Trout, *Nucleation from Solution.* Science, 2013. **341**(6148): p. 855-856.
61. Vekilov, P.G., *The two-step mechanism of nucleation of crystals in solution.* Nanoscale, 2010. **2**(11): p. 2346-2357.
62. Chen, J., et al., *Pharmaceutical Crystallization.* Cryst. Growth Des., 2011. **11**(4): p. 887-895.

63. Georgalis, Y., et al., *Lysozyme Aggregation Studied by Light Scattering. I. Influence of Concentration and Nature of Electrolytes.* Acta Crystallographica Section D, 1997. **53**(6): p. 691-702.
64. Georgalis, Y., et al., *Lysozyme Aggregation Studied by Light Scattering. II. Variations of Protein Concentration.* Acta Crystallographica Section D, 1997. **53**(6): p. 703-712.
65. Igarashi, K., et al., *The initial stage of crystallization of lysozyme: a differential scanning calorimetric (DSC) study*. Journal of Crystal Growth, 1999. **204**(1–2): p. 191-200.
66. Chattopadhyay, S., et al., *SAXS Study of the Nucleation of Glycine Crystals from a Supersaturated Solution.* Crystal Growth & Design, 2005. **5**(2): p. 523-527.
67. Garetz, B.A., J. Matic, and A.S. Myerson, *Polarization Switching of Crystal Structure in the Nonphotochemical Light-Induced Nucleation of Supersaturated Aqueous Glycine Solutions.* Physical Review Letters, 2002. **89**(17): p. 175501.
68. Gebauer, D. and H. Colfen, *Prenucleation clusters and non-classical nucleation.* Nano Today, 2011. **6**: p. 564-584.
69. Gebauer, D., et al., *Proto-Calcite and Proto-Vaterite in Amorphous Calcium Carbonates.* Angewandte Chemie International Edition, 2010. **49**(47): p. 8889-8891.
70. Pouget, E.M., et al., *The Initial Stages of Template-Controlled CaCO3 Formation Revealed by Cryo-TEM.* Science, 2009. **323**(5920): p. 1455-1458.
71. Hart, H., L.E. Craine, and D.J. Hart, *Organic Chemistry: A Short Course*. Eleventh ed. 2003, Boston, New York: Houghton Mifflin.
72. Moss, G.P., *Basic terminology of stereochemistry.* Pure & Appl. Chem., 1996. **68**(12): p. 2193-2222.
73. Bunn, C.W., *Shapes of Crystals*, in *Chemical Crystallography*. 1945, Oxford Clarendon Press: Oxford. p. 39.
74. Day, C., *Crushing a solution of left-handed and right-handed crystals breaks it's chiral symmetry.* Physics Today, 2005. **58**(4): p. 21-22.
75. Van Dijk, W.J.D., *Tower with Internal Perforated Plate Suitable for Extracting Liquids by Treatment with other Liquids and for similar Concurrent Processes*. 1935: U. S.
76. Karr, A.E., *Performance of a reciprocating-plate extraction column.* AIChE Journal, 1959. **5**(4): p. 446-452.
77. Bellhouse, B.J., et al., *A High Efficiency Membrane Oxygenator and Pulsatile Pumping System, and Its Application To Animal Trials.* ASAIO Journal, 1973. **19**(1): p. 72-79.
78. Sobey, I.J., *On flow through furrowed channels. Part 1. Calculated flow paterns.* Journal of fluid mechanics, 1980. **96**: p. 1-26.
79. Stephanoff, K.D., I.J. Sobey, and B.J. Bellhouse, *On flow through furrowed channels. Part 2. Observed flow patterns.* Journal of fluid mechanics, 1980. **96**: p. 27-32.
80. Knott, G.F. and M.R. Mackley, *On Eddy Motions near Plates and Ducts, Induced by Water Waves and Periodic Flows.* Philosophical Transactions of the Royal Society of London. Series A, Mathematical and Physical Sciences, 1980. **294**(1412): p. 599-623.
81. Mackley, M.R., *Using Oscillatory flow to improve performance.* The Chemical Engineer, 1987. **433**: p. 18-20.
82. Brunold, C.R., et al., *Experimental observations on flow patterns and energy losses for oscillatory flow in ducts containing sharp edges.* Chemical Engineering Science, 1989. **44**(5): p. 1227-1244.

83. Dickens, A.W., M.R. Mackley, and H.R. Williams, *Experimental residence time distribution measurements for unsteady flow in baffled tubes.* Chemical Engineering Science, 1989. **44**(7): p. 1471-1479.
84. Mackley, M.R. and P. Stonestreet, *Heat transfer and associated energy dissipation for oscillatory flow in baffled tubes.* Chemical Engineering Science, 1995. **50**(14): p. 2211-2224.
85. Ni, X. and S. Gao, *Mass transfer characteristics of a pilot pulsed baffled reactor.* Journal of Chemical Technology & Biotechnology, 1996. **65**(1): p. 65-71.
86. Mackley, M.R. and X. Ni, *Mixing and dispersion in a baffled tube for steady laminar and pulsatile flow.* Chemical Engineering Science, 1991. **46**(12): p. 3139-3151.
87. Ni, X. and S. Gao, *Scale-up correlation for mass transfer coefficients in pulsed baffled reactors.* The Chemical Engineering Journal and the Biochemical Engineering Journal, 1996. **63**(3): p. 157-166.
88. Ni, X., Y. Zhang, and M. I., *Correction of polymer particle size with droplet size in suspension polymerization of methylmethacrylate in a batch oscillatory baffled reactor.* Chem. Eng. Sci., 1999. **54**: p. 841-850.
89. Liu, S., et al., *Measurements of velocities of single particles for steady and oscillatory flows in plain and baffled tubes.* Trans. IChemE, 1995. **73**(A): p. 727-732.
90. Brown, C.J. and X. Ni, *Online evaluation of paracetamol antisolvent crystallization growth rate with video imaging in an oscillatory baffled crystallizer.* Crystal Growth and Design, 2011. **11**: p. 719-725.
91. Caldeira, R. and X. Ni, *Evaluation and establishment of a cleaning protocol for the production of vanisal sodium and aspirin using a continuous oscillatory baffled reactor.* Organic process research and development, 2009. **13**: p. 1080-1087.
92. Fitch, A.W., H. Jian, and X. Ni, *An investigation of the effect of viscosity on mixing in an oscillatory baffled column using digital particle image velocimetry and computational fluid dynamics simulation.* Chemical Engineering Journal, 2005. **112**(1-3): p. 197-210.
93. Mackay, M.E., M.R. Mackley, and Y. Wang, *Oscillatory flow within tubes containing wall or central baffles.* Trans. IChemE, 1991. **69**(A): p. 506-513.
94. Howes, T., M.R. Mackley, and E.P.L. Roberts, *The simulation of chaotic mixing and dispersion for periodic flows in baffled channels.* Chemical Engineering Science, 1991. **46**(7): p. 1669-1677.
95. Wang, Y., et al., *Simulation of cross-flow filtration for baffled tubular channels and pulsatile flow.* Journal of Membrane Science, 1994. **95**(3): p. 243-258.
96. Roberts, E.P.L. and M.R. Mackley, *The development of asymmetry and period doubling for oscillatory flow in baffled channels.* Journal of Fluid Mechanics, 1996. **328**: p. 19-48.
97. Ni, X., et al., *A study of velocity vector profile and strain rate distribution for laminar and oscillatory flows in a baffled tube using particle image velocimetry.* Journal of flow visualization and image processing, 1995. **2**(2): p. 135-147.
98. Fitch, A.W., X. Ni, and J. Stewart, *Characterisation of flexible baffles in an oscillatory baffled column.* Journal of Chemical Technology & Biotechnology, 2001. **76**(10): p. 1074-1079.
99. Ni, X. and P. Gough, *On the discussion of the dimensionless groups governing oscillatory flow in a baffled tube.* Chemical Engineering Science, 1997. **52**(3209-3212).

100. Binnie, A.M., *A double-refraction method of detecting turbulence in liquids.* Proceedings of the Physical Society, 1945. **57**(5): p. 390.
101. Sarpkaya, T., *Experimental determination of the critical Reynolds number for pulsating Poiseuille flow.* Trans. ASME D, J. Basic Engng., 1966. **88**: p. 589-598.
102. Sobey, I.J., *Observation of waves during oscillatory channel flow.* Journal of fluid mechanics, 1985. **151**: p. 395-426.
103. Rouse, A., J. Basic Engng, 1964. **86**: p. 129-130.
104. Zhang, Y., X. Ni, and I. Mustafa, *A study of oil–water dispersion in a pulsed baffled reactor.* Journal of Chemical Technology & Biotechnology, 1996. **66**(3): p. 305-311.
105. Gough, P., X. Ni, and K.C. Symes, *Experimental Flow Visualisation in a Modified Pulsed Baffled Reactor.* Journal of Chemical Technology & Biotechnology, 1997. **69**(3): p. 321-328.
106. Ni, X., et al., *A Systematic Study of the Effect of Geometrical Parameters on Mixing Time in Oscillatory Baffled Columns.* Trans. IChemE, 1998. **76**(5): p. 635-642.
107. Ni, X., Y. Zhang, and I. Mustafa, *An investigation of droplet size and size distribution in methylmethacrylate suspensions in a batch oscillatory-baffled reactor.* Chemical Engineering Science, 1998. **53**(16): p. 2903-2919.
108. Ni, X. and C.C. Stevenson, *On the effect of gap size between baffle outer diameter and tube inner diameter on the mixing characteristics in an oscillatory-baffled column.* J. Chem. Technol. Biotechnol. , 1999. **74**(6): p. 587-593.
109. Ni, X., G. Nelson, and I. Mustafa, *Flow patterns and oil—water dispersion in a 0.38 m diameter oscillatory baffled column.* The Canadian Journal of Chemical Engineering, 2000. **78**(1): p. 211-220.
110. Aoun Nabli, M., P. Guiraud, and C. Gourdon, *Numerical experimentation: a tool to calculate the axial dispersion coefficient in discs and doughnuts pulsed solvent extraction columns.* Chemical Engineering Science, 1997. **52**(14): p. 2353-2368.
111. Nagata, S., *Mixing: Principles and Applications*. 1975, Tokyo: Kodansha Ltd.
112. Jealous, A.C. and H.F. Johnson, *Power Requirements for Pulse Generation in Pulse Columns.* Industrial & Engineering Chemistry, 1955. **47**(6): p. 1159-1166.
113. Mackley, M.R., *Process innovation using oscillatory flow within baffled tubes.* Trans. IChemE, 1991. **69**(A): p. 197-199.
114. Baird, M.H.I. and P. Stonestreet, *Energy dissipation in oscillatory flow within a baffled tube.* Trans. IChemE, 1995. **73**(5): p. 503-511.
115. Liao, A., *Characterisation of Crystallisation of L-Glutamic Acid in a Batch Oscillatory Baffled Crystalliser*, in *Chemical Engineering*. 2008, Heriot-Watt University: Edinburgh.
116. Nelson, G., *Scale-up study of suspension polymerisation in an oscillatory baffled reactor*, in *Mechanical and Chemical Engineering*. 2001, Heriot-Watt University: Edinburgh.
117. Daugherty, R.L., J.B. Franzini, and E.J. Finnemore, *Fluid Mechanics with Engineering Aspects*. 1989, Singapore: McGraw-Hill Book Co.
118. Baird, M.H.I. and N.V.R. Rao, *Power dissipation and flow patterns in reciprocating baffle-plate columns.* The Canadian Journal of Chemical Engineering, 1995. **73**(4): p. 417-425.
119. Ni, X. and M.R. Mackley, *Chemical reaction in batch pulsatile flow and stirred tank reactors.* The Chemical Engineering Journal, 1993. **52**(3): p. 107-114.

120. Davey, R.J., et al., *Crystal Polymorphism as a Probe for Molecular Self-Assembly during Nucleation from Solutions: The Case of 2,6-Dihydroxybenzoic Acid.* Crystal Growth & Design, 2000. **1**(1): p. 59-65.
121. Ferrari, E.S., et al., *Crystallization in Polymorphic Systems: The Solution-Mediated Transformation of β to α Glycine.* Crystal Growth & Design, 2002. **3**(1): p. 53-60.
122. Ostwald, W.F.Z., *Studien uber die Bildung und Umwandlung fester Korper.* Phys. Chem. (Leipzig), 1897. **22**: p. 289.
123. Doki, N., et al., *Scaleup experiments on seeded batch cooling crystallization of potassium alum.* AIChE Journal, 1999. **45**(12): p. 2527-2533.
124. Yokota, M., et al., *Scale-up effect on the rate of contact nucleation caused by collisions of crystals with an impeller.* Chemical Engineering Science, 1999. **54**(17): p. 3831-3838.
125. Towler, C.S., et al., *Impact of Molecular Speciation on Crystal Nucleation in Polymorphic Systems: The Conundrum of γ Glycine and Molecular 'Self Poisoning'.* Journal of the American Chemical Society, 2004. **126**(41): p. 13347-13353.
126. Pincock, R.E., et al., *Probability Distribution of Enantiomorphous Forms in Spontaneous Generation of Optically Active Substances.* Science, 1971. **174**(4013): p. 1018-1020.
127. Pincock, R.E. and K.R. Wilson, *Spontaneous generation of optical activity.* Journal of Chemical Education, 1973. **50**(7): p. 455-null.
128. Kondepudi, D.K., J. Laudadio, and K. Asakura, *Chiral Symmetry Breaking in Stirred Crystallization of 1,1'-Binaphthyl Melt.* Journal of the American Chemical Society, 1999. **121**(7): p. 1448-1451.
129. Penzien, K. and G.M.J. Schmidt, *Reactions in Chiral Crystals: An Absolute Asymmetric Synthesis.* Angewandte Chemie International Edition in English, 1969. **8**(8): p. 608-609.
130. Kondepudi, D.K., *Chiral Autocatalysis and Selectivity in the Vicinity of Solid Surfaces,* in *Chirality: Physical Chemistry*. 2002, American Chemical Society. p. 302-318.
131. Belyustin, A.V. and E.D. Rogacheva, *Growth of Crystals*. 4 ed, ed. A.V. Shubinikov and N. Sheftal. 1966, New York: Consultants Bureau.
132. Pagni, R.M. and R.N. Compton, *Asymmetric Synthesis of Optically Active Sodium Chlorate and Bromate Crystals.* Cryst. Growth Des., 2002. **2**(4): p. 249-253.
133. Sinnott, R.K., *Equipment Selection, Specification and Design,* in *Coulson and Richardson's Chemical Engineering Volume 6 - Chemical Engineering Design*, R.K. Sinnott, Editor. 1999, Butterworth-Heinemann: Oxford. p. 471-473.
134. Denk, E.G., *Fundamental Studies in Secondary Nucleation,* in *Chem. Eng.* 1971, Tufts University.
135. Sánchez Pérez, J.A., et al., *Shear rate in stirred tank and bubble column bioreactors.* Chemical Engineering Journal, 2006. **124**(1–3): p. 1-5.
136. Wu, J., L.J. Graham, and N. Noui Mehidi, *Estimation of agitator flow shear rate.* AIChE Journal, 2006. **52**(7): p. 2323-2332.
137. Ni, X., et al., *On the measurement of strain rate in an oscillatory baffled column using particle image velocimetry.* Chemical Engineering Science, 2000. **55**(16): p. 3195-3208.
138. Smith, A.A., *A Model for Mother Liquor Recycle in Batch Processing.* Org. Process Res. Dev., 1997. **1**(2): p. 165-167.
139. Seidell, A., *Solubility of Sodium Chlorate,* in *Solubilities of inorganic and metal organic compounds*. 1940, Van Nostrand Company: New York. p. 1250.

140. Paul, E.L., V.A. Atiemo-Obeng, and S.M. Kresta, *Handbook of Industrial Mixing - Science and Practice*. 2004, John Wiley & Sons.
141. Martin, B., A. Tharrington, and X.l. Wu, *Chiral Symmetry Breaking in Crystal Growth: Is Hydrodynamic Convection Relevant?* Phys. Rev. Lett., 1996. **77**(13): p. 2826-2829.
142. Evans, T.W., G. Margolis, and A.F. Sarofim, *Mechanisms of secondary nucleation in agitated crystallizers.* AIChE J., 1974. **20**(5): p. 950-958.
143. Ayazi Shamlou, P., A.G. Jones, and K. Djamarani, *Hydrodynamics of secondary nucleation in suspension crystallization.* Chem. Eng. Sci., 1990. **45**(5): p. 1405-1416.
144. Liang, K., et al., *Examination of the Process Scale Dependence of l-Glutamic Acid Batch Crystallized from Supersaturated Aqueous Solutions in Relation to Reactor Hydrodynamics.* Ind. Eng. Chem. Res., 2004. **43**(5): p. 1227-1234.
145. Vogl, O., *Chiral crystallization and the origin of chiral life on earth.* J. Polym. Sci., Part A: Polym. Chem., 2011. **49**(6): p. 1299-1308.
146. Virone, C., et al., *Primary nucleation induced by ultrasonic cavitation.* J. Cryst. Growth, 2006. **294**(1): p. 9-15.
147. Kaisersberger, E., et al., *The influence of recycled material on the crystallization kinetics of thermoplastic polymers.* J. Thermal Anal., 1993. **40**(2): p. 821-829.
148. Young, S.W., *Mechanical Stimulus to Crystallization in Super-cooled Liquids.* J. Am. Chem. Soc., 1911. **33**(2): p. 148-162.
149. Ulrich, J. and C. Strege, *Some aspects of the importance of metastable zone width and nucleation in industrial crystallizers.* J. Cryst. Growth, 2002. **237–239, Part 3**(0): p. 2130-2135.
150. Mullin, J.W. and K.D. Raven, *Nucleation in Agitated Solutions.* Nature, 1961. **190**(4772): p. 251-251.
151. Melia, T.P. and W.P. Moffitt, *Secondary Nucleation from Aqueous Solution.* Ind. Eng. Chem. Fund., 1964. **3**(4): p. 313-317.
152. Melia, T.P. and W.P. Moffitt, *Crystallization from aqueous solution.* J. Colloid Sci., 1964. **19**(5): p. 433-447.
153. Min, K.Y. and W.I. Goldburg, *Dependence of nucleation on shear-induced initial conditions.* Phys. Rev. Lett., 1993. **71**(4): p. 569.
154. Erdemir, D., A.Y. Lee, and A.S. Myerson, *Nucleation of Crystals from Solution: Classical and Two-Step Models.* Acc. Chem. Res., 2009. **42**(5): p. 621-629.
155. Bauer, L.G., R.W. Rousseau, and W.L. McCabe, *Influence of crystal size on the rate of contact nucleation in stirred-tank crystallizers.* AIChE J., 1974. **20**(4): p. 653-659.
156. Callahan, C.J. and X.-W. Ni, *Probing into Nucleation Mechanisms of Cooling Crystallization of Sodium Chlorate in a Stirred Tank Crystallizer and an Oscillatory Baffled Crystallizer.* Cryst. Growth Des., 2012. **12**(5): p. 2525-2532.
157. Liu, Y., et al., *CFD simulations of turbulent flow in baffle-filled membrane tubes.* Separation and Purification Technology, 2009. **67**(1): p. 14-20.
158. Davey, R.J., S.L.M. Schroeder, and J.H. ter Horst, *Nucleation of Organic Crystals—A Molecular Perspective.* Angewandte Chemie International Edition, 2013. **52**(8): p. 2166-2179.
159. Ni, X.W. and N.E. Pereira, *Parameters affecting fluid dispersion in a continuous oscillatory baffled tube.* AIChE Journal, 2000. **46**(1): p. 37-45.
160. Lowry, R. *Concepts & Applications of Inferential Statistics.* 1998-2013 06/09/2013].
161. Manninen, M., et al., *Evaluation of axial dispersion and mixing performance in oscillatory baffled reactors using CFD.* Journal of Chemical Technology & Biotechnology, 2012. **88**(4): p. 553-562.

162. Callahan, C.J. and X. Ni, *An investigation into the effect of mixing on the secondary nucleation of sodium chlorate in a stirred tank and oscillatory baffled crystallizer.* CrystEngComm, 2013. **Submitted work**.
163. Shah, B.C., W.L. McCabe, and R.W. Rousseau, *Polyethylene vs. stainless steel impellers for crystallization processes.* AIChE Journal, 1973. **19**(1): p. 194-194.
164. Johnson, R.T., R.W. Rousseau, and W.L. McCabe, *Factors affecting contact nucleation.* AIChE Symposium Series, 1972. **68**(121): p. 31-41.
165. Page, A.J. and R.P. Sear, *Crystallization Controlled by the Geometry of a Surface.* Journal of the American Chemical Society, 2009. **131**(48): p. 17550-17551.
166. Bonafede, S.J. and M.D. Ward, *Selective Nucleation and Growth of an Organic Polymorph by Ledge-Directed Epitaxy on a Molecular Crystal Substrate.* Journal of the American Chemical Society, 1995. **117**(30): p. 7853-7861.
167. Pivot Pins Inc., *Rockwell hardness of stainless steel*. [cited 2014 4th March]; Available from: http://www.pivotpins.com/pdf/mechanical_properties_of_steel.pdf.
168. Bearing Works Inc., *Rockwell Hardness of PTFE*. [cited 2014 4th March]; Available from: http://www.bearingworks.com/content_files/pdf/retainers/PTFE%20datasheet.pdf.
169. Kondepudi, D.K., R.J. Kaufman, and N. Singh, *Chiral Symmetry Breaking in Sodium Chlorate Crystallizaton.* Science, 1990. **250**(4983): p. 975-976.
170. Kipping, F.S. and W.J. Pope, *Stereochemistry and Vitalism.* Nature, 1898. **59**: p. 53.
171. Kondepudi, D.K., et al., *Kinetics of chiral symmetry breaking in crystallization.* J. Am. Chem. Soc., 1993. **115**(22): p. 10211-10216.
172. Kondepudi, D.K., et al., *Stirring Rate as a Critical Parameter in Chiral Symmetry Breaking Crystallization.* Journal of the American Chemical Society, 1995. **117**(1): p. 401-404.
173. Botsaris, G.D., R.-Y. Qian, and A. Barrett, *New insights into nucleation through chiral crystallization.* AIChE Journal, 1999. **45**(1): p. 201-203.
174. Kuhs, M., J. Zeglinski, and Å.C. Rasmuson, *Influence of History of Solution in Crystal Nucleation of Fenoxycarb: Kinetics and Mechanisms.* Crystal Growth & Design, 2014. **14**(3): p. 905-915.